

THE INFLUENCE OF SILICA STRUCTURE ON
THE PROPERTIES OF SUPPORTED NICKEL CATALYSTS.

THESIS
SUBMITTED FOR THE DEGREE
OF
DOCTOR OF PHILOSOPHY
OF THE
UNIVERSITY OF GLASGOW
BY
FRASER JOHN ROBERTSON B.Sc.
DEPARTMENT OF CHEMISTRY

FEBRUARY 1994

(c) Fraser J. Robertson, 1994.

ProQuest Number: 13833405

All rights reserved

INFORMATION TO ALL USERS

The quality of this reproduction is dependent upon the quality of the copy submitted.

In the unlikely event that the author did not send a complete manuscript and there are missing pages, these will be noted. Also, if material had to be removed, a note will indicate the deletion.



ProQuest 13833405

Published by ProQuest LLC (2019). Copyright of the Dissertation is held by the Author.

All rights reserved.

This work is protected against unauthorized copying under Title 17, United States Code
Microform Edition © ProQuest LLC.

ProQuest LLC.
789 East Eisenhower Parkway
P.O. Box 1346
Ann Arbor, MI 48106 – 1346

ACKNOWLEDGEMENTS

I would like to express my sincere gratitude to my academic supervisors, Professor G. Webb and Dr. R. J. Cross, and my industrial supervisors, Drs. S. D. Jackson and R. W. Griffiths, for suggesting the topic of this thesis and the guidance and helpful advice they have given during the course of this work.

In addition, I would like to thank the academic staff and Ph.D. students from the universities of Cambridge and Surrey (Professor J. R. Jones, Dr. L. F. Gladden, Mr. A. P. Sharratt, Mrs. M. Vignaux and Miss P. Chiaranussati) with whom I collaborated during this study.

Additionally, I acknowledge Drs. M. A. Keane, G. McLellan, K. C. Campbell and D. Stirling for constructive discussions in relation to this work. Thanks are also due to my colleagues in the catalysis research group for encouragement and advice when I needed it most.

Furthermore, I wish to thank innumerable technical staff, especially Miss R. Millar, Mr. D. Thom and Mr. W. McCormack, without whom this project would have been impossible.

I also gratefully acknowledge the award of a grant from the ICI Strategic Research Fund for this research project.

SUMMARY

A series of silica-supported nickel catalysts has been prepared under standard conditions by impregnation of a range of silica supports with nickel(II) nitrate solutions. The catalysts, in their unreduced and reduced states, and the supports have been characterised using temperature programmed reduction (T.P.R.), neutron diffraction, small angle neutron scattering (S.A.N.S.), ^{29}Si magic angle spinning nuclear magnetic resonance (MAS NMR) spectroscopy, carbon monoxide chemisorption and transmission electron microscopy (T.E.M.).

Using these characterisation techniques it was established that, in unreduced calcined catalysts, two distinct forms of nickel oxide can exist on the surface of the support; the ratio of the two forms being dependent on the fundamental structure of the silica. One form, which predominated in calcined catalysts prepared from supports containing a small proportion of strained three-fold siloxane rings in their structures, reduced at low temperature and had a negligible interaction with the silica: a three-fold siloxane ring is a ring structure consisting of three [Si-O] units. The other form, which was the predominant nickel oxide species in calcined catalysts prepared from supports whose structures contained a large proportion of three-fold siloxane rings, reduced at high temperature and interacted with the silica. The nickel particles formed upon reduction of the more reducible oxide species were large and sintered readily having no anchorage to the support. In contrast, reduction of the

less reducible oxide species led to nickel particles which were small, thermally stable and anchored to the support. In consequence, reduced catalysts prepared from silicas with large proportions of three-fold siloxane rings in their structures possessed good and thermally stable nickel dispersions.

The observation that the relative amounts of the two forms of nickel oxide were related to the proportion of three-fold siloxane rings in the silica structure has allowed a model for the interaction between nickel oxide and silica in calcined catalysts to be developed. This model can account for observations in the literature which previous models have found difficult to explain.

Ethene hydrogenation was used as a test reaction to ensure that the reduced catalysts were behaving in a comparable manner to similar catalysts reported in the literature. It was found, in agreement with other workers, that the reaction was surface insensitive and that deactivation occurred during a series of hydrogenation reactions performed using the catalysts. This deactivation was probably due to the formation and build-up of carbonaceous residues on the metal surfaces of the catalysts. The use of ethene hydrogenation as a test reaction, combined with the T.P.R. characterisation results, demonstrated that the catalysts in their reduced and unreduced states behaved similarly to previously reported analogous studies. Since the catalysts were not anomalous, at least with respect to ethene hydrogenation and their T.P.R. characteristics, the conclusions reached in this

dissertation can be extended to silica-supported nickel catalysts prepared by impregnation in general.

CONTENTS

	Page
Acknowledgements.	i
Summary.	ii
Contents.	v
<u>Chapter One</u> <u>Introduction</u>	1
1.1 General Introduction.	1
1.2 Preparation of Silica-Supported Nickel Catalysts.	2
1.3 Dispersion, Average Metal Particle Size and Metal Surface Area of Supported Metal Catalysts.	3
1.3.1 Definition of Dispersion.	3
1.3.2 Relationship Between Nickel Dispersion and Particle Size.	4
1.3.3 Relationship Between Dispersion, Average Nickel Particle Size and Nickel Surface Area.	5
1.4 Experimental Methods for Determining Dispersion, Nickel Surface Area and Average Particle Size.	6
1.4.1 Chemisorption Measurement.	6
1.4.1(a) The Adsorption of Carbon Monoxide on Supported Nickel Catalysts.	9
1.4.2 Transmission Electron Microscopic Analysis.	20
1.4.3 Other Methods.	24

1.5	The Influence of the Support on the Reducibility of the Supported Metal Precursor and the Properties of the Supported Metal.	24
1.5.1	The Influence of the Support on the Reducibility of the Supported Metal Precursor.	24
1.5.2	The Influence of a Reducible Support on the Properties of Supported Metal.	31
1.5.3	The Influence of a Non-reducible Support on the Properties of Supported Metal.	40
1.6	The Preparation, Uses and Structures of Silicas.	43
<u>Chapter Two</u>	<u>The Object of the Present Work</u>	46
2.1	Organisation of the Project.	46
2.2	Aims and Objectives.	46
<u>Chapter Three</u>	<u>Apparatus and Experimental Procedure</u>	49
3.1	Preparation of the Catalysts.	49
3.2	Unreduced Catalyst Characterisation.	52
3.2.1	Temperature Programmed Reduction.	52
3.2.1.1	Apparatus.	52
3.2.1.2	Experimental Procedure.	53
3.2.1.3	Quantitative Determination of Hydrogen Uptake.	55
3.3	Reduced Catalyst Characterisation.	56
3.3.1	Catalyst Reduction and Carbon Monoxide Adsorption Experiments.	56

3.3.1(a)	Chemisorption of Carbon Monoxide in Hydrogen Carrier Gas.	57
3.3.1(b)	Chemisorption of Carbon Monoxide in Helium Carrier Gas.	61
3.3.2	Transmission Electron Microscopy.	62
3.4	Reaction Chemistry.	65
3.4.1	Static Reduction.	65
3.4.1.1	Static Reduction Procedure.	67
3.4.1.2	Ethene Hydrogenation After Static Reduction.	68
3.4.2	Flow Reduction.	70
3.4.2.1	Flow Reduction Procedure.	70
3.4.2.2	Ethene Hydrogenation After Flow Reduction.	71
<u>Chapter Four</u>	<u>Results</u>	73
4.1	Characterisation of the Unreduced Catalysts.	73
4.1.1	Chemical Compositions, BET Surface Areas and Porosities of the Catalysts.	73
4.1.2	Temperature Programmed Reduction.	74
4.1.2(a)	T.P.R. - Control Experiments.	75
4.1.2(b)	T.P.R. of the Uncalcined Catalysts	75
4.1.2(c)	T.P.R. of the Calcined Catalysts	78
4.2	Characterisation of the Reduced Catalysts.	83
4.2.1	Carbon Monoxide Chemisorption.	83
4.2.1(a)	Carbon Monoxide Chemisorption in Hydrogen Carrier Gas.	83

4.2.1(b)	Carbon Monoxide Chemisorption in Helium Carrier Gas.	86
4.2.2	Transmission Electron Microscopic Analyses.	89
4.3	Reaction Chemistry.	92
4.3.1	Catalysts Reduced by the Static Method.	93
4.3.2	Catalysts Reduced by the Flow Method.	98
<u>Chapter Five</u>	<u>Discussion</u>	104
5.1	The Influence of the Support on the Nature of the Deposited Nickel Precursor States and the Resultant Nickel Particles Formed Upon Reduction.	104
5.1.1	Uncalcined Catalysts.	104
5.1.2	Calcined Catalysts.	108
5.1.3	The Influence of the Support on the Average Nickel Particle Size.	128
5.1.4	General Conclusions on the Nature of Nickel Metal Precursors in Uncalcined and Calcined Catalysts.	138
5.2	Reaction Chemistry.	140
5.3	General Summary.	157
<u>Appendix A</u>	<u>Silica Support Data</u>	160
A1	ICI Silica Support.	160
A2	Cab-O-Sil M-5 Silica Support.	161
A3	CS1030E Silica Support.	161
A4	CS2040 Silica Support.	162

		Page
<u>Appendix B</u>	<u>Summary of Support Characterisation</u>	164
B1	Introduction.	164
B2	Neutron Diffraction Studies.	164
B3	Magic Angle Spinning NMR.	166
B4	Small Angle Neutron Scattering.	167
<u>Appendix C</u>	<u>Catalyst Characterisation and Reaction</u>	
	<u>Chemistry</u>	171
C1	Introduction.	171
C2	T.P.R. Studies.	171
C3	Reductive Amination of Ethanol.	175
References.		180

CHAPTER ONE

CHAPTER ONEINTRODUCTION1.1 General Introduction

Nickel catalysts, whether supported or unsupported, are employed in a wide variety of industrial manufacturing processes. For example, nickel on silica and unsupported Raney nickel catalysts are used extensively in fat hardening (1). In this economically important process, animal and vegetable oils, which are rich in polyunsaturated triacylglyceride species, are partially hydrogenated by catalytic means. This partial hydrogenation leads to oils that are more resistant to oxidation and therefore have a longer shelf life. The processed oils also tend to have a more appropriate physical form, i.e. solid, compared to the natural materials and this allows for easier handling and for more applications (1).

Catalysts containing nickel as the active component are also used in the steam reforming of hydrocarbons (1). In this process, methane (from natural gas) is reacted with steam, in the presence of a catalyst, to form synthesis gas. Synthesis gas is a mixture of hydrogen, carbon monoxide and carbon dioxide and can be used as a fuel (town gas), a feedstock gas to produce organic materials such as methanol or treated to yield hydrogen. Methanol is produced on a massive scale by passing synthesis gas over a copper/zinc oxide/alumina catalyst.

In addition, Raney nickel (sometimes referred to as skeletal nickel) finds application in numerous synthetic preparations in organic chemistry (2, 3).

1.2 Preparation of Silica-Supported Nickel Catalysts

One of the most common and industrially important methods of catalyst preparation is impregnation (1, 4, 5). In this technique a solution of a nickel salt, typically nickel(II) nitrate, is added to a silica. These components are thoroughly mixed and dried to give the uncalcined form of the catalyst, i.e. essentially the silica-supported nickel salt.

Another common method of catalyst preparation is the precipitation technique. In this technique, an insoluble nickel salt is precipitated onto a silica support. This is normally achieved by the slow addition of a solution of sodium hydroxide or sodium carbonate to a suspension of silica in an aqueous nickel(II) nitrate solution to deposit nickel(II) hydroxide or basic nickel carbonate respectively onto the silica (5 - 7). A variant of this procedure is deposition-precipitation, whereby nickel(II) hydroxide is precipitated by adding urea to a suspension of silica in an aqueous nickel(II) nitrate solution. Progressive precipitation of nickel(II) hydroxide occurs when this mixture is heated to ca. 363 K by the gradual release of hydroxide ions into solution from hydrolysis of the urea (5, 6, 8 - 13).

The unreduced catalysts produced by these methods can be directly reduced (activated) by thermal treatment in hydrogen to give supported nickel. More commonly, however, an uncalcined catalyst is first heated (calcined) in a flow of nitrogen or air to give the calcined form of the catalyst, i.e. essentially silica-supported nickel(II) oxide. The calcined catalyst is then reduced. In this

study all the catalysts were prepared by an impregnation method and were usually precalcined before reduction.

1.3 Dispersion, Average Metal Particle Size and Metal Surface Area of Supported Metal Catalysts

1.3.1 Definition of Dispersion

One of the prime considerations in the manufacture and reduction of supported metal catalysts, especially those containing precious metals, is to obtain a high degree of metal dispersion (surface-to-volume ratio of the active component) in the reduced catalyst which is stable under reaction conditions (8, 13 - 19). The active component in supported metal catalysts is usually the metal, although in reforming catalysts the support is also catalytically active; reforming catalysts are therefore termed bifunctional catalysts (1, 14, 20). The dispersion (D) of the metal is defined as the ratio of surface metal atoms (N_s) to the total number of metal atoms (N_{tot}) and is defined mathematically by the expression (14, 21, 22);

$$D = N_s/N_{tot} \quad (1.1).$$

This expression gives the number of surface metal atoms expressed as a fraction of the total number of metal atoms (D is also often quoted as a percentage value). Naturally, the value of D calculated using equation 1.1 is an average quantity but it retains its meaning for catalysts composed of particles of different sizes and shapes, i.e. polydispersed catalysts (21, 22). Further, for macroscopic particles and for very small particles the values of D are ca. zero and one, respectively. The value of D for a

supported metal catalyst is inversely proportional to the average metal particle size (21), hence the larger the value of D the smaller the average particle size.

1.3.2 Relationship Between Nickel Dispersion and Particle Size

For supported metal catalysts, where the active component is usually present as discrete metal particles, a relationship exists between D and the average size of these particles. If V is the total volume and S the total surface area of metal, then equation 1.1 may be rewritten as (21);

$$D = \frac{fA}{p\sigma N} \frac{S}{V} \quad (1.2),$$

where f is the fraction of the metal surface effectively exposed to reactants during a chemical reaction, A is the atomic weight of the metal atoms, p is the density of the metal, σ is the average cross-sectional area occupied by a metal atom at the surface and N is the Avogadro constant. If the supported metal particles are now assumed to be spheres of equal diameter (d_s) and given that $V = 4/3\pi r^3$ and $S = 4\pi r^2$ (where r is the radius of the spheres, i.e. $d_s = 2r$) then;

$$\frac{S}{V} = \frac{4\pi r^2}{4/3\pi r^3} = \frac{3}{r} = \frac{6}{d_s} \quad (1.3)^a.$$

Substituting equation 1.3 into 1.2 leads to the expression;

$$D = \frac{6fA}{d_s p \sigma N} \quad (1.4).$$

a. Equally valid for cubic particles with edges of length d_s .

Rearranging equation 1.4 gives;

$$d_s = \frac{6fA}{D\rho_s N} \quad (1.5).$$

Assuming that $f = 1$, i.e. that all the surface is effectively exposed to the reactants during a chemical reaction, and given that for nickel; $A = 58.71$ g, $\rho = 8.90 \times 10^{-21}$ g nm⁻³ and $\sigma = 0.065$ nm² atom⁻¹ (16, 21, 23 - 29), then;

$$d_s \text{ (nm)} = \frac{1.01}{D} = \frac{101}{D(\%)} \quad (1.6)$$

Equation 1.6 is identical to that used by Smith, Thrower and Vannice (23) in their evaluation of d_s for nickel on silica and nickel on alumina catalysts.

1.3.3 Relationship Between Dispersion, Average Nickel Particle Size and Nickel Surface Area

Nickel surface area (S_{Ni}) is another useful parameter and is usually expressed as m² nickel per gram of nickel. S_{Ni} values are most commonly used to normalise reaction rates between catalysts of differing metal surface areas, i.e. by expressing the rate per m² of nickel. Expressions relating S_{Ni} to both D and d_s can be derived by first considering the expression (21);

$$S_{Ni} = N_s \sigma \quad (1.7),$$

where N_s is the number of surface nickel atoms expressed per gram of nickel and σ is the average cross-sectional area of a surface nickel atom expressed in m². N_s is therefore related to S_{Ni} by;

$$N_s [\text{atom (g Ni)}^{-1}] = S_{\text{Ni}} [\text{m}^2 (\text{g Ni)}^{-1}] \times 10^{18} [\text{nm}^2/\text{m}^2] \times 1/0.065 [\text{atom/nm}^2] \quad (1.8).$$

i.e.;

$$N_s [\text{atom (g Ni)}^{-1}] = 1.54 \times 10^{19} S_{\text{Ni}} \quad (1.9).$$

Since D is defined as (equation 1.1);

$$D (\%) = \frac{N_s [\text{atom (g Ni)}^{-1}]}{N_{\text{tot}} [\text{atom (g Ni)}^{-1}]} \times 100,$$

insertion of equation 1.9 into this expression gives;

$$D (\%) = \frac{1.54 \times 10^{19} \times S_{\text{Ni}}}{1.03 \times 10^{22}} \times 100 = 0.15 \times S_{\text{Ni}} \quad (1.10).$$

Substituting expression 1.10 into equation 1.6 therefore gives;

$$d_s = \frac{101}{0.15 \times S_{\text{Ni}}} = \frac{674}{S_{\text{Ni}}} \quad (1.11).$$

Expression 1.11 is identical to that used by Montes, de Bosscheyde, Hodnett, Delannay, Grange and Delmon (9).

1.4 Experimental Methods for Determining Dispersion, Nickel Surface Area and Average Particle Size

1.4.1 Chemisorption Measurement

Selective chemisorption of a gas is very commonly utilised as a technique to determine the D, d_s and S_{Ni} parameters for a reduced catalyst. The technique depends on the fact that suitably chosen gases selectively chemisorb on the metal surface and not on the support surface of a supported metal catalyst. Typical gases used in

chemisorption experiments include carbon monoxide, hydrogen and oxygen.

Two main experimental approaches have been developed to determine the amount of adsorbate gas chemisorbed by a catalyst (21):

a. Pulse Flow Method. This is a relatively recent method of chemisorption measurement. In this technique, a flow of hydrogen or helium (30) is maintained over a sample of reduced catalyst which is kept at a constant specified temperature. Pulses consisting of a known quantity of adsorbate gas are then introduced into the gas stream and allowed to pass through the catalyst bed. The amount of gas adsorbed per pulse can then be determined by use of a suitable detection device, typically a calibrated thermal conductivity detector (T.C.D.). The gas pulsing is continued until no more gas is adsorbed. If the cumulative amount of gas adsorbed is then plotted against the total amount of gas pulsed through the catalyst bed, the amount of gas chemisorbed by the catalyst corresponds to the plateau region of the graph. This graph is referred to as an adsorption isotherm.

b. Volumetric Method. In this method, aliquots of gas are admitted separately to an evacuated vacuum apparatus of known volume containing a sample of reduced catalyst, which is maintained at a constant specified temperature. After each admission of gas, adsorption is allowed to occur over a suitable time as to allow equilibrium to be achieved. The amount of gas remaining in the vacuum system after each addition can then be calculated from the residual pressure and hence the amount of gas adsorbed by the catalyst

determined. The pressure in the reaction vessel is raised by admitting further aliquots of the adsorbing gas. As the surface of the catalyst becomes saturated, increasing the pressure in the reaction vessel has little effect on the amount of material adsorbed. Extrapolation to zero pressure from the plateau region of a total amount of gas adsorbed versus pressure graph leads to a value for the unimolecular coverage of the adsorbate on the metal surface.

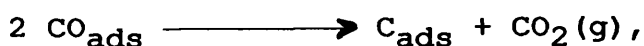
Studies have shown that, for nickel and other metal catalysts, both the pulse flow and volumetric methods lead to comparable results when examining separate samples of the same catalyst reduced under identical conditions (21, 30 - 32).

Both of the methods described above give the amount of adsorbate gas taken up by a particular catalyst. If the adsorption stoichiometry of the adsorbate with the surface atoms of the supported metal is known or assumed, then a value for the number of surface metal atoms (N_s) can be calculated. From this, a value for D can be obtained by use of equation 1.1 if the metal content of the catalyst is known. The value of D obtained can then be used to calculate d_s and S_{Ni} values for that catalyst by applying equations 1.6 and 1.11, respectively.

In this work, a pulse flow technique was employed to determine the amount of gas chemisorbed by the reduced catalysts. The adsorbate gas chosen for the chemisorption measurements was carbon monoxide. The complexity of carbon monoxide adsorption on supported nickel catalysts has led to a preponderance of papers in the literature and discussion of these warrants a separate subsection (see below).

1.4.1(a) The Adsorption of Carbon Monoxide on Supported Nickel Catalysts

The chemisorption of carbon monoxide on dispersed nickel metal is associative at room temperature (21, 33 - 38). At higher temperatures (> 400 K), as well as the adsorbed carbon monoxide species, some disproportionation of the carbon monoxide into a surface carbon species and carbon dioxide occurs (34 - 36, 39);



with complete reaction occurring at temperatures in excess of 573 K (34, 36, 38). The disproportionation reaction leads to the formation of nickel carbide platelets on the nickel surface as observed by electron microscopy (40).

The interaction of adsorbates with metal surfaces has been extensively studied by infrared spectroscopy (41, 42). The adsorption of carbon monoxide on nickel gives rise to strong and readily measured absorption bands in the infrared region of the electromagnetic spectrum (42). Hence many studies have utilised infrared spectroscopy to characterise the nature of the bonding between carbon monoxide molecules and nickel surfaces. If the nature of the bonding can be determined, this may lead to a correct estimation for the bonding stoichiometry between the adsorbate molecules and surface metal atoms in chemisorption experiments (43). Once this stoichiometry is determined, an accurate value for the dispersion of metal in a supported catalyst can be calculated and hence correct values for d_s and S_{Ni} (31, 43).

In practice, the application of infrared spectroscopy for the determination of the nature of carbon monoxide

bonding with supported nickel catalysts has aroused controversy with regard to the interpretation of spectra.

The earliest infrared work performed on silica-supported nickel was reported in the 1950's by Eischens, Pliskin and Francis (44, 45). By comparison of the observed absorption bands at 2075 and 2041 cm^{-1} (44, 45) with the bands due to the C-O stretching frequencies of terminal^a carbonyl ligands in iron carbonyl compounds, e.g. $\text{Fe}_2(\text{CO})_9$, Eischens *et al.* assigned these bands to linearly-bound carbon monoxide. Similarly, the bands observed at 1912 and 1850 cm^{-1} were assigned to carbon monoxide bound in a bridging fashion between two nickel atoms.

Eischens *et al.* found that the position and number of absorption bands varied with surface coverage and they attributed this to surface heterogeneity. It was therefore suggested that a convenient division between the C-O stretching frequencies for linear- and bridge-bonded carbon monoxide molecules could be distinguished at 2000 cm^{-1} . Absorption bands occurring below this division were attributed to bridge-bonded carbon monoxide, whereas absorption bands above this were attributed to linearly-bonded carbon monoxide. This interpretation of the absorption bands found support from O'Neill and Yates (15) and Yates and Garland (46) among others.

Subsequently, in the 1960's, this hypothesis was criticised by Blyholder (47) on the basis of results obtained from Hückel molecular orbital calculations. He argued that if the surface heterogeneity was taken into

a. The term terminal carbonyl refers to the situation where one carbonyl ligand is linearly-bonded to one metal atom.

account, then all the experimental data could be equally well explained by assuming that all the carbon monoxide molecules were adsorbed in the linear form.

Blyholder argued, on qualitative grounds, that carbon monoxide molecules are more strongly adsorbed on more exposed nickel atoms, e.g. atoms at the edges and corners of particles; these atoms are less coordinated by other nickel atoms. On adsorbing on an exposed nickel atom, therefore, the stretching frequency of the C-O bond may be shifted to the $1800 - 1900 \text{ cm}^{-1}$ region, i.e. the region according to Eischens *et al.* where the stretching frequency of bridge-bonded carbon monoxide occurs. Blyholder claimed this shift to lower frequency may be due to the increased back-bonding from the more electron rich exposed metal atom to the empty $2\pi^*$ antibonding orbital of the adsorbed carbon monoxide molecule. This increased back-bonding weakens the C-O bond and lowers the C-O stretching frequency of the adsorbed carbon monoxide molecule to below 2000 cm^{-1} .

On the other hand, nickel atoms which are coordinated to a greater number of other nickel atoms donate less electron density to the $2\pi^*$ antibonding orbital of an adsorbed carbon monoxide molecule. This means that the C-O stretching frequency remains high at greater than 2000 cm^{-1} . Using this as a hypothesis, therefore, Blyholder estimated that linearly-adsorbed carbon monoxide could give rise to absorption bands in the region ca. $2100 - 1800 \text{ cm}^{-1}$.

In addition, Blyholder (47) also cited examples from the literature (48, 49) of substituted metal-carbonyl compounds possessing linearly-bound carbonyl groups and having absorption bands of below 2000 cm^{-1} in their infrared

spectra. In the discussion of his paper, however, Blyholder did not rule out the existence of bridging carbon monoxide species.

More recent publications have indicated by the combined use of infrared spectroscopy and saturation magnetisation techniques that the original interpretation of the infrared data by Eischens *et al.* was correct (33, 36, 50). Primet, Dalmon and Martin (33) calculated the average bond order (n) of adsorbed carbon monoxide molecules with surface nickel atoms in a series of five reduced silica-supported nickel catalysts by determining the decrease of saturation magnetisation per adsorbed molecule. They calculated that $n = \text{ca. } 1.85$ for all the catalysts (cf. $n = 1$ for linearly-adsorbed carbon monoxide and $n = 2$ for bridge-bonded carbon monoxide). Interestingly, the value of n did not vary with:

- i. temperatures between 293 - 373 K;
- ii. average nickel particle sizes between 2.5 - 12 nm;
- iii. degree of surface coverage.

On the basis of the above results it can be seen that carbon monoxide was not adsorbed exclusively in a linear manner. This implies that the original hypothesis of Eischens *et al.* is correct, i.e. that both linear and bridged forms of adsorbed carbon monoxide occur on supported nickel catalysts, with the bridged form being predominant.

In addition to the magnetic measurements described above, Primet *et al.* (33, 36) performed infrared spectroscopy on the same catalysts during carbon monoxide adsorption experiments. They reported that two sets of absorption bands were present: one set in the region 2070 -

2040 cm^{-1} (they denoted these A bands) and a band at 1935 cm^{-1} (B band). The A bands were assigned to the C-O stretching frequency of linearly-bound carbon monoxide and the B band was the corresponding stretching frequency of 2 fold-bridge bonded carbon monoxide. Other multivalent bound carbon monoxide molecules (Ni_3CO and Ni_4CO) were observed to give rise to a small shoulder on the B band at ca. 1800 cm^{-1} . The ratio, r , of the integrated optical densities for bands A and B was also calculated;

$$r = A_A / (A_A + A_B)$$

where A_A and A_B are the integrated optical densities of bands A and B, respectively. The ratio was ca. 0.3 for fully reduced catalysts and indicated, together with the magnetically determined value of n , that the linear species was present in smaller amounts relative to the bridged species. This view was also shared by Rochester and Terrell in their analyses of infrared spectra recorded during carbon monoxide adsorption on moderately dispersed reduced nickel on silica catalysts (51).

Further, it was also noted by Primet *et al.* (33) that as the degree of reduction of the catalyst decreased the linear species became more abundant, i.e. r was observed to increase and n decrease. The authors suggested that the presence of unreduced surface residues led to a decrease in the probability of two adjacent nickel atoms being on the surface and hence to a decrease in the number of bridged species. Similar effects have been observed by infrared spectroscopy when carbon monoxide was adsorbed on partially carbided nickel on silica catalysts (36) and also nickel on

alumina catalysts that had been partially poisoned by mercury vapour (46) or carbon disulphide vapour (52).

The above hypothesis is further strengthened by work performed by several researchers on supported nickel-copper alloys (50, 53). In these studies it was found that as the copper content of the alloy increased the band attributed to bridge-bonded carbon monoxide decreased in intensity relative to the band assigned to linearly-bonded carbon monoxide. A similar argument to that presented above for catalysts with unreduced residues on the surface could be invoked to explain this phenomenon, i.e. that the copper was acting as a diluent for the nickel atoms (50, 53, 54). The sites for bridge-bonded carbon monoxide, therefore, became fewer at higher concentrations of copper. Magnetic measurements also confirmed that n decreases with increasing copper content in such alloys (50).

In light of the increasing evidence for the existence of bridge-bonded carbonyl species, Blyholder (55) performed further calculations and concluded that multi-bridged carbon monoxide species give rise to the strongest carbon monoxide bonding and the lower C-O stretching frequencies (ca. 1935 cm^{-1}). In contrast, linearly-bonded carbon monoxide species give rise to a band ca. 2075 cm^{-1} .

Also in retrospect, the model metal-carbonyl compounds chosen by Blyholder (48, 49) to illustrate that terminal carbonyls can display C-O stretching frequencies similar to those assigned by Eischens *et al.* to bridged species were found to be anomalous (41). The lower C-O stretching frequencies observed for these compounds could have arisen due to the influence of the other ligands in the compounds,

e.g. amines and phosphines. These groups could donate electron density to the metal atoms which in turn would strengthen the back-bonding from the metal d-orbitals to the empty carbonyl $2\pi^*$ antibonding orbitals. This increase in electron donation would weaken the C-O bond and lower its stretching frequency. This is similar to what occurs when carbon monoxide is adsorbed on nickel doped with potassium, where the potassium donates electrons to the nickel which strengthens the Ni-CO bond (56, 57). Similar adsorbed electron-donating species were not present on the nickel catalysts in the carbon monoxide adsorption studies described above, where infrared spectroscopy and magnetic saturation techniques established that both linear- and bridge-bonded carbon monoxide species are present on fully reduced, unpoisoned nickel catalysts.

For a general discussion of the infrared data, it should be noted that the positions and numbers of the absorption bands determined originally by Eischens *et al.* can be influenced by:

- i. The degree of reduction of the catalyst (33, 41);
- ii. The surface coverage of adsorbate (15, 33, 41, 45, 52, 58);
- iii. The crystallite size (33, 41, 46, 59 - 61);
- iv. Adsorption on nickel atoms in differing environments, e.g. different crystal planes (41, 47, 55, 59, 62) or atoms in contact with the support (33, 41);
- v. The method of catalyst preparation, e.g. impregnation, ion-exchange, etc. (59);
- vi. The type of support (15, 33, 41, 42, 60, 63);
- vii. The temperature (36).

In addition to the above factors, the date of the literature report also influences the determination of the intensities and positions of the absorption bands. The older literature details work performed using classical infrared spectrometers where the region of interest (2200 - 1600 cm^{-1}) coincides partly with the Si-O absorption band of the support (33). Hence accurate evaluation of the positions and intensities of absorption bands due to adsorbed carbon monoxide was difficult. Modern spectrometers can subtract out the absorption bands due to the catalyst itself leaving the spectrum of adsorbed carbon monoxide. This improves the accuracy of the determination of the intensities and positions of adsorption bands due to adsorbed carbon monoxide.

Due to the factors listed above, it is necessary to summarise the infrared data by a generalised scheme such as that proposed by Sheppard and Nguyen (41). In this scheme, bands occurring within the region 2025 - 2090 cm^{-1} are assigned to the stretching frequency of the C-O bond in linearly-adsorbed carbon monoxide, bands occurring between 1910 - 1975 cm^{-1} are assigned to the bridge-bonded carbon monoxide C-O stretching frequency and absorption bands in the region 1750 - 1890 cm^{-1} assigned to the stretching frequency of the C-O bond in carbon monoxide adsorbed on more than two nickel atoms [multicentred adsorption] (33, 41, 50, 58).

A further complicating factor in the adsorption of carbon monoxide on nickel can be the formation of subcarbonyl species, i.e. $\text{Ni}(\text{CO})_2$, $\text{Ni}(\text{CO})_3$, and also the formation of the stable nickel tetracarbonyl ($\text{Ni}(\text{CO})_4$).

According to the model presented by Van Hardeveld and Hartog (61), where they approximated the shape of a supported nickel particle to a cubo-octahedron, subcarbonyl species may form on nickel atoms with a coordination number of seven nickel atoms (denoted C_7 where the subscript is the coordination number) or less due to appropriate steric considerations. Such atoms exist at the vertices (C_4) and the edges (C_7) of a cubo-octahedral particle.

Although the cubo-octahedron was suggested by the authors to be one of the most stable particle shapes, in reality nickel crystallites only tend to approximate to cubo-octahedra (16, 41, 61). Despite this, some researchers have observed these subcarbonyl species and also gas phase nickel tetracarbonyl by infrared spectroscopy; the C-O stretching frequencies occur for these species at ca. $2055 - 2065 \text{ cm}^{-1}$ (46, 51, 59, 61 - 65). In agreement with the model presented by Van Hardeveld and Hartog, the subcarbonyl species appear to become more prevalent in highly dispersed catalysts, where the proportion of nickel atoms in edge and corner sites relative to nickel atoms with higher coordination numbers is large (46, 51, 59, 63).

The formation of nickel tetracarbonyl has also been observed during the measurement of adsorption isotherms on reduced nickel on silica and nickel on alumina catalysts at room temperature using the volumetric method (23, 25, 46, 63, 66, 67). In this method, the catalyst is exposed to relatively high pressures of carbon monoxide ($P_{CO} = 50 - 250$ Torr) and long catalyst-adsorbate contact times, typically several hours. This problem is minimised by using the pulse flow chemisorption technique as the time of contact

between the carbon monoxide gas and the catalyst bed is very short.

The final concern when using carbon monoxide chemisorption as a catalyst characterisation technique is exemplified by the recently reported adsorbate-induced morphology changes in very highly dispersed reduced palladium on silica and palladium on alumina catalysts (43). In this study it was found that the sizes of small particles of supported palladium metal were affected by the action of chemisorbing carbon monoxide. Adsorption-induced restructuring (also known as facetting) occurs when an adsorbate strongly bonds to a surface, i.e. has a high heat of adsorption, and the surface atoms undergo rearrangement (68). This process has been observed by low energy electron diffraction (LEED) on well defined nickel single crystal surfaces [e.g. Ni(100)] whereby the surface rearranges to maximise the number of nickel atoms interacting with the carbon atom of an adsorbed carbon monoxide molecule (69). It is, therefore, possible that such interactions will occur during the chemisorption of carbon monoxide on reduced supported nickel catalysts as the heat of adsorption of carbon monoxide on nickel is moderately high at 298 K [ca. 144 kJ mole⁻¹ (70)]. The effects of this restructuring, should it occur, would be more pronounced on very well dispersed crystallites (43). Care, therefore, must be taken to minimise or assess such effects on highly dispersed catalysts, e.g. by using relatively low temperatures in adsorption experiments or by comparing data derived from chemisorption experiments with

corresponding data derived from another technique such as electron microscopy.

During chemisorption experiments, in addition to the metal, the support may irreversibly chemisorb the adsorbate gas. For silica, however, this is usually not a major concern as the uptake of carbon monoxide has been found to be very small or zero at room temperature (23, 71, 72).

To summarise, the adsorption of carbon monoxide on silica-supported nickel leads to a variety of adsorption stoichiometries. From infrared data and magnetic measurements, the predominant adsorbed form of carbon monoxide appears to be a molecule bridging two nickel atoms; recent publications still support this view (73). However, for well dispersed catalysts, nickel tetracarbonyl and subcarbonyl formation as well as crystallite reconstruction may reduce the accuracy of chemisorption measurements.

In order to avoid estimating the stoichiometry of the adsorbate-surface metal bond, some researchers have assumed that at saturation coverage the adsorbate molecules are close packed. Hence the surface area can be calculated from the sum of the cross-sectional areas of the adsorbed carbon monoxide molecules (30, 74). Each chemisorbed carbon monoxide molecule is assumed to occupy a cross-sectional area of ca. 0.13 nm^2 (30, 75, 76). If this procedure is adopted it leads to a S_{Ni} value which is approximately the same as that determined by the assumption that one carbon monoxide molecule bonds to two nickel atoms. If this assumption of bonding stoichiometry is valid, an adsorbed carbon monoxide molecule is equivalent to an area of 0.13 nm^2 . LEED studies (41, 77) conducted on well

defined nickel single crystal planes have indicated that the adsorbed overlayer of carbon monoxide on the nickel is compressed beyond close packed at high surface coverages to form an out-of-register layer. In this structure the adsorbed carbon monoxide molecules are no longer equidistant from the metal surface. This compression presumably reflects the fact that a proportion of the carbon monoxide molecules are adsorbed linearly on one nickel atom and therefore steric crowding occurs.

1.4.2 Transmission Electron Microscopic Analysis

The technique of electron microscopy most commonly employed for the characterisation of supported metal catalysts is transmission electron microscopy (T.E.M.). This technique can image structures in a working range of ca. 1 - 100 nm (78) and is found to give accurate and reliable particle size distribution data for reduced nickel on silica catalysts (13). Microscopic techniques with greater resolution than T.E.M. do exist, e.g. scanning tunnelling electron microscopy (S.T.E.M.), whereby extremely small particles of the order of atomic dimensions can be imaged (79). As yet, however, these techniques have seldom been used for supported catalyst characterisation due to the expense and difficulties in their application (78, 80).

Numerous studies utilising T.E.M. for the characterisation of reduced supported nickel catalysts appear in the literature (9 - 11, 13, 23, 29, 61, 66, 81 - 85). The number of studies using T.E.M. as a characterisation method reflects the fact that it is a very useful technique, particularly for reduced nickel on silica

catalysts, with the often excellent contrast between the silica and nickel particles facilitating particle size measurement (13, 21). Conversely, T.E.M. characterisation of nickel particles on titania, or especially alumina supports, is more difficult as the metal particles do not display as sharp a contrast with the support (13, 23, 29).

In the case of reduced nickel on silica catalysts it is possible to image particles with diameters of ca. 1 nm (1, 13, 21, 23, 86). T.E.M. is also the most direct way of determining the particle size distribution of a catalyst (1, 21). The measurement of a significant number of nickel particle diameters in a catalyst sample (often several hundred) can lead to a meaningful particle size distribution (1, 21).

T.E.M. also has advantages over other techniques for the determination of particle size, such as magnetic susceptibility, chemisorption and X-ray diffraction (X.R.D.). In addition to yielding information on the average particle size, T.E.M. gives a distribution of particle sizes and information on the particle shape (13, 21, 69, 87). Data on the particle shape for supported catalysts is only accessible by electron microscopy techniques (13). Furthermore, information can be obtained on the catalyst texture and the extent, if any, of the nickel interaction with the support (13).

The measurement of the diameters of supported particles imaged by T.E.M. depends on three fundamental assumptions stated by Flynn, Wanke and Turner (86):

- i. The size of a metal particle is equal to the size of its image recorded on the micrograph (corrected for magnification);
- ii. The detection of a particle of a given size implies that all particles of that size and all larger particles are being detected;
- iii. The image contrast of the metal particles is distinguishable from contrast arising from the support material.

Flynn *et al.* also showed that caution should be applied to the interpretation of T.E.M. particle size data, especially for particles with diameters of less than ca. 2.5 nm in the case of reduced platinum on alumina catalysts. For reduced nickel on silica catalysts this value is less than 2 nm (21). The error in the measurement of supported particle diameters of this size or smaller increases as the particle size decreases because of deviation from perfect focus (defocus). Defocus arises in T.E.M. analyses of supported catalysts because of the relative thicknesses of the samples (typically greater than 30 nm). This leads to particles having a range of different elevations in the direction of the electron beam and therefore, in general, particles have different focus conditions. This could lead to identical particles in separate micrographs appearing to have different sizes.

Flynn *et al.* suggested that the lowest meaningful division of particle diameters into classes is 1 nm. Particle size distribution data are, therefore, usually presented in the form of a histogram with particle sizes divided into a minimum of 1 nm sized classes with the lowest

class incorporating 0.1 - 1 nm diameter particles and the second incorporating particles of diameters 1.1 - 2 nm, etc. (23). From these particle size distribution histograms it is possible to calculate the surface weighted average diameter as defined below (9, 13, 21, 22, 24, 31);

$$d_s = \frac{\sum_i (n_i \cdot d_i^3)}{\sum_i (n_i \cdot d_i^2)} \quad (1.12),$$

where n_i is the number of particles whose sizes lie between the class boundaries of the i^{th} class and whose size is represented by the class mark d_i .

The value of d_s obtained by use of equation 1.12 is identical to the average size obtained by chemisorption measurement using equation 1.6 (21). Hence, from a particle size distribution provided by electron microscopy, a value for d_s can be obtained and similarly for D and S_{Ni} by using equations 1.6 and 1.11, respectively.

A further advantage of T.E.M. is that it is sometimes possible to image silica-supported nickel oxide particles (9, 85, 88, 89) thereby allowing unreduced calcined catalysts to be characterised. A difficulty presented in such studies is the relative lack of contrast between the support and the nickel oxide particles (as opposed to nickel metal particles) and so only comparatively large nickel oxide particles can be seen (89).

Although T.E.M. particle size analysis is very accurate, it does suffer from some disadvantages. Firstly, the technique is usually unable to differentiate between catalytically inactive and catalytically active nickel (21). Catalytically inactive nickel may be nickel that is chemically combined with the support or where a catalytic

poison is adsorbed on the nickel surface. For this reason, the S_{Ni} , D and d_g parameters derived from chemisorption experiments are probably more applicable when considering catalytic reactions (16, 21). Secondly, T.E.M. also suffers from the disadvantage that very small crystallites cannot be imaged and therefore the d_g values obtained from T.E.M. may be slightly larger than those obtained for the same catalysts by using chemisorption techniques (23). T.E.M. is also an expensive and time-consuming technique to employ, with many hundreds of particle diameter measurements per sample required to ensure the accuracy of the resulting particle size distribution data (13).

1.4.3 Other Methods

Chemisorption and T.E.M. techniques for the determination of the dispersion, average metal particle size and metal surface area are amongst the most useful and commonly used techniques. Other techniques exist, however, whereby these parameters can be determined. Included in these techniques are X.R.D., X-ray photoelectron spectroscopy and magnetic susceptibility measurements (21).

1.5 The Influence of the Support on the Reducibility of the Supported Metal Precursor and the Properties of the Supported Metal

1.5.1 The Influence of the Support on the Reducibility of the Supported Metal Precursor

Most supported nickel catalysts are derived from a nickel salt, typically nickel(II) nitrate or nickel(II) hydroxide, which has been deposited onto the support

material. To eliminate the possibility of the formation of undesirable compounds during reduction [e.g. nitric oxide, nitrogen dioxide or possibly ammonia from supported nickel(II) nitrate (28)], uncalcined catalysts are commonly calcined in a flow of air or nitrogen before reduction. This procedure leaves essentially nickel oxide deposited on the support (90). Reduction is then performed on the calcined catalyst. The emphasis of this section will therefore primarily concern the reduction of silica-supported nickel oxide.

It is well known that unsupported nickel oxide is much easier to reduce than supported nickel oxide (18, 90 - 98). For example, Roman and Delmon (18) found that 4 grams of unsupported nickel oxide was completely reduced in 40 minutes under a flow of hydrogen at a temperature of 538 K. In contrast, under identical conditions, only 7 % of the supported nickel oxide in 4 grams of an impregnated and calcined 18.9 % w/w nickel on silica catalyst was reduced.

Roman and Delmon concluded that the inhibiting effect of the support on the rate of nickel oxide reduction could not be ascribed wholly to diffusion limitations imposed on the transport of hydrogen gas; reduction was found to be immensely speeded by the addition of a small amount of a foreign metal as a promoter, e.g. copper or platinum. These promoters were added in small amounts, less than 1 % w/w, without significantly changing the texture of the catalyst.

Roman and Delmon also found that the reduction of supported nickel oxide apparently never goes to completion even at the highest temperature used in their study (679 K)

and despite the presence of promoters. They speculated that a fraction of the silica-supported nickel oxide was "unreducible" because it was either almost completely encapsulated by the support or possibly bound up with the support as poorly crystallised nickel hydrosilicate. Evidence from X.R.D. indicated that the supported crystallites were nickel oxide, with no evidence for bulk chemical compound formation between the nickel oxide and the silica.

It is generally agreed that the rate-determining step in the reduction process is the formation of metallic nuclei on the metal oxide crystallites [nucleation] (9, 18, 90, 95, 99). Nucleation occurs when reduction has removed a sufficient number of oxygen ions from a metal oxide crystallite to cause the metal oxide lattice to rearrange and eliminate these anion vacancies and hence form metal nuclei.

Roman and Delmon (18) devised two explanations to account for the inhibitory effect of the support on the rate of nickel oxide reduction. Firstly, that the reduction process only nucleates on sufficiently large crystallites with thick nickel oxide domains. Secondly, that nucleation occurs only on particular sites, e.g. special crystal defects, regardless of nickel oxide crystallite size. Hence for highly dispersed nickel oxide, reduction may be hindered because the nickel oxide domains may be very thin or there may be a lack of nucleus forming sites on some isolated crystallites. Furthermore, when nucleation occurs on a particular supported nickel oxide crystallite, complete reduction of all the supported nickel oxide is hindered by

the lack of crystallite continuity over the surface of the support. This is not the situation in unsupported nickel oxide where the crystallites are much larger and are in contact with each other.

In summary, these proposed mechanisms imply that the rate of reduction of supported nickel oxide is limited by the smallness of the nickel oxide crystallites and also by the discontinuity of the dispersed crystallites on the support surface. In addition, a small fraction of the supported nickel oxide was, for some reason, found to be "unreducible" under the conditions of reduction used in the study by Roman and Delmon.

Temperature programmed reduction (T.P.R.) is a recently developed technique which is ideal for determining the reducibility of an unreduced catalyst and also the type (or types) of supported metal precursor species present. T.P.R. is a very sensitive and powerful technique, and yet simple and inexpensive, for monitoring the reduction processes occurring in an unreduced catalyst during thermal treatment under hydrogen (90, 97). T.P.R. does not depend on any specific property of the unreduced catalyst other than that it contains a species which is reducible by hydrogen. T.P.R., especially when used in conjunction with other techniques such as X.R.D., can provide strong evidence for the presence of, for example, metal precursor-support compounds in unreduced calcined catalysts.

T.P.R. in its commonest form consists of an apparatus capable of allowing a mixture of hydrogen in an inert carrier gas, typically 5 % v/v hydrogen in argon, to flow through a bed of unreduced catalyst. The catalyst is then

heated at a constant rate (β) under this gas flow and the uptake of hydrogen monitored by the change in the thermal conductivity of the gas during catalyst reduction. This provides a characteristic reduction "profile" or "fingerprint" and is a sensitive method for detecting the reduction of surface species within unreduced catalysts.

The first T.P.R. study on silica-supported nickel oxide was performed by Robertson, McNicol, de Baas, Kloet and Jenkins (91). In this study, T.P.R. clearly showed that the nickel oxide phase present in a calcined 0.25 % w/w nickel on silica catalyst reduced, under the conditions of the T.P.R. experiment, at a much higher temperature than unsupported nickel oxide; the maximum hydrogen uptake, T_{max} , occurred for these materials at ca. 683 and 597 K, respectively. A shoulder, which was not present in the reduction profile of unsupported nickel oxide, was also observed on the high temperature side of the reduction peak for the supported nickel oxide.

A further study performed by Unmuth, Schwartz and Butt (100) on a calcined 4.6 % w/w nickel on silica catalyst revealed a T.P.R. profile consisting of three reduction peaks, denoted by the authors as α , β and γ in order of ascending temperature. The α peak was ascribed by Unmuth et al. to the reduction of nickel oxide occurring simultaneously with an endothermic phase transformation from a rhombohedral nickel oxide structure to a cubic sodium chloride-type structure. X.R.D. revealed that the higher temperature β peak was due to the reduction of nickel oxide. The γ peak, which appeared as a shoulder on the high temperature side of the β peak, was ascribed to the

reduction of either very small nickel oxide particles or a nickel oxide-support compound, e.g. nickel hydrosilicate. X.R.D. data was inconclusive regarding the origin of the γ peak as the diffraction peaks were broad. Complete reduction was achieved under T.P.R. conditions for most of the catalyst samples. The conditions of the T.P.R. experiments were $\beta = 10 - 23 \text{ K min.}^{-1}$, with a final reduction temperature of 758 K.

Mile, Stirling, Zammitt, Lovell and Webb (101) also conducted a T.P.R. study on calcined nickel on silica catalysts. The T.P.R. profiles for their calcined catalysts indicated that three distinct types of reducible species were present. The lowest temperature peak, $T_{\text{max}} = 523 \text{ K}$, was assigned to the reduction of nickel(III), a species which is often present in nickel(II) oxide (88, 99, 102). The peak observed at $T_{\text{max}} = 673 \text{ K}$ was assigned to the reduction of large aggregates of nickel oxide which had little interaction with the support. The authors assigned the peak observed at $T_{\text{max}} = 773 \text{ K}$ to either the reduction of surface nickel hydrosilicate or very small nickel oxide particles. Again, X.R.D. provided no evidence for the presence of a well defined nickel hydrosilicate compound, although the authors could not rule out the possibility of this compound being present in very small quantities.

The method of catalyst preparation also has an effect on the reducibility of the supported metal precursor. The studies by Robertson, Unmuth and Mile and their respective co-workers were performed using calcined catalysts prepared by impregnation. For unreduced catalysts prepared by the precipitation or deposition-precipitation methods it is

often found that a relatively large proportion of the supported nickel is chemically combined with the support as nickel hydrosilicate (5, 6, 8 - 10, 72, 85, 95, 103, 104). This compound has a layer structure derived from the brucite $\text{Ni}(\text{OH})_2$ structure with an one-sided partial replacement of hydroxide groups by interlinked SiO_4 tetrahedra of the silica framework (6, 9, 12, 103, 104). This compound is known as nickel antigorite and has the stoichiometry $\text{Ni}_3(\text{OH})_3(\text{Si}_2\text{O}_5)\text{OH}$ (10, 103, 104). Nickel antigorite is thought to be present as an interfacial layer between the silica and the precipitated nickel(II) hydroxide (6).

Coenen (6) prepared an uncalcined 24.6 % w/w nickel on silica catalyst by the deposition-precipitation method. After calcination, T.P.R. revealed that the majority of the nickel was present as a compound which was very difficult to reduce, with T_{max} occurring at ca. 853 K. Comparison of this T.P.R. profile with one obtained under identical conditions for pure nickel antigorite indicated that the majority of the nickel in the unreduced catalyst was in the form of the hydrosilicate compound. Only a very small proportion of the supported nickel was found to be easily reducible.

As described earlier, some investigators have assigned the high temperature peaks in T.P.R. profiles of calcined catalysts prepared by impregnation to the reduction of nickel antigorite. There is, however, no conclusive proof for the presence of bulk nickel antigorite from techniques such as X.R.D., X-ray photoelectron spectroscopy and electron spin resonance (9, 11, 17, 18, 85, 88, 89, 96, 97, 99, 101).

1.5.2 The Influence of a Reducible Support on the Properties of Supported Metal

After reduction, the support can, in certain circumstances, interact with a metal so strongly that the ability of the metal to chemisorb gases such as carbon monoxide and hydrogen at room temperature is impaired or even completely suppressed. A reduced catalyst in which this behaviour is observed is termed to be in a strong metal support interaction (S.M.S.I.) state.

S.M.S.I. behaviour was first observed by Tauster and co-workers for the group VIII noble metals (ruthenium, rhodium, palladium, osmium, iridium and platinum) supported on titania [TiO_2] (105), and also for iridium supported on Ta_2O_5 , Nb_2O_5 and V_2O_3 (106). They discovered that catalysts prepared from these components and reduced in hydrogen at high temperatures (typically 773 K) behaved unconventionally with respect to chemisorption of gases. It was found that the catalysts adsorbed relatively little carbon monoxide or hydrogen at room temperature, whereas catalysts reduced at lower temperatures (ca. 473 K), with comparable average particle sizes, adsorbed much more. When group VIII noble metals were supported on silica or alumina, the chemisorption properties were not affected significantly, even by reduction temperatures up to 973 K (106).

The behaviour of a catalyst in a S.M.S.I. state can be illustrated by the following example. Tauster et al. (105) studied the effect of the reduction conditions on the chemisorption capacity of a 2 % w/w palladium on titania catalyst. After reduction at 448 K, the catalyst exhibited

H/M and CO/M ratios of 0.93 and 0.53, respectively, where M is the total number of palladium atoms in the sample. This indicated that the palladium was highly dispersed on the surface of the support. On reducing the same catalyst at 773 K, the uptakes of both the hydrogen and carbon monoxide were almost negligible (H/M = 0.05 and CO/M = 0.02). This indicated that the average particle diameter was greater than 15 nm according to the hydrogen uptake figure (assuming one adsorbed hydrogen atom per surface palladium atom). In fact, X.R.D. line broadening studies gave a diffraction pattern that was indistinguishable from that obtained from the titania support alone. This indicated that the average particle diameter was less than 5 nm as no peaks due to palladium metal were observed in the diffraction pattern. In addition, T.E.M. did not show the presence of any metal particles greater than ca. 1 nm in diameter. The decrease in chemisorption capacity, therefore, was not due to any loss of metal surface area by particle sintering suffered by the catalyst during high temperature reduction.

Intriguingly, it was discovered in the same study that the capacity of the reduced 2 % palladium on titania catalyst in the S.M.S.I. state for hydrogen chemisorption was almost completely restored by thermal treatment under oxygen at 673 K followed by a low temperature re-reduction under hydrogen at 448 K. On hydrogen adsorption, the H/M ratio for the re-reduced catalyst was found to be 0.89 (cf. 0.93 for the catalyst initially reduced at 448 K). If the catalyst was then treated in hydrogen at 773 K, the hydrogen chemisorption was again almost completely suppressed (H/M = 0.03). Furthermore, if the catalyst in the S.M.S.I. state

was simply treated with a low temperature reduction without any oxidation treatment, it was still found to be in the S.M.S.I. state.

Tauster *et al.* (105) considered that the possibility of metal particle encapsulation by the support was unlikely because the argon BET surface area of the sample was not significantly affected by high temperature reduction. Moreover, the restoration of the normal chemisorption capacity by oxidation followed by low temperature reduction argued against encapsulation. Poisoning of the metal by impurities in the supports was also considered unlikely as Tauster *et al.* found that the degree of suppression of chemisorption did not correlate with either the sulphur or chlorine contents of the two titania supports used in the study. The effect of the initial titania surface area was also ruled out: a 2 % palladium catalyst prepared using thermally treated titania support (argon BET surface area about half that of the untreated support) showed similar chemisorption suppression after reduction at 773 K as a 2 % palladium catalyst prepared from the untreated support.

Since the pioneering work of Tauster *et al.* on supported group VIII noble metals, subsequent studies have shown that similar chemisorption suppression behaviour occurs, albeit to a less pronounced degree, when any other group VIII metal is supported on titania and reduced at high temperature (107). Nickel displays S.M.S.I. behaviour when supported on titania and several studies have shown that on reducing the metal catalyst at high temperature both the suppression of hydrogen (13, 23, 25, 60, 108 - 111) and of carbon monoxide chemisorption occur (23, 25, 60, 108, 111).

The degree of chemisorption suppression is less than that observed for the more noble group VIII metals, e.g. iridium, platinum, rhodium and palladium (107). The extent of hydrogen and carbon monoxide chemisorption suppression also increases with the severity of reduction conditions for all group VIII metals supported on titania (107, 109, 110, 112 - 114). This has been clearly observed for nickel on titania catalysts (107). Oxidation at 623 K of nickel on titania catalysts in the S.M.S.I. state followed by re-reduction in hydrogen at 473 K restores the chemisorption capacities of the catalysts (110).

Further studies on the S.M.S.I. state formed by group VIII metals supported on materials other than titania have also been conducted, for example nickel on Nb_2O_5 (115 - 117), ruthenium on V_2O_3 (118) and rhodium on Nb_2O_5 (119, 120) catalysts. The degree of chemisorption suppression is often more severe in these examples than for the same metal supported on titania. For instance, the reduction of a 10 % w/w nickel on Nb_2O_5 catalyst at 573 K decreased the H/M_s ratio to 0.16, where M_s is the number of surface metal atoms estimated from X.R.D. data (115). Reduction of the same catalyst at 773 K lowered this ratio to 0.02. Analogous results obtained using a 10 % w/w nickel on titania catalyst reduced at 573 and 773 K gave H/M_s ratios of 0.80 and 0.15, respectively (115).

In the case of reduced nickel on titania catalysts, the formation of nickel tetracarbonyl during carbon monoxide chemisorption is also found to be suppressed relative to reduced nickel supported on silica or alumina (25, 108). This phenomenon also occurs for reduced nickel on Nb_2O_5

catalysts, although in this case, at high carbon monoxide pressures, gaseous nickel tetracarbonyl was identified by infrared spectroscopy, even though no adsorbed carbon monoxide was detected (63).

Tauster and Fung (106) quantified the reducibility of all the supports used in their study by reducing the pure supports statically under hydrogen at 1000 K. The reducibility of each support was then expressed as the ratio of water and hydrogen partial pressures at equilibrium. In a further study, Tauster and co-workers (121) showed that the amount of hydrogen chemisorption on reduced supported iridium metal decreased as the reducibility of the support increased. The ascending order of reducibility for the supports used in this study was $\text{Sc}_2\text{O}_3 < \text{Y}_2\text{O}_3 \ll \text{HfO}_2 < \text{ZrO}_2 \ll \text{Ta}_2\text{O}_5 < \text{TiO}_2 < \text{Nb}_2\text{O}_5$. This pattern of greater suppression of chemisorption for catalysts prepared from supports more easily reduced was maintained over reduction temperatures ranging from 473 K to 973 K.

The reduction of the titania support itself during the high temperature reduction of titania-supported metals has been observed in several studies (122 - 128). Baker, Prestridge and Garten (128) showed by electron diffraction that, if platinum supported on a thin film of titania was reduced in hydrogen at temperatures greater than 825 K, then the support was converted to Ti_4O_7 . If pure titania was treated in a similar manner, only the rutile form of titania was detected: anatase to rutile phase transformation for pure titania occurs at ca. 973 K (129). Indeed, the reduction of the titania is occasionally evident visually as

titanium(III) ions impart a light blue colour to the support (126, 127).

T.P.R. studies have also shown that the reduction of the support is initiated at lower temperatures and occurs to a far greater extent for platinum on titania catalysts than for pure titania (122, 123, 125). The reduction of titania to Ti_4O_7 has also been observed upon reduction, at temperatures greater than 1080 K, of nickel supported on a thin film of titania (130, 131). For high surface area supports it is found that only a relatively small fraction of the titania support is reduced (125).

Another feature of a catalyst in a S.M.S.I. state is the formation on reduction of thin raft-like metal particles which are generally hexagonal in shape. Particles of this morphology have been observed by electron microscopy for platinum supported on a thin film of titania (132), platinum on titania catalysts (125), nickel on titania catalysts (13, 23, 131, 133) and iron on titania catalysts (134, 135). This particle morphology is not universal, however, for all reduced catalysts that display strong suppression of chemisorption, e.g. palladium on titania (136), rhodium on titania and iridium on titania catalysts (137).

Four types of models, which may not be mutually exclusive, have been proposed to account for S.M.S.I. behaviour:

a. Morphological Models: As described previously, metal particles can adopt raft-like morphologies when a catalyst is in a S.M.S.I. state. It has been suggested that structural changes in the metal particles result in the

predominance of a particular crystallite face on the surface of the particles. This changes the catalytic and adsorption properties of the high-temperature-reduced catalyst relative to the low-temperature-reduced catalyst (138, 139).

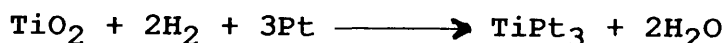
The discovery that some catalysts which exhibit S.M.S.I. behaviour do not have raft-like particles indicates that this model is incorrect. However, for catalysts in the S.M.S.I. state where raft-like particles are present, the particle morphology may indeed affect the catalytic and sorption behaviour.

b. Interfacial Metal-Support Compound Formation: This model was first proposed by Tauster and co-workers (105, 106) in their original work on catalysts in the S.M.S.I. state. It is based on the observation that in substituted hexagonal barium titanates [general formula; $\text{BaM}_{1/3}\text{Ti}_{2/3}\text{O}_{3-x}$, where M is a metal cation and $x \geq 0$; examples include M = cobalt(II), platinum(IV), iridium(IV) and titanium(III)] there is hetero-atomic bonding between the titanium(IV) and M cations. The authors suggested that at the interface between the titania support and reduced platinum particles in platinum on titania catalysts overlap may be possible between the d-orbitals of the titanium(IV) cations and the d-orbitals of the platinum atoms. The authors speculated that in such a bond electron density would be transferred from the platinum atoms to the titanium(IV) cations, thereby drastically modifying the sorption properties of the metal.

This model was subsequently modified by Horsley (140). He took into account that for catalysts in the S.M.S.I. state, the support is observed to be partially reduced

during the high temperature reduction. For titania this could lead to the possibility of bonding via d-orbital overlap between a titanium(III) cation and a supported platinum atom. Also, by considering a partially reduced support it meant that the platinum atom could occupy an anion vacancy and this permitted a close approach of the atom to the titanium(III) cation. As a basis for his model of the Ti-Pt bond, Horsley chose the $(\text{PtTiO}_5)^{7-}$ cluster. For this cluster, he calculated that the titanium(III) cation would donate electron density to the platinum atom. This would increase the metal d-orbital occupancy. According to Schwab (141), this would suppress hydrogen and carbon monoxide chemisorption as both adsorbate molecules donate electron density to the metal upon adsorption (and in the case of hydrogen, subsequent dissociation).

c. Alloy Formation: The possibility of alloy formation occurring in catalysts during high temperature reduction was also considered as an alternative hypothesis to interfacial metal-support compound formation (105, 106). Tauster *et al.* (105) considered the thermodynamic feasibility of the following reaction occurring in platinum on titania catalysts reduced at 773 K;



According to the authors, the formation of TiPt_3 will be thermodynamically favoured at 773 K, provided that the $P(\text{H}_2\text{O})/P(\text{H}_2)$ ratio is less than 2.5×10^{-3} , where $P(\text{H}_2\text{O})$ and $P(\text{H}_2)$ are the partial pressures of water and hydrogen, respectively.

Experimental observation showed that the maximum amount of water in the outlet gas stream during reduction of

platinum on titania catalysts at 773 K under a flow of hydrogen gave a $P(H_2O)/P(H_2)$ ratio of ca. 1.2×10^{-4} (105). Under these conditions, therefore, the formation of a titanium-platinum alloy was thermodynamically possible.

Similar explanations have been advanced for other types of catalyst in the S.M.S.I. state, e.g. by Tatarchuk and Dumesic for iron on titania catalysts reduced at 875 K (142).

d. Decoration Model: This model has been considered by a number of researchers (131, 143 - 146). In this model it is proposed that titania and other easily reduced support materials are partially reduced by spillover hydrogen to give suboxide species in the vicinity of supported metal particles. In the case of titania, these suboxides can be represented by the general formula TiO_x , with $X < 2$. These suboxide species are believed to migrate over the surface of the metal and so decorate the surface with partially reduced support residues. These residues are believed to modify the sorption and catalytic properties of the metal.

The advantage of this model over the interfacial metal-support compound model is that it can account for the experimental data which shows that a reduced catalyst with large metal particles (> 10 nm) can still be in a S.M.S.I. state (109, 112, 146). The interfacial compound hypothesis would be expected to have only localised effects along the support-metal interface and therefore only well dispersed metals would be affected. The two models, however, are not incompatible as the spreading of the suboxide species over the particle surface may be triggered by the favourable

energetics of compound formation between this species and the surface metal atoms.

Baker, Chludzinski and Dumesic (147) have suggested on the basis of electron microscopy evidence that, at least in the case of a nickel/titania system, thermal oxidation of a deposited overlayer of TiO_x on the surface of the nickel particles reforms crystallites of titania. The formation of these crystallites re-exposes the majority of the nickel surface to the gas phase. Therefore, the decoration process may be at least partially reversible.

1.5.3 The Influence of a Non-reducible Support on the Properties of Supported Metal

Metal-support interactions involving group VIII metals supported on oxides that are not easily reduced, so called "non-reducible" supports, have been reported. To bring about these interactions requires more severe conditions than those necessary for systems involving more reducible supports and, generally, the interactions have less pronounced effects on the properties of the reduced catalyst. For example, suppression of hydrogen chemisorption for platinum on alumina catalysts reduced at 773 K or above has been observed (148 - 153). As with high-temperature-reduced noble group VIII metals supported on titania, it was found that thermal treatment of these catalysts in oxygen followed by low temperature re-reduction restored the hydrogen chemisorption capacities (148 - 153). Again the poisoning of the metal by impurities in the alumina supports was ruled out as a cause of the suppression of chemisorption (153).

In comparison to catalysts like platinum on titania, where hydrogen chemisorption is almost completely suppressed (105), platinum on alumina catalysts still exhibit considerable hydrogen chemisorption after high temperature reduction. For instance, reduction of a 5.0 % w/w platinum on alumina catalyst at 573 K gave a H/M ratio of 0.95 (153). If the catalyst was reduced at 773 K, this ratio decreased to 0.31 while the metal crystallite size remained constant. Oxidation and re-reduction was found to restore this ratio to the original value of 0.95. Similar results were obtained by Dautzenburg and Wolters using a 0.8 % w/w platinum on alumina catalyst (149).

The explanation for this behaviour most commonly advanced is that during reduction spillover of atomic hydrogen from the metal onto the support occurs. This spillover hydrogen reduces the support (149 - 151, 153, 154) with the possible result of platinum-aluminium alloy formation. This explanation is supported by evidence that alumina reduction does occur during the reduction of platinum on alumina catalysts (151, 153). Oxidation of these catalysts is thought to form platinum(II) oxide and alumina phases from the alloy phase. Re-reduction at low temperatures therefore generates platinum crystallites supported on alumina with no re-formation of the alloy.

The suppression of hydrogen chemisorption has also been observed for silica-supported catalysts after high temperature reduction. This type of behaviour has been reported to occur with platinum on silica (155) and nickel on silica catalysts (156) after reduction at 1120 K or above. Electron microscopy data (155) and magnetic

susceptibility measurements (156) ruled out the possibility that extensive particle sintering led to the suppression of hydrogen chemisorption. Following thermal oxidation and low temperature re-reduction treatments, the high-temperature-reduced catalysts had almost identical chemisorption capacities to those reduced using the low temperature reduction procedure alone.

Two possible explanations have been proposed for this behaviour. Powell and Whittington (157) found that on annealing a platinum film deposited on silica, distinct platinum particles were formed. As the temperature was increased, these particles grew in size due to sintering. When these model catalysts were annealed at temperatures of 1200 K and 1375 K, scanning electron microscopy revealed that the platinum particles became partially immersed in the silica support. Powell and Whittington suggested that this process may occur to a limited extent at lower temperatures for reduced platinum on silica catalysts. However, in view of the reversible nature of the metal-support interaction for the silica-supported catalysts discussed above this explanation seems unlikely.

A second and more plausible explanation has been advanced by Praliaud and Martin (156). These workers found that the magnetic susceptibility data obtained for a 20 % w/w nickel on silica catalyst after reduction at 1180 K indicated that the formation of a nickel-silicon alloy had occurred. This explanation is analogous to that described previously for platinum on alumina catalysts. Again, the alloy formation was thought to be reversible on oxidation and low temperature re-reduction as with the

platinum/alumina system. The suggestion of nickel-silicon alloy formation has found support from other researchers (95, 158). In addition, further indication of nickel-silicon alloy formation for nickel on silica catalysts reduced at high temperatures is provided by the observation of Dubois and Nuzzo (159). They observed that hydrogen dissociation did not occur and molecular carbon monoxide was only weakly chemisorbed on the (111) face of nickel silicide (NiSi_2). The presence, therefore, of a nickel-silicon alloy may inhibit hydrogen and carbon monoxide chemisorption.

1.6 The Preparation, Uses and Structures of Silicas

Silicas find widespread applications in industry, with the main types of silica, their methods of preparation and some of their uses noted below (160):

- i. Naturally occurring silicas, e.g. diatomaceous earth, kieselguhr (both of which are amorphous silicas) and α -quartz (crystalline silica). Diatomaceous earth and kieselguhr are mined and are principally used in filtration plants. The α -quartz used by industry (particularly the electronics industry) is mainly synthetically produced due to purity considerations;
- ii. Silica gels. These are amorphous forms of silica with very porous structures. They are produced by acidification of aqueous solutions of soluble silicates, usually sodium silicate. This acidification leads to the formation of supersaturated solutions of silicic acid ($\text{Si}(\text{OH})_4$) which then undergo condensation polymerisation to form gelatinous precipitates of silica. These precipitates are then washed

free of electrolytes and dehydrated by roasting or spray drying. The properties of these silicas depend critically on the conditions of preparation, with typical samples having BET surface areas in the range $200 - 500 \text{ m}^2\text{g}^{-1}$ and bulk densities in the range $0.6 - 0.8 \text{ g cm}^{-3}$. Silica gels find application as desiccants, catalyst supports, insulators, chromatographic supports and in the food industry as well as many other applications;

iii. Fumed (pyrogenic) silicas. These silicas are produced by the high temperature hydrolysis of silicon tetrachloride in an oxygen-hydrogen flame. Fumed silicas have very small particle sizes, with typical BET surface areas in the region $150 - 400 \text{ m}^2\text{g}^{-1}$, and very low bulk densities, typically $0.03 - 0.06 \text{ g cm}^{-3}$. Such silicas are mainly used as thixotropic thickening agents in epoxy and polyester resins and plastics, and as reinforcing fillers in silicon rubbers;

iv. Vitreous (glassy) silicas. These silicas are glasses produced by fusing quartz at high temperatures (ca. 2000 K). They find application in specialist glassware which needs to be chemically resistant and have high thermal shock resistance.

Silica is an extremely complex material and its study has led to the publication of many books and articles (160, 161). A species can be defined as silica if it is found to approximate to SiO_2 in analysis. Silica is essentially constructed from SiO_4 tetrahedra with corner oxygens shared between two silicon atoms. The structure of non-crystalline silica at distances beyond that defined by the local coordination tetrahedra has not yet been adequately described and it has been concluded that the structure is

best described as a chemically ordered continuous random network (161).

Different silicas may vary in crystallinity, solubility, surface silanol (Si-OH) concentration, surface area, porosity, pore volume, pore size, particle size, purity and hydrophobicity dependent on their method of preparation and variables thereof (160).

Further information on the preparation, and the physical and chemical properties of silicas, with particular reference to the silicas used in this study, is given in Appendices A and B.

CHAPTER TWO

CHAPTER TWO

THE OBJECT OF THE PRESENT WORK

2.1 Organisation of the Project

The work reported in this dissertation forms part of a collaborative study, funded by the ICI Strategic Research Fund, involving three university research groups:- Dr. L. Gladden (Department of Chemical Engineering, University of Cambridge), Prof. J. R. Jones (Department of Chemistry, University of Surrey) and Prof. G. Webb (Department of Chemistry, University of Glasgow).

These three research groups, in conjunction with Dr. S. D. Jackson (Catalysis Centre, ICI Research and Technology, Billingham) and Dr. R. W. Griffiths (General Chemicals Group, ICI Research and Technology, Runcorn), have been involved in an extensive study of the preparation, characterisation and properties of silicas and silica-supported metal catalysts, with a view to gaining a better understanding of the effects of the support structure on the nature of the supported metal and catalytic activity.

2.2 Aims and Objectives

Silicas and silica-supported metal catalysts have been largely neglected in terms of their structural characterisation and the effects of structure on catalytic behaviour. This is a direct consequence of the incredible complexity of silicas and of the inability to prepare well characterised silicas reproducibly.

Recent technological developments have led to the preparation of a new generation of silicas with well defined

and well characterised properties. These advances offer an opportunity to develop a better understanding of the fundamental structural properties of silica-supported metal catalysts and of the effects of structure on catalytic behaviour.

By varying, in a controlled manner, structural variables of silicas (e.g. surface area, pore size, pore volume, pore size distribution and distribution of strained siloxane rings) it was anticipated to be able to identify and clarify the role of the support in determining the nature and the catalytic activity of supported materials. This should ultimately provide a means of predicting catalyst behaviour on the basis of structural data. An ability to make such predictions will allow desirable activities and selectivities to be engineered into a catalyst at the preparation stage. To meet these objectives, the three university research groups have been involved in an integrated research programme, each concentrating in the areas of their expertise.

The work detailed in this dissertation covers aspects of several catalyst characterisation techniques including temperature programmed reduction (T.P.R.), carbon monoxide chemisorption and transmission electron microscopy. It was anticipated that, by extensive characterisation of a range of nickel on silica catalysts in their unreduced and reduced states, correlations would be observed between the characterisation results and the physical and chemical properties of the supports from which the catalysts were prepared by impregnation. Hence a detailed picture was expected to emerge of the influence of the support on the

nature of the supported nickel metal precursors in the unreduced catalysts and, consequently, the nickel particles in the reduced catalysts.

By use of a simple test reaction, ethene hydrogenation, and by the T.P.R. characteristics of the unreduced catalysts, it was hoped to be able to demonstrate that the silica-supported nickel catalysts used in this study were not anomalous in their behaviour relative to analogous studies of similar catalysts reported in the literature. This being the case, conclusions reached in this study will be quite general for nickel on silica catalysts prepared by impregnation.

Thus, through detailed consideration of the data presented in this thesis, together with data obtained from the other research centres and from the literature, a fundamental understanding was expected to be gained of how the support affects the nature and catalytic activity of silica-supported nickel.

CHAPTER THREE

CHAPTER THREEAPPARATUS AND EXPERIMENTAL PROCEDURE3.1 Preparation of the Catalysts

Four silicas with different physical and chemical properties were chosen to be the support materials from which the catalysts used in this study were subsequently prepared. These supports were ICI silica (produced by ICI, Winnington), CS1030E silica (PQ Corporation), CS2040 silica (PQ Corporation) and Cab-O-Sil silica (M-5 grade, Cabot Corporation); data on these support materials can be found in Appendices A and B. Catalysts were prepared containing either a nominal 1 % w/w or 10 % w/w nickel loading using the ICI, CS1030E and Cab-O-Sil silica supports. Two catalysts, both containing ca. 1 % w/w nickel, were prepared using the CS2040 silica. As described later in this section, these latter catalysts were prepared by aqueous and non-aqueous preparative methods, respectively.

The 1 % w/w and 10 % w/w nickel catalysts based on the ICI, Cab-O-Sil and CS1030E supports were prepared by aqueous impregnation of the silicas with an acidic (pH ca. 1) standardised solution of nickel(II) nitrate supplied by ICI, Clitheroe. This solution was analysed by atomic absorption spectrophotometry and found to contain 23.6 ± 0.6 % w/v nickel. The impregnation procedure was performed by adding the appropriate volume of the stock solution, usually 25.00 or 250.00 ml to give 1 % or 10 % nickel loadings, respectively, to the silicas (usually 500 grams). To ensure thorough mixing, de-ionised water was initially added to the silicas to form aqueous slurries prior to the

aforementioned additions of the stock solution. The volume of de-ionised water added varied from 700 ml for the ICI support to 3.5 l for the Cab-O-Sil support.

As previously stated, two 1 % w/w nickel catalysts were prepared by different methods using the CS2040 silica. This silica is known to undergo pore diameter contraction on drying after exposure to aqueous media (see Appendices A and B, Section 4.1.1 and ref. 161). Two batches of this support were impregnated using an aqueous and a non-aqueous method, respectively. In the aqueous method, the CS2040 silica (200 grams) was impregnated by a solution consisting of 10 grams of "AnalaR" nickel(II) nitrate (BDH Ltd.) in 800 ml of de-ionised water to give a metal loading of ca. 1 % w/w nickel. In the non-aqueous impregnation procedure, the method of preparation was identical to that described above, except that 850 ml of acetone (M & B Pronalys^{*}ar) was used in place of de-ionised water as the solvent for the 10 grams nickel(II) nitrate. The catalyst impregnated by the aqueous method is designated by the suffix aq. and that of the non-aqueous route by non-aq.

With the exception of the two impregnated Cab-O-Sil silica mixtures, all other impregnated silica mixtures were separately and thoroughly mixed using a rotary evaporator. The excess solvent was then removed from these mixtures by rotary evaporation *in vacuo* at 353 K. The drying process was then completed by drying overnight (ca. 17 hours) in an air oven at 353 K.

The volume of the two nickel(II) nitrate and Cab-O-Sil silica mixtures necessitated the addition of glass beads to each mixture to facilitate proper mixing. After each

mixture had been thoroughly mixed, using a rotary mixer, a stream of hot air was passed over it for 16 hours, whilst the mixture was continually rotated. The drying process for the two mixtures was completed by drying in an air oven at 353 K overnight.

Each uncalcined catalyst so obtained was then divided into two batches; one batch was to be used in experiments as the supported nickel salt and required no further treatment, while the other was calcined for use in experiments requiring the calcined form of the catalyst. The calcination procedure was performed by heating the batches of uncalcined catalysts separately in a tube furnace to 723 K at a heating rate of 50 K h^{-1} under a flow of dry air (flow-rate = $60 \text{ cm}^3 \text{ min}^{-1}$). The final temperature was maintained for two hours, after which time the calcined catalysts were allowed to cool to ambient temperature. To summarise therefore, the following uncalcined and calcined catalysts with nominal nickel loadings as noted were prepared:

- i. 1 % and 10 % w/w nickel supported on ICI silica
- ii. 1 % and 10 % w/w nickel supported on CS1030E silica
- iii. 1 % and 10 % w/w nickel supported on Cab-O-Sil silica
- iv. 1 % w/w nickel supported on CS2040 silica (non-aq.)
- v. 1 % w/w nickel supported on CS2040 silica (aq.)

The unreduced catalysts were then distributed to Cambridge, Surrey and Glasgow Universities.

3.2 Unreduced Catalyst Characterisation

3.2.1 Temperature Programmed Reduction

Temperature programmed reduction (T.P.R.) was the major method employed at Glasgow for the characterisation of the prepared uncalcined and calcined catalysts. As stated in Section 1.5.1, the only requirement for the successful application of T.P.R. is the presence of a species in the unreduced catalyst which is reducible by hydrogen. T.P.R. is, therefore, ideally suited for use in a characterisation study of silica-supported nickel nitrate or silica-supported nickel oxide, where both the supported nickel metal precursors are reducible by hydrogen.

3.2.1.1 Apparatus

A diagram of the T.P.R. apparatus is illustrated in Figure 3.1. Similar apparatus, as well as the technique of T.P.R., have been described previously (100, 162). The apparatus was constructed from 1/8 inch diameter *Copper* tubing with connections made using Swagelok unions. Whitey three-way valves and Nupro needle valves were employed in the apparatus construction to control gas flows. The reactor, shown in Figure 3.2, was of an U-tube type design and constructed from silica. A sample of an unreduced catalyst was positioned in this reactor on a quartz sinter. The temperature of the catalyst bed was monitored by a K-type thermocouple located in a thermocouple well positioned at the same level as the sinter. To enable manipulation of the reactor in and out of the tube furnace, the reactor inlet and outlet were attached via Swagelok unions to flexible 1/8 inch diameter PTFE tubing (Phase Separations

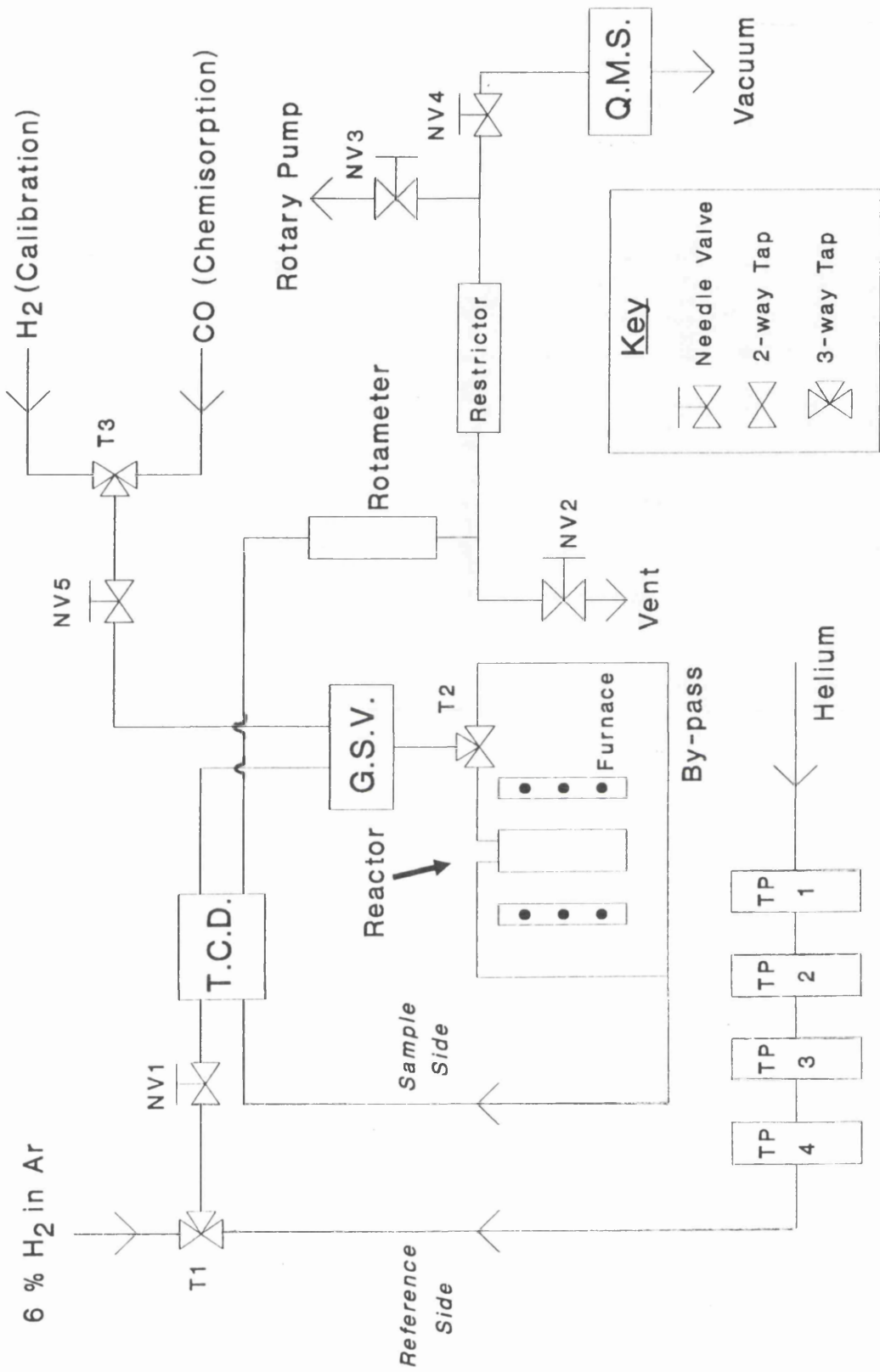
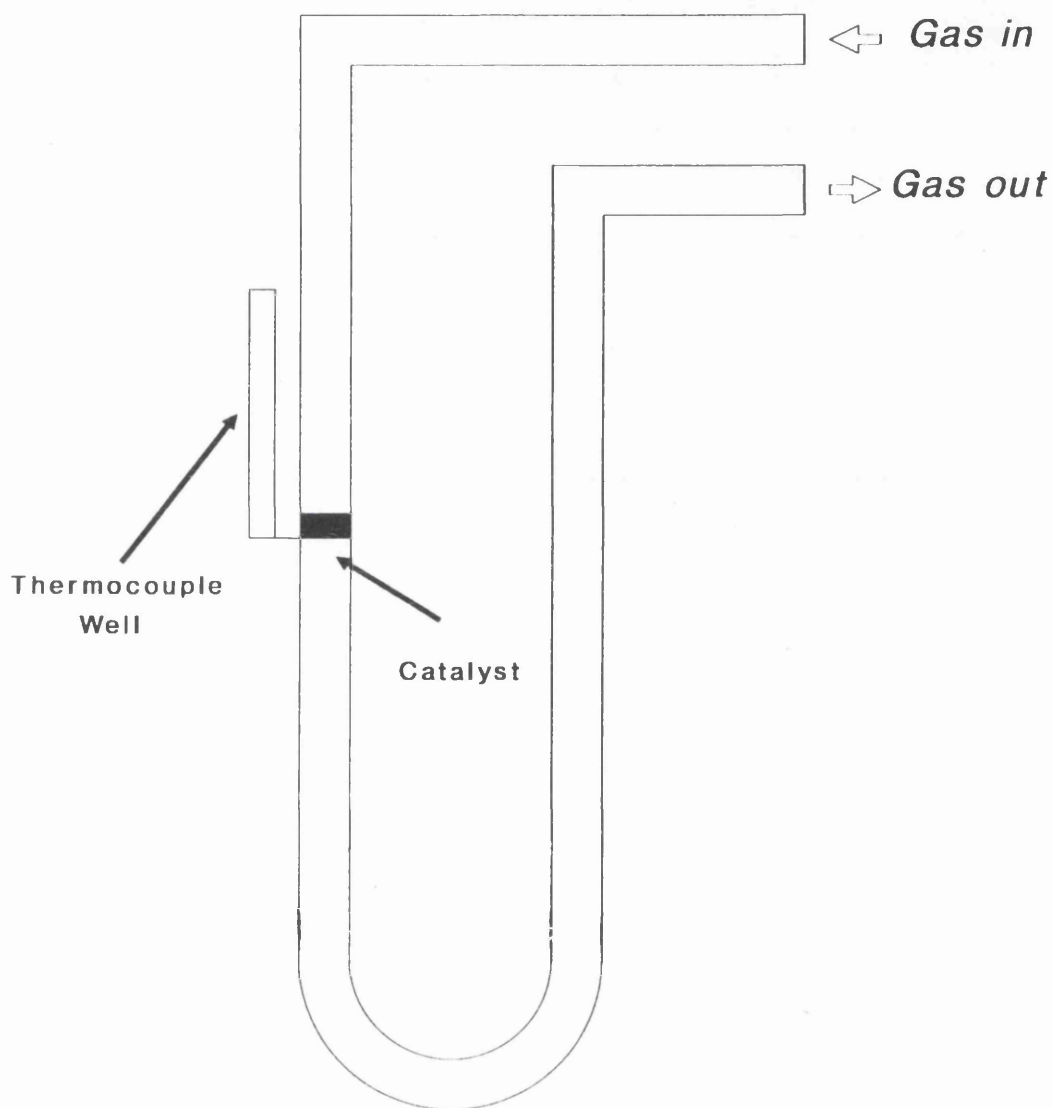


Fig. 3.1 Diagram of the T.P.R. Apparatus

Fig. 3.2 Diagram of the T.P.R. Reactor



Ltd.). The PTFE tubing was in turn connected to the apparatus brass tubing via Swagelok unions. The gas flow through the reactor was measured by a GEC-Elliott 1100 rotameter.

3.2.1.2 Experimental Procedure

An accurately weighed sample of unreduced catalyst was placed in the reactor and the bed of unreduced catalyst swept at room temperature for ca. 30 minutes with helium gas (B.O.C. Ltd.) to expel air from the system. The flow-rate of helium during this purging procedure was maintained at $25 \text{ cm}^3 \text{ min}^{-1}$ by needle valve NV1. The helium had previously been purified by passage through four traps containing, respectively, copper oxide (TP1), copper turnings (TP2), manganese(II) oxide (TP3) and Linde 5A molecular sieve (TP4).

After purging the system of air, the gas flow through the T.P.R. apparatus was changed to 6 % v/v hydrogen in argon (B.O.C. Ltd.) via tap T1. This gas mixture was allowed to flow through the reactor (at room temperature) for ca. 30 minutes at a flow-rate of $25 \text{ cm}^3 \text{ min}^{-1}$, the flow-rate again controlled by needle valve NV1. After this time, the reactor was placed in a Stanton Redcroft tube furnace. A Stanton Redcroft temperature programmer (Cambridge Process Controls 702) was employed to control the temperature of the furnace, while a thermocouple, located on the inside wall of the furnace, provided the temperature feedback to the programmer. The flow of 6 % v/v hydrogen in argon was maintained through the reactor whilst it was heated at a steady rate, $\beta \text{ K min}^{-1}$, to a pre-set

temperature. The temperature of the catalyst sample was recorded using the independent K-type thermocouple located in the thermocouple well attached to the reactor as previously described. The output of this thermocouple was recorded on one channel of a dual channel Servoscribe 2s potentiometric chart recorder. The uptake of hydrogen by the sample was monitored using a thermal conductivity detector (T.C.D.), the output of which was recorded on the other channel of the chart recorder. The resulting plot of hydrogen depletion in the outlet gas stream versus temperature is known as a T.P.R. profile.

The conditions employed for a typical T.P.R. experiment, using either an uncalcined or a calcined catalyst, involved heating the sample in a flow of 6 % v/v hydrogen in argon gas from ambient temperature to 1023 K at $\beta = 5 \text{ K min.}^{-1}$. Normally 0.2 g of unreduced catalyst was loaded into the reactor, but in the case of less dense materials (i.e. the catalysts prepared from Cab-O-Sil and CS2040 silicas) a 0.1 g sample was used thus ensuring that the bed of unreduced catalyst was always approximately the same depth (ca. 0.25 cm) in all experiments.

Each of the unreduced catalysts listed in Section 3.1 was characterised by T.P.R. Furthermore, for all T.P.R. experiments involving the calcined catalysts, the outlet gas stream was monitored using a Spectromass Dataquad mass spectrometer operating in the "Peak Select" mode. The quadrupole mass spectrometer (Q.M.S.) was set up to monitor the peaks at $m/e = 18$ (water) and at $m/e = 2$ (hydrogen).

Additionally, control experiments were performed using:

- i. Pure ICI silica;

- ii. The two empty silica reactors used in the T.P.R. experiments;
- iii. Unsupported nickel oxide.

The unsupported nickel oxide used in control experiment (iii) was prepared by calcining 0.0950 g of "AnalaR" nickel(II) nitrate hexahydrate (BDH Ltd.) using the same procedure employed to calcine the uncalcined catalysts (Section 3.1). In this way, useful comparisons can be made between the T.P.R. profile of unsupported nickel oxide and those profiles obtained for the calcined catalysts. Control experiments (i) and (ii) were performed to ensure that the observed uptakes of hydrogen during T.P.R. experiments could only be attributed to the presence of nickel species in the unreduced catalysts.

3.2.1.3 Quantitative Determination of Hydrogen Uptake

The uptakes of hydrogen by the calcined catalysts during T.P.R. experiments were quantified as follows:

Before heating each calcined catalyst, at least eight separate aliquots of pure hydrogen, each 50 μ l in size (pressure = 760 Torr), were pulsed into the 6 % v/v hydrogen in argon gas flow. The hydrogen was introduced to the system via tap T3, and the aliquots of hydrogen pulsed into the 6 % v/v hydrogen in argon flow via an eight port gas sampling valve (G.S.V., supplied by Valco Instruments Co. Inc.) fitted with two 50 μ l sampling loops. The aliquots of hydrogen so introduced were directed to flow through the reactor by-pass via tap T2. Comparison of the T.P.R. profile areas (corrected for chart recorder sensitivity) with the average area detected by the T.C.D. for the 50 μ l

hydrogen calibration injections enabled the hydrogen uptake for each calcined catalyst to be calculated.

3.3 Reduced Catalyst Characterisation

3.3.1 Catalyst Reduction and Carbon Monoxide Adsorption Experiments

Carbon monoxide chemisorption is very commonly employed as a technique to determine the metal dispersion, metal surface area and average particle size of the metal in a reduced supported metal catalyst. The technique depends on the fact that carbon monoxide chemisorption is restricted to the metal surfaces of silica-supported metal catalysts (see Section 1.4.1 for further details).

Detailed below are the two methods of carbon monoxide chemisorption employed in this study. In the first method described, carbon monoxide chemisorption was performed on the catalysts in hydrogen carrier gas at a temperature of 273 K. Prior to these carbon monoxide chemisorption experiments, the calcined catalysts were reduced systematically at a temperature of 673 K in a flow of pure hydrogen.

In the second method, carbon monoxide chemisorption was performed on the catalysts in helium carrier gas at a temperature of 273 K. As this was, chronologically, the earlier method to be employed in this study, the calcined catalysts were reduced using different reduction conditions (on an empirical basis) to enable an estimation of the optimum reduction conditions to be made.

3.3.1(a) Chemisorption of Carbon Monoxide in Hydrogen

Carrier Gas

The apparatus used in this study, a diagram of which is shown in Figure 3.3, was a glass gas flow/vacuum system and was similar in design to that described by other workers (163). The carrier gas flow was split such that one part of the flow (designated the *reference side* in Figure 3.3) was directed through a mass flow controller into a short reference column located in a Shimadzu GC-14A gas chromatograph (G.C.) and then through the reference side of the installed T.C.D.

The other part of the flow (designated the *sample side*) passed through a pressure regulator and then into the flow/vacuum system. The gas flowed through this system via a sample loop and then through the reactor. The gas sampling system and the reactor were both equipped with bypass facilities. The carrier gas was then directed to flow through an empty one metre stainless steel column located in the G.C. and into the sample side the T.C.D. The T.C.D. operated at a bridge current of 120 mA and a temperature of 373 K. The approximate detection limit for carbon monoxide in hydrogen carrier gas was determined to be 3×10^{17} molecules (see Section 4.2.1(a) for details). The reference and sample gas flow-rates through the T.C.D. were balanced, each having been measured by a bubble flowmeter. The eluant gases from the G.C. were then analysed by an on-line quadrupole mass spectrometer (a Spectromass Selector).

The sample loop, shown in Figure 3.4, consisted of a series of three three-way sprung-greased taps. The taps were arranged so that a standard volume ($4.44 \pm 0.04 \text{ cm}^3$)

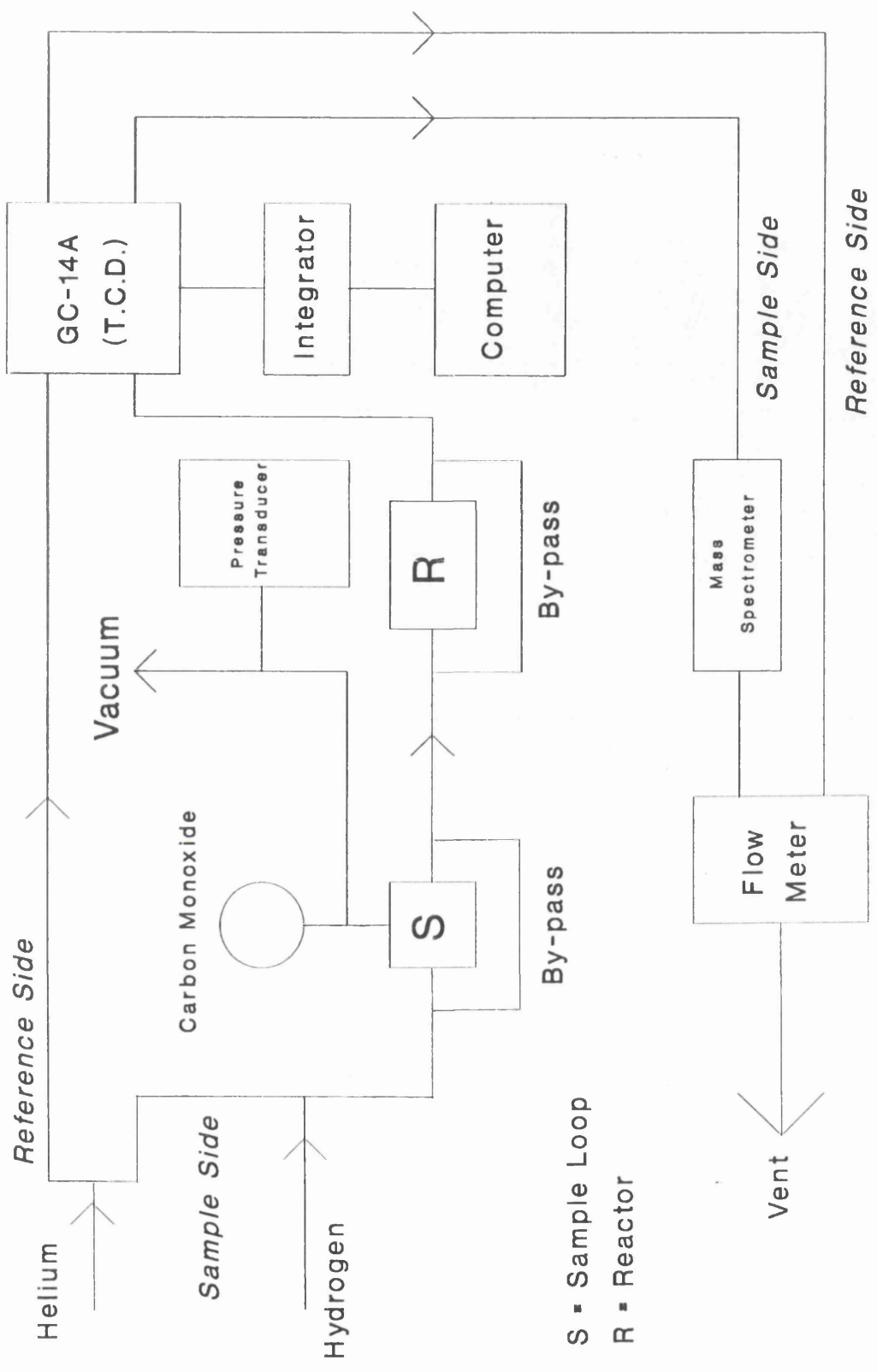


Fig. 3.3 Schematic Block Diagram of the Gas Adsorption Apparatus

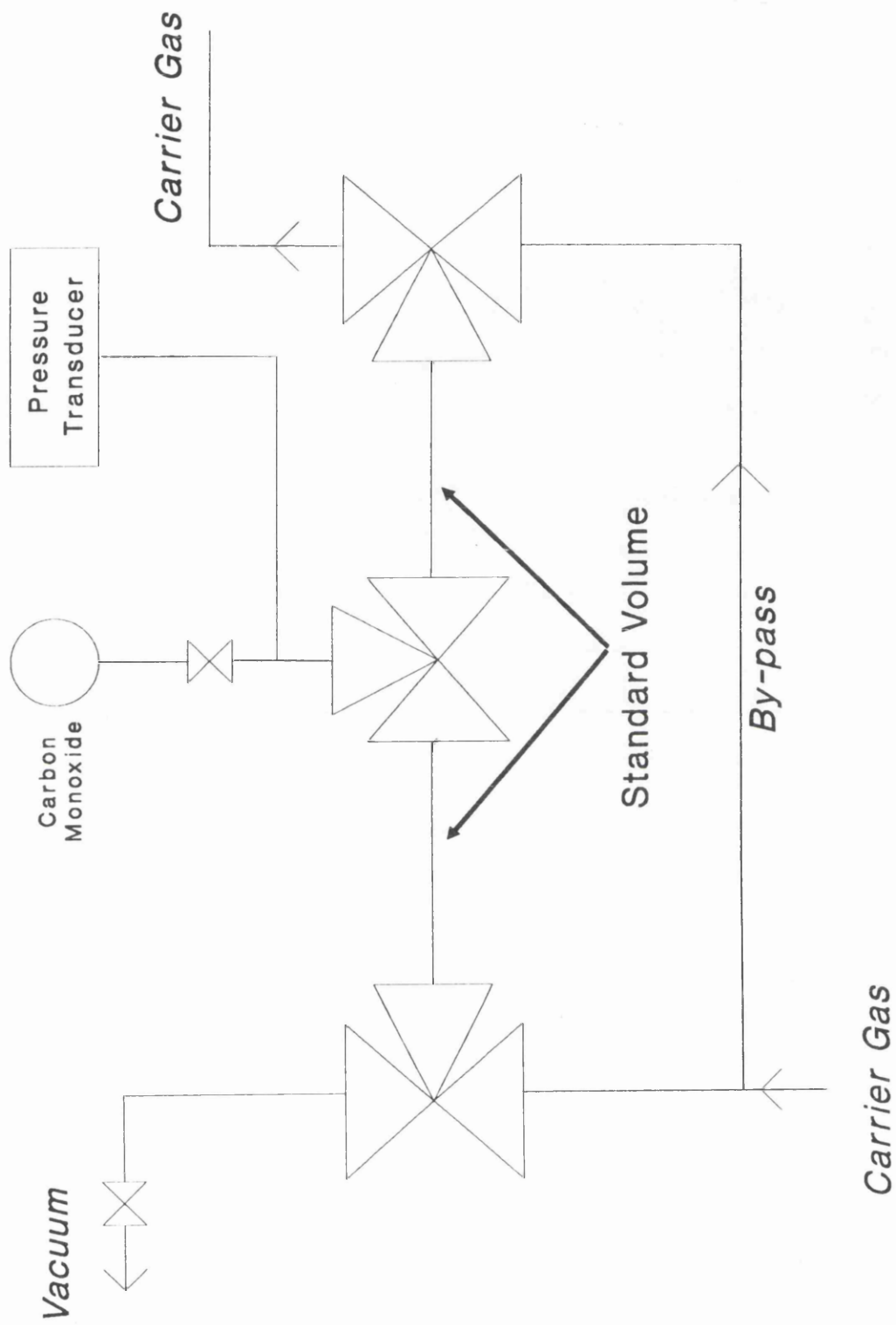


Fig. 3.4 Diagram of the Gas Sample Loop

could be isolated from the flow system and evacuated. During evacuation of this volume, the carrier gas flow was made to by-pass the sample loop. A known pressure of carbon monoxide, measured by an Edwards pressure transducer (model number EMV 251), was introduced via the vacuum system to the evacuated standard volume. The standard volume was then isolated from the vacuum system and the carrier gas flow re-directed through this volume thereby sweeping a known amount of carbon monoxide toward the catalyst bed. Using this technique, therefore, a known quantity of carbon monoxide was pulsed through the catalyst bed. Gases eluting from the catalyst bed were analysed by the G.C. and periodically by the mass spectrometer.

The signal produced by the T.C.D. on detection of a gas pulse was electronically integrated by a Spectra-Physics Chromjet integrator and the data relayed to a personal computer operating LABNET software. During the initial pulses of carbon monoxide over the reduced catalysts in the chemisorption experiments described below, the reactor eluants were also analysed by the mass spectrometer as well as the T.C.D. This was to ensure that only unadsorbed carbon monoxide was present and that no chemical reactions (e.g. methanation or oxidation) had occurred during passage of the carbon monoxide through the catalysts beds. This being the case, the peak areas detected by the T.C.D. arose solely from unadsorbed carbon monoxide in the hydrogen carrier gas. The mass spectrometer repeatedly scanned the mass range $m/e = 0$ to 50 using a scan time of 30 seconds. The resulting m/e peaks were plotted on a chart recorder (a BBC, model number SE430).

Before the commencement of the carbon monoxide adsorption experiments, an experiment was performed to determine the T.C.D. response to varying amounts of carbon monoxide. This was accomplished in the following manner:

Aliquots consisting of either 0.29×10^{19} , 0.59×10^{19} , 1.18×10^{19} or 2.36×10^{19} molecules of carbon monoxide (B.O.C. Ltd.) were introduced separately into the sample loop. Each aliquot of gas was injected into the hydrogen carrier gas flow which was directed through the reactor by-pass into the G.C. The area of the peak detected by the T.C.D. was then determined. Identical quantities of carbon monoxide were repeatedly injected into the carrier gas flow until three concordant results ($\pm 2.5\%$) were obtained for the detected peak areas. The mean of the three detected peak areas for each quantity of gas was then calculated and the results plotted on a graph of the detector response, i.e. peak area detected, versus the number of carbon monoxide molecules [Section 4.2.1(a)].

Chemisorption experiments were then performed on two separate samples of each reduced calcined catalyst. In each experiment, an accurately weighed sample (ca. 0.2 g) of a calcined catalyst was reduced at 673 K using the conditions described below. To expel air from the apparatus, the reactor was initially flushed for 20 minutes (at room temperature) with pure hydrogen (B.O.C. Ltd.) at a flow-rate of $25 \text{ cm}^3 \text{ min}^{-1}$ (as measured by the bubble flowmeter). The hydrogen used in this purge had previously been deoxygenated by passage through a bed of activated palladium bronze (reduced 1 % w/w palladium (ex-palladium(II) chloride) on tungsten(VI) oxide) and then

through a bed of Linde 5A molecular sieve to remove traces of water. After purging, the bed of unreduced catalyst was heated under this flow of hydrogen at $\beta = 5 \text{ K min.}^{-1}$ to 673 K and held at this temperature for three hours. These conditions were adopted as the standard conditions for reduction of the calcined catalysts using a flow of hydrogen.

After the three hour reduction period, the reduced catalysts were cooled to ambient temperature and the flow of hydrogen increased to $40 \text{ cm}^3 \text{ min.}^{-1}$. Each catalyst sample was then further cooled to $273.0 \pm 0.2 \text{ K}$ in an ice/sodium chloride mixture, whilst the flow of hydrogen carrier gas was maintained. After cooling, the sample was by-passed and three equivalent aliquots of carbon monoxide (B.O.C. Ltd.) introduced into the hydrogen flow to ensure the gas detection systems (the T.C.D. and mass spectrometer) were functioning correctly and that consistent peak areas were detected. The hydrogen carrier gas was then re-directed to flow through the sample and aliquots of carbon monoxide gas, normally identical in size to those pulsed through the reactor by-pass, were directed through the catalyst bed. Pulsing was continued until at least three concordant peak areas ($\pm 2.5 \%$) were obtained by which time surface saturation was deemed to have occurred. This variation in the peak areas for the eluted pulses was comparable to that observed for the peak areas detected when the three equivalent aliquots of carbon monoxide were pulsed through the reactor by-pass immediately before each adsorption experiment.

The size of the carbon monoxide aliquots pulsed through each catalyst bed was varied according to the particular catalyst, ranging from 5.9×10^{17} to 1.18×10^{19} molecules, but throughout each experiment the aliquots were normally constant in size.

3.3.1(b) Chemisorption of Carbon Monoxide in Helium

Carrier Gas

Reduction and carbon monoxide chemisorption experiments were performed using the T.P.R. apparatus (Figure 3.1). In this series of experiments, selected calcined catalysts were reduced by heating samples at a constant rate to a specified final temperature under a flow of 6 % v/v hydrogen in argon (flow-rate = $25 \text{ cm}^3 \text{ min.}^{-1}$). Each sample was then left to reduce at the final temperature under a flow of either the 6 % v/v hydrogen in argon or, in some cases, pure hydrogen for a specified time; the catalysts and reduction conditions used are noted below in Table 3.1. At the end of the reduction period the reactor was swept out with helium (flow-rate = $25 \text{ cm}^3 \text{ min.}^{-1}$) at the final reduction temperature for ca. 30 minutes. The furnace was then removed and the reactor cooled to $273.0 \pm 0.2 \text{ K}$, whilst the flow of helium carrier gas was maintained. Temperature equilibration was achieved by allowing the reactor to stand at 273.0 K for a further 20 minutes. Several $50 \mu\text{l}$ carbon monoxide pulses (at a pressure of 760 Torr) were then passed through the catalyst bed by means of the G.S.V.

The uptake of carbon monoxide by the reduced catalysts was quantified in the following way. Immediately before the carbon monoxide pulses were directed through the

Experiment Number	Catalyst	Reduction Temp. (K)	Reduction Conditions
1	10 % Ni/ICI silica	793	16 h. reduction at 793 K.
2	10 % Ni/ICI silica	723	Once at 723 K, catalyst reduced in pure H ₂ for 2 h.
3	10 % Ni/CS1030E silica	723	"
4	1 % Ni/ICI silica	723	"
5	1 % Ni/ICI silica	723	"
6	1 % Ni/CS2040 silica (non-aq.)	1073	Once at 1073 K, catalyst swept with He immediately.

All reductions were performed on samples of the calcined catalysts. The catalysts were heated at $\beta = 5 \text{ K min.}^{-1}$ to the final reduction temperature in a flow of 6 % v/v hydrogen in argon ($25 \text{ cm}^3 \text{ min.}^{-1}$).

Table 3.1

Reduction Conditions Used in CO Chemisorption Experiments
in Helium Carrier Gas

catalyst bed, several 50 μ l carbon monoxide pulses were introduced into the helium carrier gas which was directed to flow through the reactor by-pass. The peak areas detected by the T.C.D. for these calibration pulses were then determined and hence the average area of a peak produced by 50 μ l of carbon monoxide calculated. The difference between this average area and the peak area detected for a carbon monoxide pulse after elution from a catalyst bed in a chemisorption experiment (i.e. unadsorbed carbon monoxide) gave the amount of carbon monoxide adsorbed per pulse by the catalyst. Hence, the sum of the amounts of carbon monoxide adsorbed by a catalyst over all pulses in a chemisorption experiment gave the total amount of carbon monoxide adsorbed by the catalyst under pulse-flow conditions.

3.3.2 Transmission Electron Microscopy

Reduced and passivated samples of the calcined catalysts were examined by transmission electron microscopy (T.E.M.): the process of passivation is described below and permitted the reduced samples to be manipulated in air. T.E.M. analyses allow the determination of the average particle diameters, and hence, the dispersions and the metal surface areas of the reduced catalysts to be made. These parameters can be directly compared to the analogous parameters calculated using data from carbon monoxide chemisorption experiments (Section 1.4.2).

A schematic diagram of the apparatus used to reduce and passivate catalyst samples for T.E.M. analyses is shown in Figure 3.5. The helium (B.O.C. Ltd.) was purified by passage through a trap containing Linde 5A molecular sieve

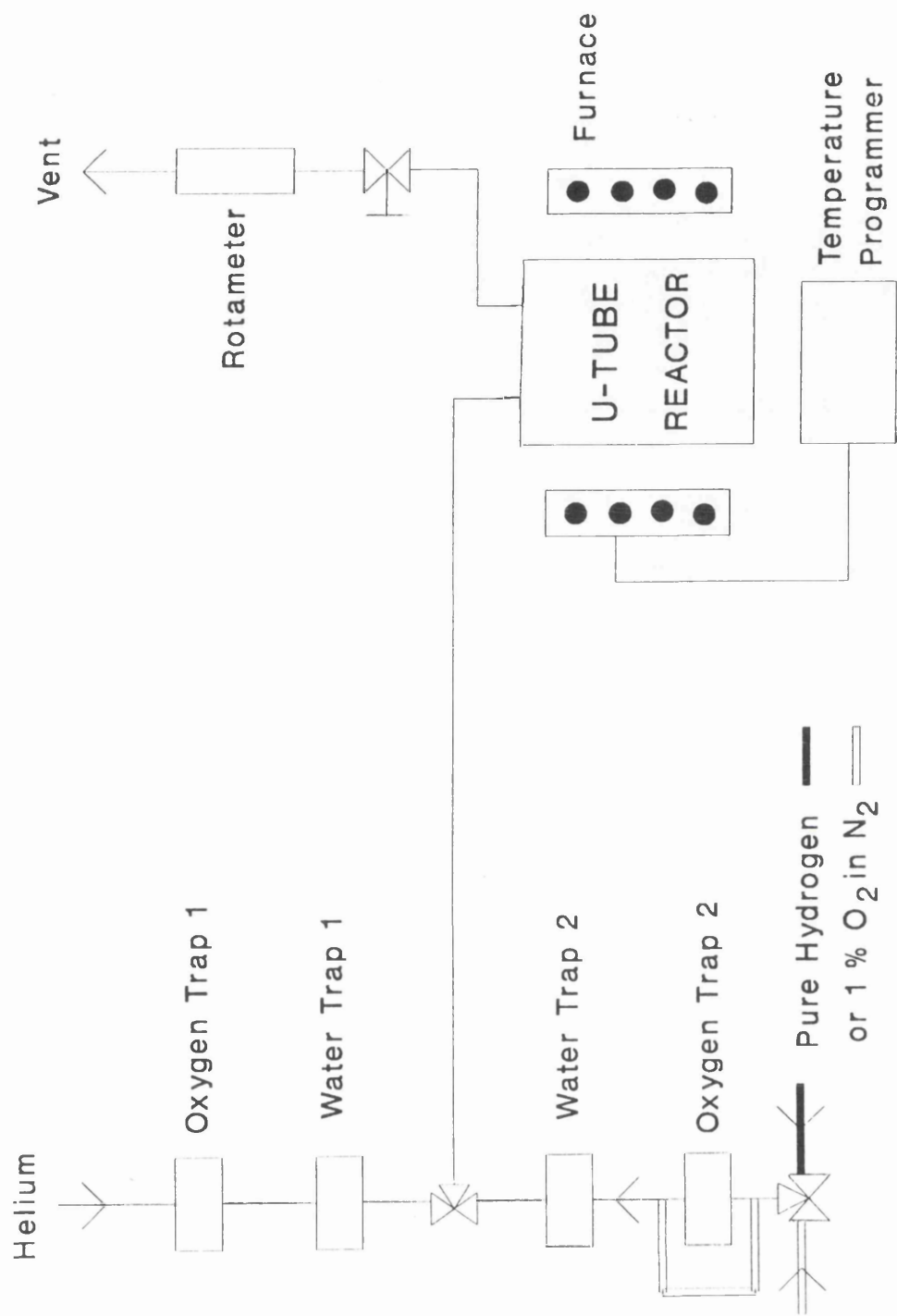


Fig. 3.5 Schematic Diagram of the Apparatus for Reduction and Passivation of Catalysts for T.E.M. Analyses

(Water Trap 1) in series with a trap containing activated palladium bronze (Oxygen Trap 1). The hydrogen (B.O.C. Ltd.) was purified in a similar manner to the helium via Water Trap 2 in series with Oxygen Trap 2. The 1 % v/v oxygen in nitrogen (B.O.C. Ltd.), used in the passivation procedure of the reduced catalyst samples, was dried by passing the gas mixture through a trap containing Linde 5A molecular sieve (Water Trap 2). The calcined catalysts (ca. 0.2 g) were separately loaded into a T.P.R. reactor (Figure 3.2) which was surrounded by a Stanton Redcroft tube furnace. The temperature of this furnace was controlled in an identical manner to that described in Section 3.2.1.2.

All the catalysts examined by T.E.M. analyses were reduced according to the standard procedure detailed in Section 3.3.1(a). After reduction, each catalyst was flushed with helium (flow-rate = $25 \text{ cm}^3\text{min}^{-1}$) at 673 K for ca. 90 minutes and then cooled to room temperature under flowing helium. Finally, each catalyst sample was passivated under a flow of 1 % v/v oxygen in nitrogen for one hour (flow-rate = $25 \text{ cm}^3\text{min}^{-1}$) before exposure to the atmosphere. This passivation treatment was similar to other procedures reported in the literature (8, 9, 60, 164).

The catalysts were subjected to such a long helium sweep at high temperature before the passivation treatment to ensure that all the reversibly adsorbed hydrogen species were removed from the catalysts (8, 165, 166). This removal of adsorbed hydrogen avoided the possibility of an exothermic reaction occurring upon exposure of the catalysts to the diluted oxygen during the passivation procedure.

Such a reaction is known to lead to sintering of the metal particles in nickel on silica catalysts (8).

The reduced and passivated catalyst samples were prepared for the T.E.M. analyses by crushing them and dispersing the resulting powders separately in toluene (23). A drop of each suspension was placed onto a carbon film supported on a 400-mesh copper grid and the dispersing medium allowed to evaporate.

A JEOL JEM-1200EX transmission electron microscope was employed in the T.E.M. investigation of the catalysts, except for the microscopic analysis of the 1 % nickel on CS2040 silica (aq.) catalyst. For this catalyst, an ABT EM-002B transmission electron microscope was used as an alternative. By using this microscope, which was fitted with a Link Analytical Energy Dispersive Analysis of X-rays (E.D.A.X.) detector, an E.D.A.X. microanalysis was obtained on a single supported nickel particle in the 1 % nickel on CS2040 silica (aq.) catalyst. Micrographs were recorded for the catalysts at various magnifications and further magnified by photo-enlargement.

Several different areas of each prepared catalyst sample were scanned by T.E.M. and micrographs of these areas recorded. From this set of micrographs, a selection of micrographs were chosen to represent "typical" areas within the sample. The diameters of a large number of separate particles were then measured using the criteria outlined in Section 4.2.2 from which particle size distributions were obtained.

3.4 Reaction Chemistry

Ethene hydrogenation was the test reaction chosen for investigation at Glasgow (the Surrey group also studied, in depth, the kinetics and mechanism of the reductive amination of ethanol to give predominantly ethylamine - see Appendix C for details). By using ethene hydrogenation as a test reaction it was hoped to establish that the reduction conditions detailed below were sufficient to lead to metallic nickel formation and consequently active catalysts. Also, by observing the behaviours of the reduced catalysts toward ethene hydrogenation, it was anticipated, by comparison with literature data, to be able to determine if any of the catalysts were anomalous in behaviour with respect to this reaction.

In this study two different reduction procedures were employed to reduce the calcined catalysts for ethene hydrogenation. The first, described below, was performed by successively adding several hydrogen aliquots to a sealed and heated reactor containing a sample of a calcined catalyst, i.e. static reduction. Each addition of hydrogen was preceded by evacuation of the reactor. The second method employed was the standard reduction procedure, previously described in Section 3.3.1(a), for calcined catalysts in a flow of hydrogen, i.e. flow reduction.

3.4.1 Static Reduction

A diagram of the apparatus is shown in Figure 3.6. The apparatus consisted of a conventional glass vacuum-system which was capable of being evacuated to a pressure of ca. 10^{-5} Torr by the use of a mercury diffusion pump (D.P.)

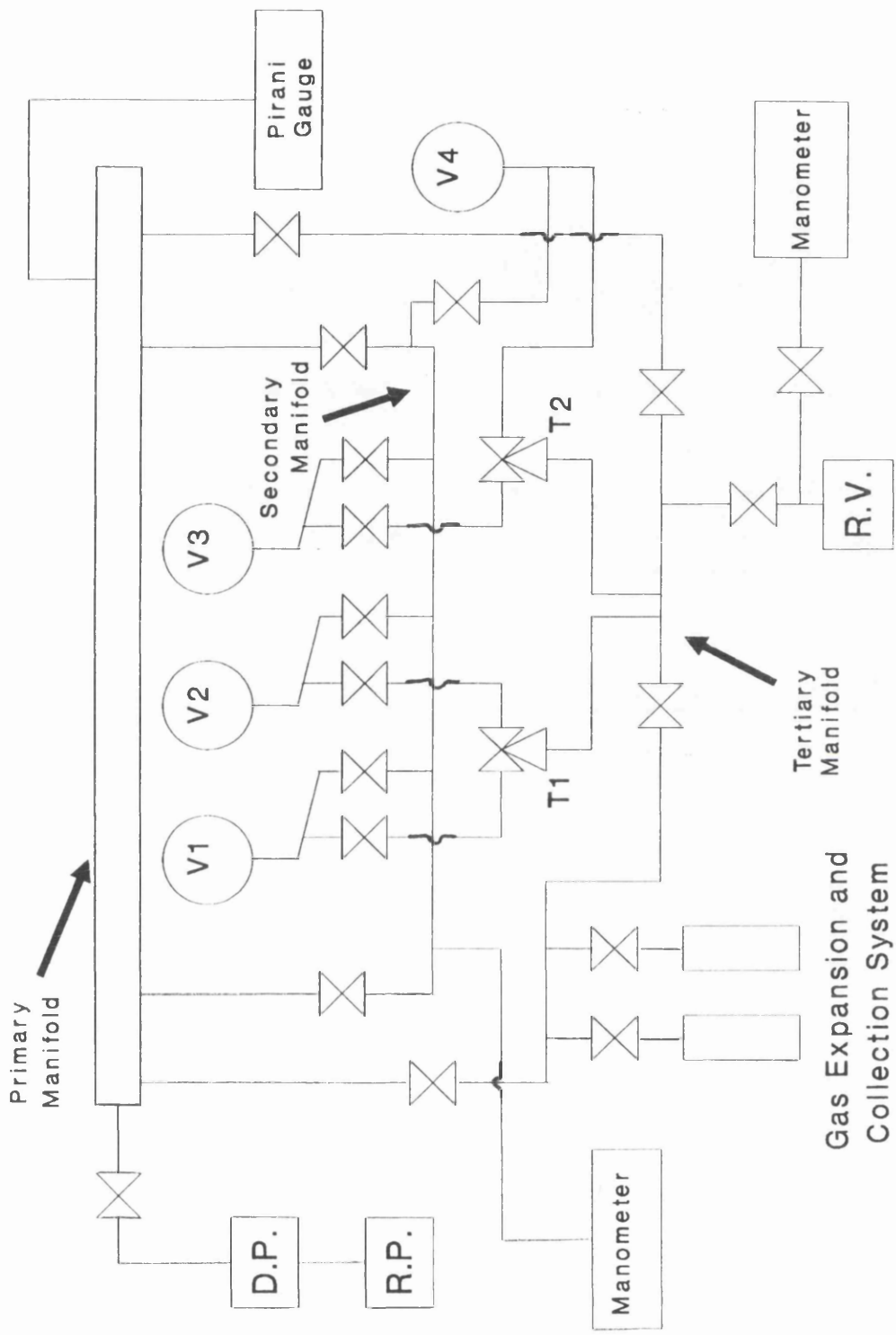
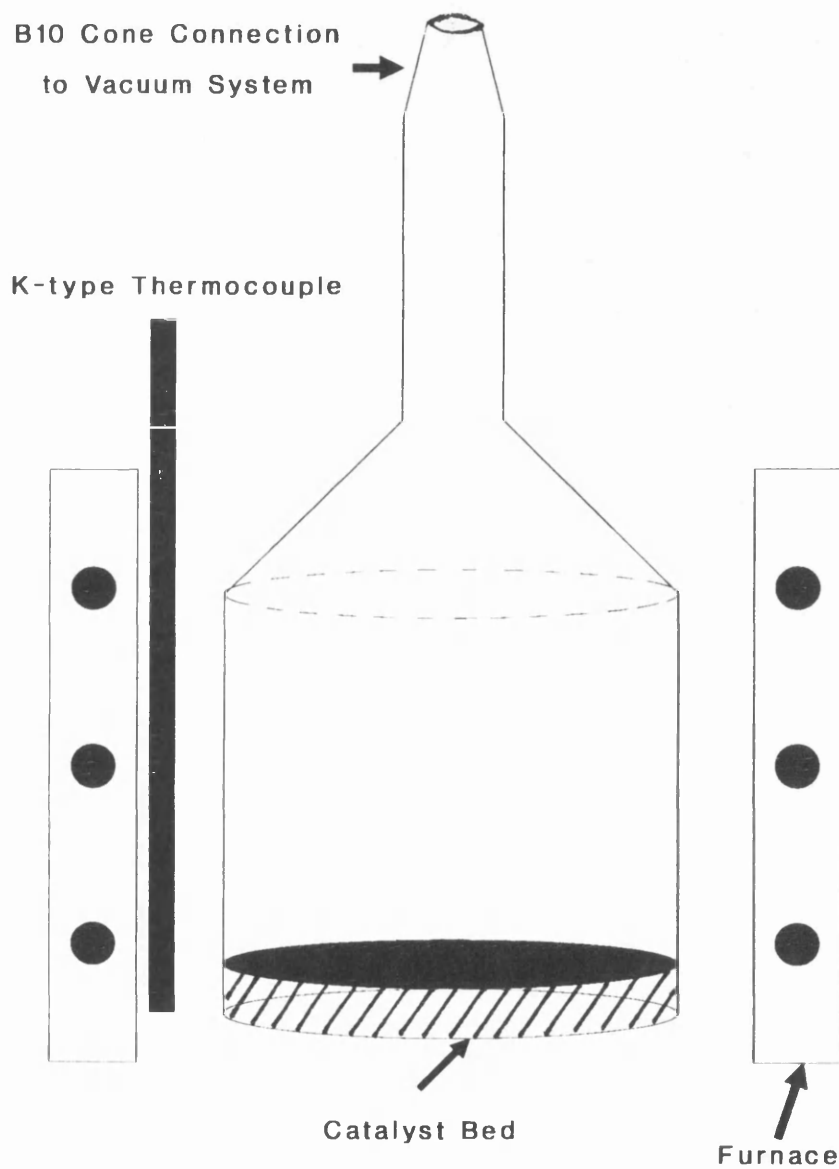


Fig. 3.6 Diagram of the Vacuum System for Static Reduction and Ethene Hydrogenation

backed by a rotary pump (R.P.). The apparatus had three nominal manifolds. The primary manifold was used as the main pumping manifold, the secondary manifold was used mainly for the filling of the gas storage bulbs V1, V2, V3 and V4 and the tertiary manifold incorporated the reaction vessel (R.V.). The storage bulbs V1, V2 and V3 contained hydrogen (B.O.C. Ltd.), a 2:1 hydrogen:ethene mixture (by volume) and ethene (B.O.C. Ltd.), respectively. The hydrogen stored in bulb V1 had been deoxygenated by passage over activated palladium bronze and then through a trap which was maintained at 77 K, using liquid nitrogen, to remove water vapour. The ethene contained in bulb V3 was purified by condensing the gas three times at liquid nitrogen temperature and removing residual gas by evacuation. The 2:1 hydrogen:ethene mixture contained in bulb V2 was mixed from the hydrogen and ethene stored in bulbs V1 and V3, respectively.

The storage bulbs were connected to the tertiary manifold by capillary tubing to minimise the dead volume in the apparatus. The reactor was also connected to this manifold via a glass B10 cone and socket joint. A greased tap isolated the reaction vessel from the vacuum-system. The reactor, illustrated in Figure 3.7, was constructed from Pyrex and was cylindrical in shape with a flat base. A single aperture at the top of the reactor, which tapered into the B10 cone connection, allowed the unreduced catalyst sample to be loaded and also permitted the admission and evacuation of gases from the reactor. The pressure in the reactor (volume = $176 \pm 1 \text{ cm}^3$) was monitored during the hydrogenation reactions using a mercury manometer. The

Fig. 3.7 Diagram of the Reactor for Static Reduction of the Calcined Catalysts for Ethene Hydrogenation



three-way taps T1 and T2 allowed gas from any of the storage bulbs to be admitted into the reaction vessel.

The reaction vessel was heated during the reduction procedure by a tube furnace, the temperature being controlled by a FGH temperature programmer (model number P200); the temperature feedback was provided by a K-type thermocouple located on the inside wall of the tube furnace at the same level as the base of the reactor.

3.4.1.1 Static Reduction Procedure

An accurately weighed sample (ca. 0.2 g) of a calcined 1 % nickel on silica catalyst (or ca. 0.02 g of a calcined 10 % nickel on silica catalyst) was loaded into the reactor. The reactor was then attached to the vacuum-system and evacuated to a pressure of ca. 10^{-5} Torr.

Hydrogen gas was admitted into the evacuated reactor from storage bulb V1 to a pressure of 100 Torr. The reactor was then heated from room temperature to 723 K at $\beta = 5 \text{ K min.}^{-1}$. When the temperature reached 373 K during this heating process, the reactor was evacuated and a further 100 Torr aliquot of hydrogen added. Similar replacements of the hydrogen atmosphere were made at temperature intervals of 100 K, thereafter. An additional 100 Torr aliquot of hydrogen was added at 673 K and the temperature raised to the final reduction temperature. Once the reactor had reached 723 K, it was evacuated and an aliquot consisting of 200 Torr of hydrogen admitted. This hydrogen aliquot was then evacuated after 30 minutes. A further four changes of hydrogen (each charge at a pressure of 200 Torr) were made at one hourly intervals with the

final charge of hydrogen left in the reactor overnight (ca. 16 hours). After this time, the reactor was evacuated for ca. 30 minutes at 723 K and then allowed to cool under evacuation to room temperature. This cooling was complete in about 30 minutes.

3.4.1.2 Ethene Hydrogenation After Static Reduction

Following reduction using the procedure described above, the reactor was cooled to 273.0 ± 0.2 K and the temperature allowed to equilibrate for ca. 15 minutes. The reactor was then isolated from the vacuum and approximately 100 Torr of the 2:1 hydrogen:ethene mixture admitted to the reactor and the pressure noted at various times using the mercury manometer.

The reaction was allowed to continue, typically for 80 minutes, and then the reactor evacuated for ca. five minutes. Another 100 Torr sample of the gas mixture was then admitted and the reaction again monitored by the pressure change with time. Six reactions were normally performed using a reduced sample of catalyst without re-reduction of the catalyst. If the cycle of six hydrogenation reactions using a particular catalyst was interrupted, e.g. overnight, then a 200 Torr aliquot of hydrogen was admitted to the evacuated reactor after the last reaction had been monitored. The cycle of reactions was continued the next day by initially removing the added hydrogen from the reactor by evacuation for 30 minutes at room temperature. The reactor was then cooled to 273.0 K before admission of a further aliquot of the hydrogenation mixture.

A slight modification of the above procedure was introduced for the experiments performed using the 1 % nickel catalysts. A cycle of six ethene hydrogenation reactions was performed using each reduced catalyst as before, but in the first hydrogenation reaction only, ca. 2 Torr of [^{18}O]-carbon dioxide (MSD isotopes) was added to the reactor with the 100 Torr aliquot of the hydrogenation gas mixture. The [^{18}O]-carbon dioxide was added to the first hydrogenation reaction mixture in order to detect if residual exchangeable oxygen was present on the metal surface of the catalyst after reduction (see Section 4.3.1 for details). After the reaction time of the first hydrogenation reaction had elapsed, the gases present in the reactor were condensed at a temperature of 77 K in the gas collection system. These gases were then analysed by a KRATOS MS-12 single focus mass spectrometer. The mass spectrometric analyses allowed the amounts of [^{16}O]-oxygen exchange by the catalysts to be quantified. The reproducibility of the mass spectrometric analysis was investigated by analysing thirteen separate samples of the "as supplied" standard [^{18}O]-carbon dioxide.

A control experiment using an oxidised sample of 1 % nickel on ICI silica was also performed. In this experiment, the calcined 1 % nickel on ICI silica catalyst was reduced in the normal way and the reactor evacuated and cooled to 273.0 K. After cooling, 724 Torr of dry air was admitted to the reactor and left for 30 minutes before evacuation. As in the case of the first hydrogenation cycles performed using the reduced 1 % nickel on silica catalysts, an aliquot consisting of 100 Torr of the hydrogen

and ethene mixture plus 2 Torr of [^{18}O]-carbon dioxide was added to the reactor containing the oxidised catalyst. The pressure of the gas in the reactor was then monitored over 80 minutes. After this time, the condensable gases were analysed by mass spectrometry.

3.4.2 Flow Reduction

A schematic diagram of the apparatus used in the flow reduction and ethene hydrogenation studies is shown in Figure 3.8. The hydrogen and helium (both supplied by B.O.C. Ltd.) used in these experiments were purified by passage through a water trap containing Linde 5A molecular sieve in series with an oxygen trap containing activated palladium bronze.

3.4.2.1 Flow Reduction Procedure

An accurately weighed sample (ca. 0.2 g) of a calcined 1 % nickel on silica catalyst (or ca. 0.02 g of a calcined 10 % nickel on silica catalyst) was placed on a glass sinter situated in an U-tube type Pyrex reactor of similar design to that of the T.P.R. reactor (Figure 3.2). The reactor was fitted with a thermocouple well located at the same level as the sinter. The reaction vessel was heated during the reduction procedure by a tube furnace, the temperature being controlled by a FGH temperature programmer (model number P200); the temperature feedback was provided by a K-type thermocouple located in the thermocouple well incorporated in the reactor.

The calcined catalysts were reduced using the standard flow reduction procedure described in Section 3.3.1(a). After the three hour reduction period, the reactor was

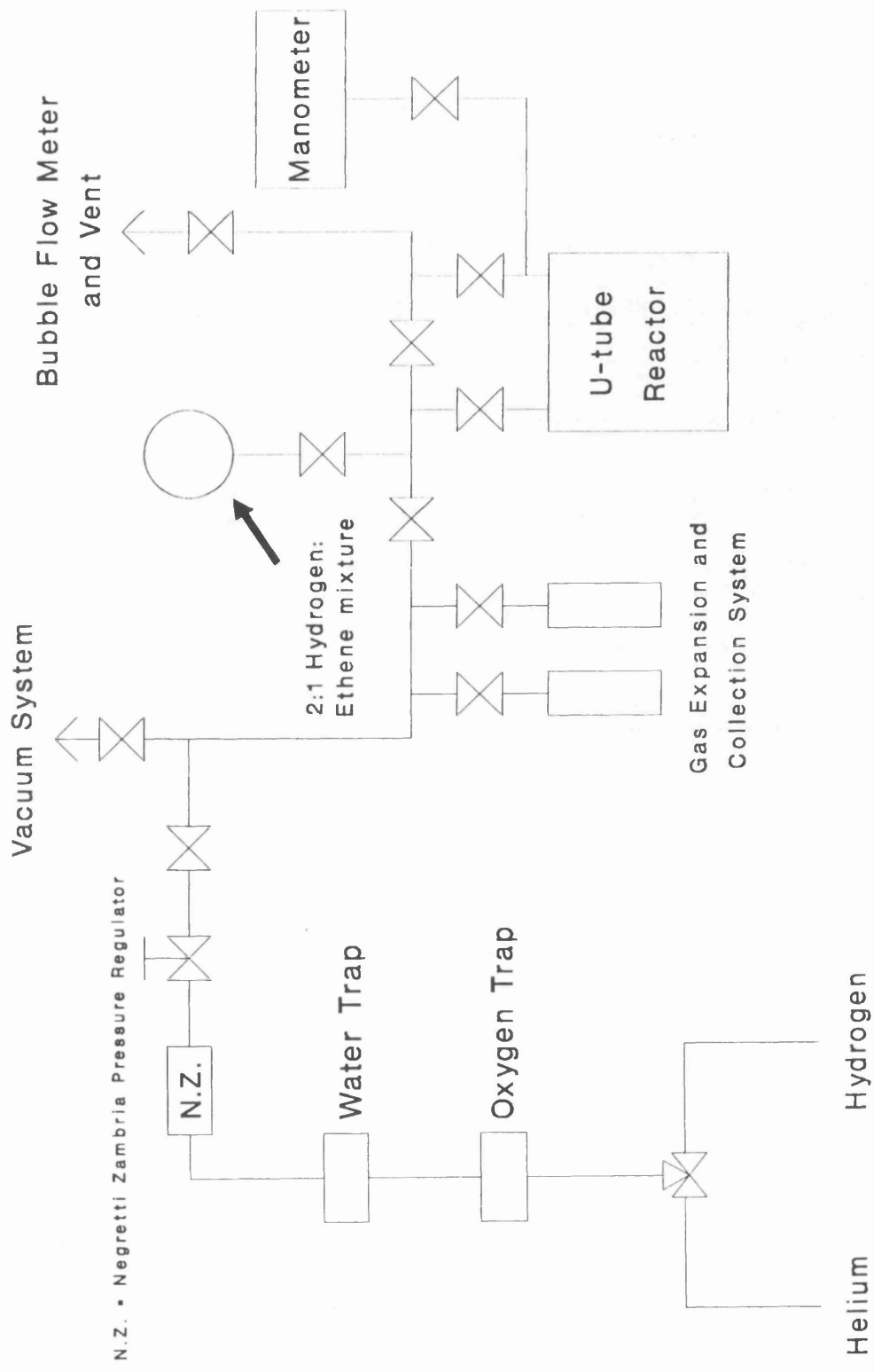


Fig. 3.8 Diagram of the Flow/Vacuum System for Flow Reduction and Ethene Hydrogenation

flushed with helium for 1.5 hours at a flow rate of 25 $\text{cm}^3\text{min}^{-1}$, whilst the temperature was maintained at 673 K.

3.4.2.2 Ethene Hydrogenation After Flow Reduction

After reduction, the reactor was removed from the furnace and allowed to cool to room temperature under flowing helium (ca. 20 minutes). The reactor was further cooled to 273.0 ± 0.2 K and the temperature allowed time to equilibrate (ca. 15 minutes).

The identical ethene hydrogenation procedure to that described in Section 3.4.1.2 for the 1 % nickel on silica catalysts reduced by the static method was employed, i.e. ca. 100 Torr of a 2:1 hydrogen:ethene mixture plus ca. 2 Torr of [^{18}O]-carbon dioxide were added to the evacuated reactor (volume = 152 ± 1 cm^3). The change in pressure was then observed over 80 minutes. After this time, the condensable gases were collected at a temperature of 77 K in the gas collection system and analysed by the KRATOS MS-12 single focus mass spectrometer. A single ethene hydrogenation reaction was performed using each flow-reduced catalyst in order to determine the initial specific rates of ethene hydrogenation for the catalysts (see Section 4.3.2).

A control experiment was also performed using an oxidised sample of 1 % nickel on ICI silica. In this experiment, the calcined 1 % nickel on ICI silica catalyst was reduced in the normal way and the reactor evacuated and cooled to 273.0 K. After cooling, 702 Torr of dry air was admitted to the reactor and left for 30 minutes prior to evacuation. The hydrogen, ethene and [^{18}O]-carbon dioxide mixture was then added in the usual way, and the pressure of

gas in the reactor monitored over 80 minutes. After this time, the condensable gases were recovered and analysed by mass spectrometry.

CHAPTER FOUR

CHAPTER FOURRESULTS4.1 Characterisation of the Unreduced Catalysts4.1.1 Chemical Compositions, BET Surface Areas and Porosities of the Catalysts

The nickel loadings of the catalysts were determined by digestion of the calcined catalysts, separately, in nitric acid. The nickel(II) nitrate solutions so formed were analysed by atomic absorption spectrophotometry. The nickel contents of the catalysts were then determined by comparison of the experimental data with a calibration curve constructed from data obtained using standardised nickel(II) nitrate solutions. The analyses were performed at ICI, Billingham and the relevant data presented below in Table 4.1. The nitrogen BET and mercury porosimetry data for the catalysts reported by the Cambridge group (Dr. L. Gladden *et al.*) are also shown in this table.

The data presented in Table 4.1 highlight the wide variations in the BET surface areas (ca. 200 to 400 m²g⁻¹) and porosities of the catalysts (average pore diameters between 0 and 18.2 nm and pore volumes ranging between 0 and 1.6 cm³g⁻¹). Comparison of the porosity data for both the non-aqueously and aqueously impregnated CS2040 silica catalysts with that for the pure CS2040 silica (Section A4, Appendix A and also Table B1, Appendix B) reveals that the non-aqueous impregnation of the silica followed by drying and calcination caused minimal pore diameter contraction (from 20.8 to 18.2 nm). In contrast, after drying and

calcining the aqueously impregnated silica, the average pore diameter decreased by 50 %.

Table 4.1

Nickel Contents, Nitrogen BET Surface Areas, Average Pore Diameters and Pore Volumes of the Catalysts

Catalyst	% Ni (w/w)	BET Area (m^2g^{-1})	Pore Diameter (nm)	Pore Volume (cm^3g^{-1})
10 % Ni/ICI silica	10.3	n/d ^a	n/d	n/d
10 % Ni/Cab-O-Sil silica	10.9	n/d	0.0	0.0
10 % Ni/CS1030E silica	10.9	n/d	n/d	n/d
1 % Ni/ICI silica	1.2	424	4.0	0.4
1 % Ni/Cab-O-Sil silica	1.7	209	0.0	0.0
1 % Ni/CS1030E silica	1.6	290	14.4	1.1
1 % Ni/CS2040 (aq.) silica	1.5	396	10.4	1.2
1 % Ni/CS2040 (non-aq.) silica	1.4	293	18.2	1.6

a. Not determined.

4.1.2 Temperature Programmed Reduction

Temperature programmed reduction (T.P.R.) experiments were performed on both the uncalcined and calcined catalysts according to the procedure described in Section 3.2.1.2. The T.P.R. profiles obtained showed the hydrogen consumption of the unreduced catalysts as a function of temperature during heating at $\beta = 5 \text{ K min.}^{-1}$ in a flow of 6 % v/v hydrogen in argon. In all T.P.R. experiments, the samples were heated to a final temperature of 1023 K.

4.1.2(a) T.P.R. - Control Experiments

Control experiments were performed using pure ICI silica, unsupported nickel oxide and the empty reactors as described in Section 3.2.1.2. The T.P.R. profile for unsupported nickel oxide was characterised by two overlapping hydrogen uptake peaks with maxima (denoted T_{\max}) at temperatures of 596 and 641 K, respectively. The experiments performed using the empty reactors and pure ICI silica revealed that, in the absence of nickel species, there was no measurable uptake of hydrogen during heating.

4.1.2(b) T.P.R. of the Uncalcined Catalysts

The T.P.R. profiles obtained for the uncalcined catalysts are shown in Figures 4.1 and 4.2.

Inspection of the results presented in Figure 4.1 and Table 4.2 reveals that T.P.R. profiles of the uncalcined 10 % nickel on silica catalysts possessed a common structure consisting of three distinct hydrogen uptake peaks. In all profiles, the low temperature (L.T.) peak spanned a characteristically narrow temperature range with T_{\max} within the temperature interval 560 - 573 K. The subsequent two peaks occurring at higher temperatures were much broader; the mid-temperature (M.T.) peak was characterised by a T_{\max} value lying in the temperature interval 673 - 717 K, while T_{\max} for the high temperature (H.T.) peak lay in the temperature interval 826 - 859 K.

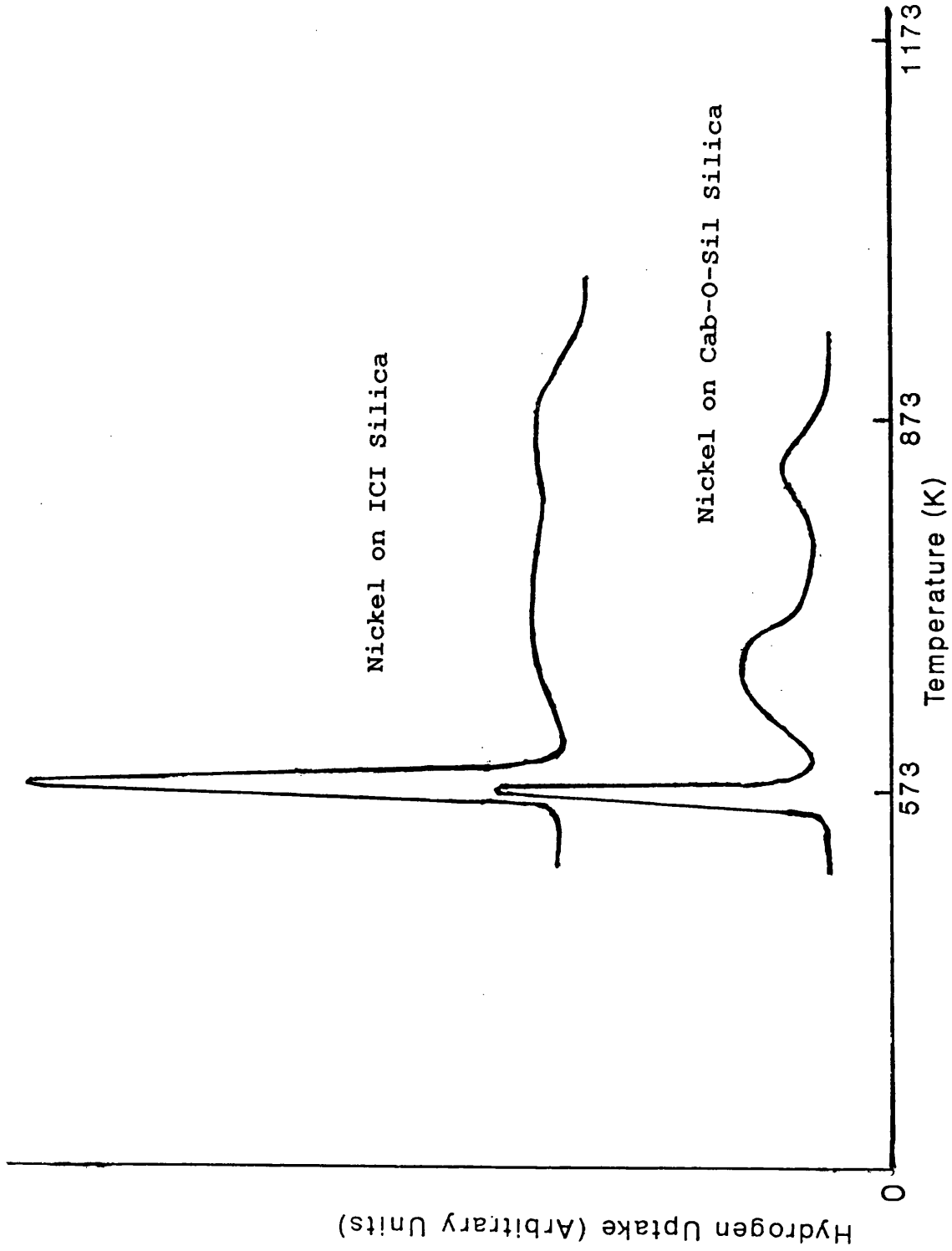


Fig. 4.1: T.P.R. Profiles of the Uncalcined 10 % w/w Nickel on Silica Catalysts

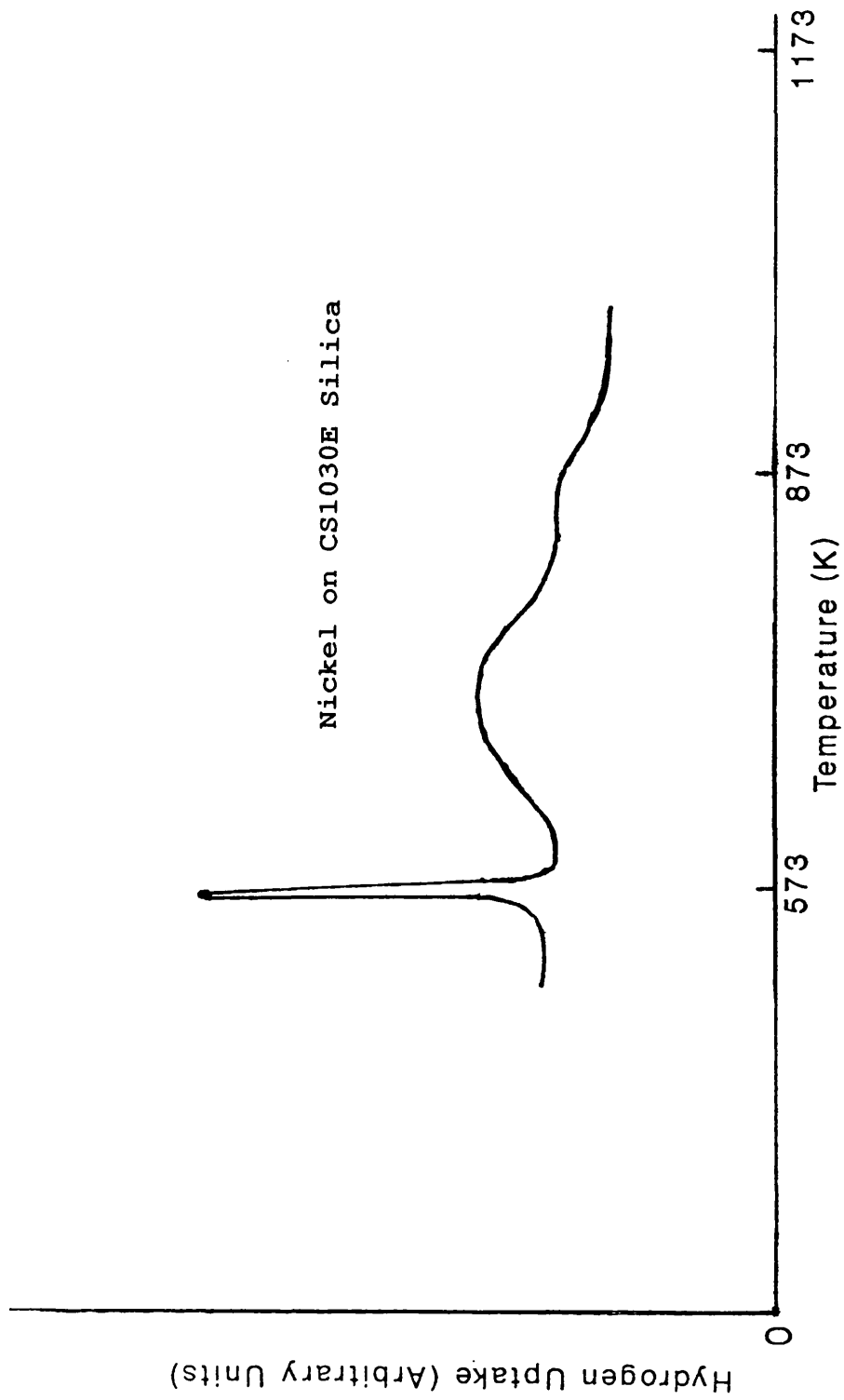


Fig. 4.1 (continued): T.P.R. Profiles of the Uncalcined 10 % w/w
Nickel on Silica Catalysts

Table 4.2

T_{\max} Data for T.P.R. Profiles of Uncalcined 10 % Nickel on
Silica Catalysts

Uncalcined Catalyst	T_{\max} (K)		
	L.T.	M.T.	H.T.
Ni/ICI silica	573	717	859
Ni/Cab-O-Sil silica	560	673	826
Ni/CS1030E silica	568	713	853

The data presented in Table 4.3 and Figure 4.2 reveal that the T.P.R. profiles for the uncalcined 1 % nickel on silica catalysts were similar to one another and that each profile consisted of three overlapping hydrogen uptake peaks. This pattern was exactly analogous to that described previously for the T.P.R. profiles of the uncalcined 10 % nickel on silica catalysts.

Table 4.3

T_{\max} Data for T.P.R. Profiles of Uncalcined 1 % Nickel on
Silica Catalysts

Uncalcined Catalyst	T_{\max} (K)		
	L.T.	M.T.	H.T.
Ni/ICI silica	528	617	745
Ni/Cab-O-Sil silica	546	629	743
Ni/CS1030E silica	544	640	805
Ni/CS2040 (aq.) silica	561	642	736
Ni/CS2040 (non-aq.) silica	551	633	735

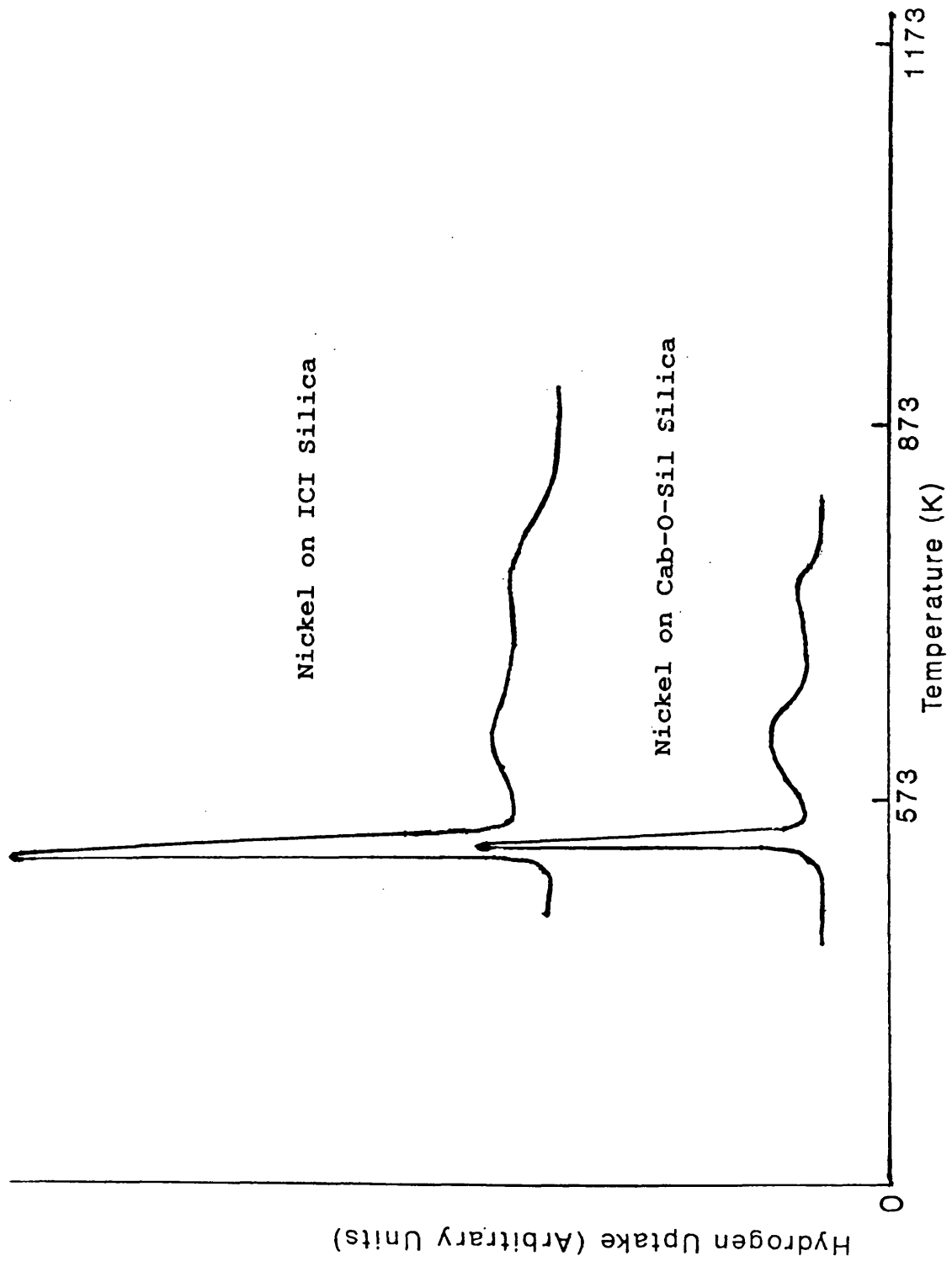


Fig. 4.2: T.P.R. Profiles of the Uncalcined 1 % w/w Nickel on Silica Catalysts

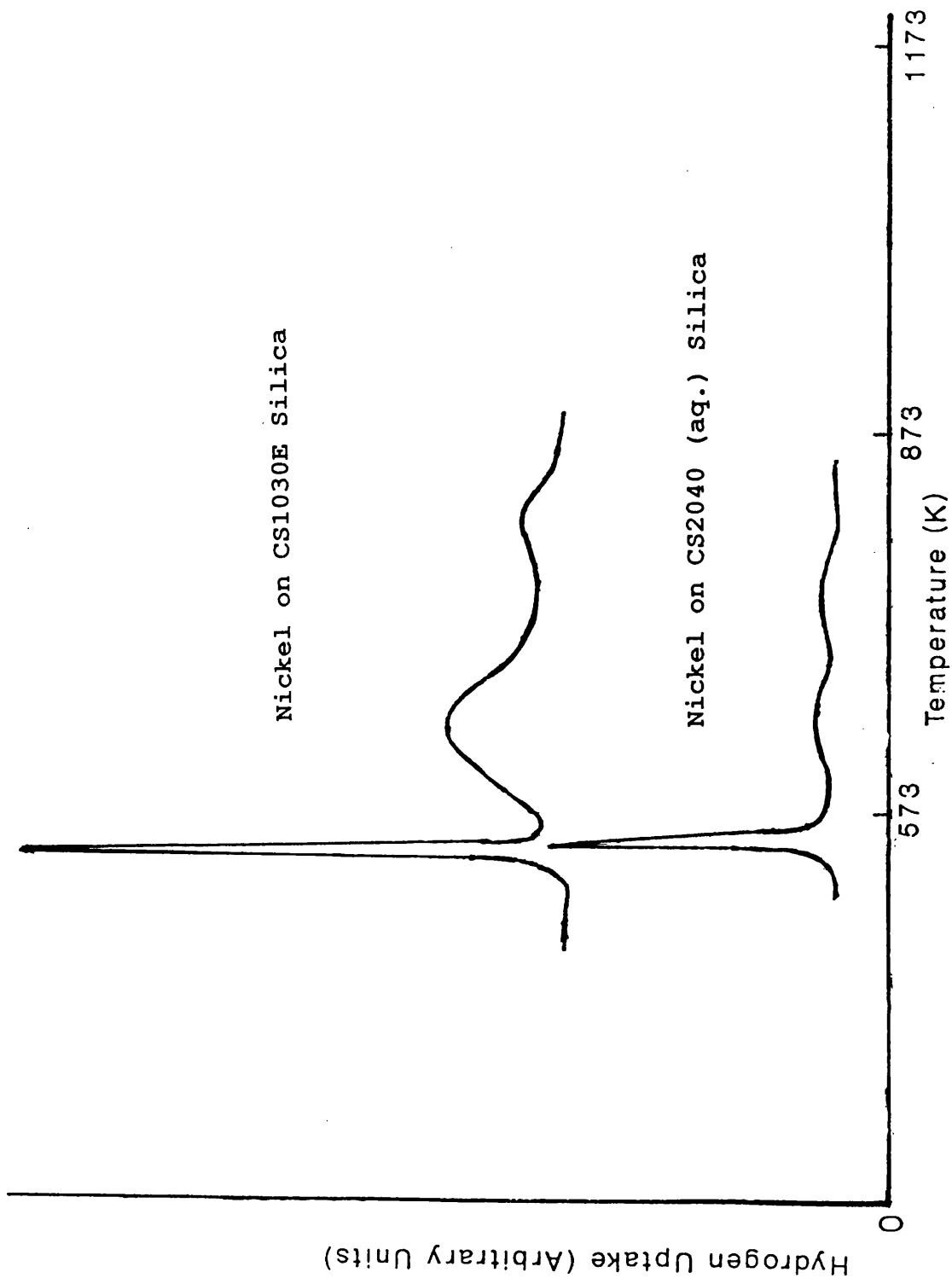


Fig. 4.2 (continued): T.P.R. Profiles of the Uncalcined 1 % w/w Nickel on Silica Catalysts

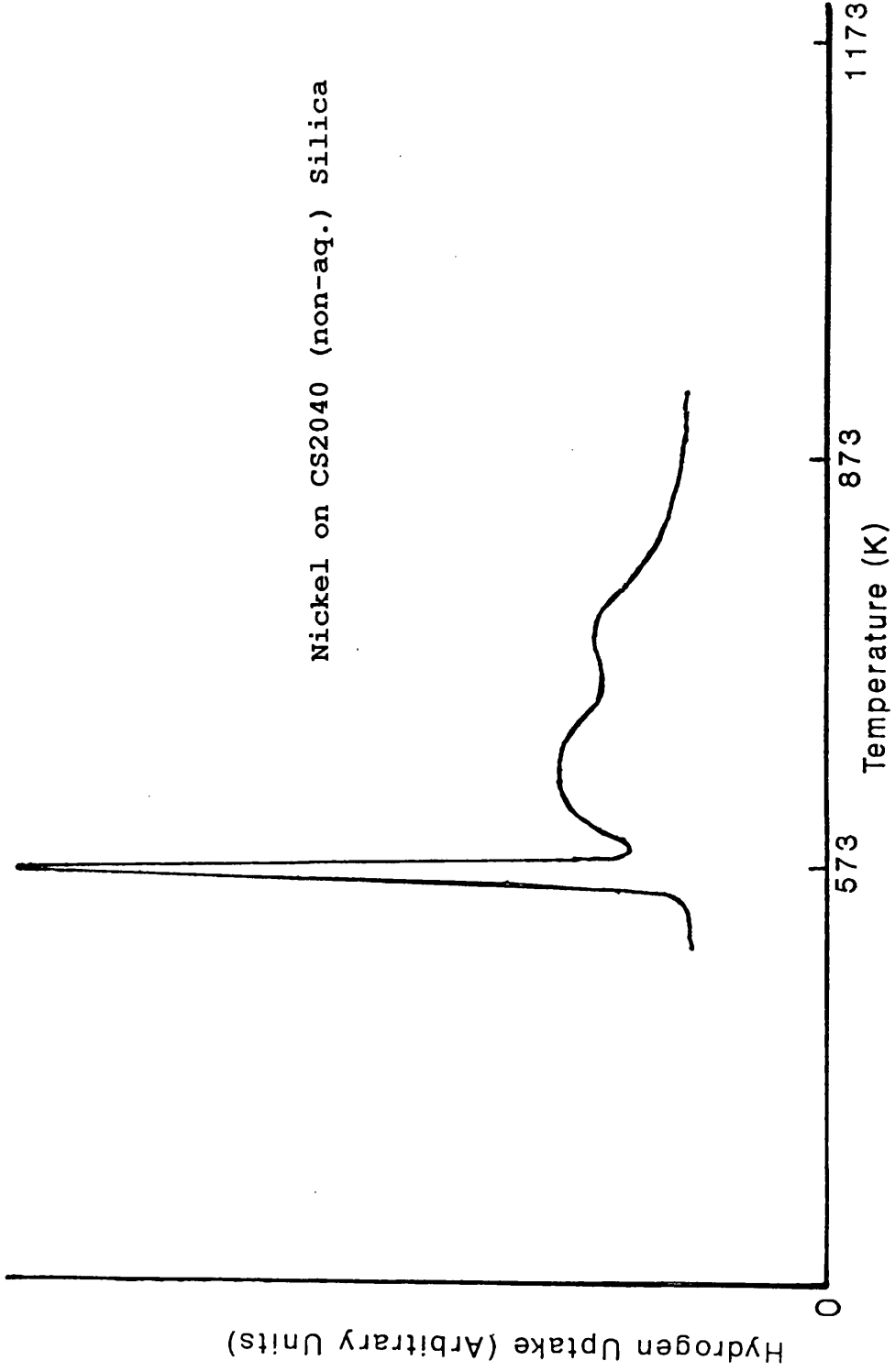


Fig. 4.2 (continued): T.P.R. Profiles of the Uncalcined 1 % w/w
Nickel on Silica Catalysts

Profiles for all the 1 % nickel on silica catalysts exhibited a characteristically sharp L.T. peak with T_{\max} in the temperature interval 528 - 561 K. In addition, a broad M.T. peak with T_{\max} in the temperature interval 617 - 642 K and a broad H.T. peak with T_{\max} in the temperature interval 735 - 805 K were observed. The T_{\max} values for the L.T., M.T. and H.T. peaks, respectively, occurred at lower temperatures for the 1 % nickel on silica catalysts relative to the T_{\max} values for the corresponding peaks for the 10 % nickel on silica catalysts, the difference in T_{\max} being greater for the corresponding M.T. and H.T. peaks.

In summary, all T.P.R. profiles for the uncalcined catalysts were similar regardless of the nickel content or the silica used as the support. The main points of similarity were:

- i. Each profile conformed to a general pattern consisting of three overlapping hydrogen uptake peaks;
- ii. For catalysts of similar metal content, the T_{\max} values of either the L.T., M.T. or H.T. peaks were similar;
- iii. The L.T., M.T. and H.T. peaks were similar in shape for all profiles; the L.T. peak spanned a much narrower temperature range than either of the broader M.T. or H.T. peaks.

A difference existed between T.P.R. profiles of uncalcined catalysts with high and low metal loadings: all the peaks occurred at relatively higher T_{\max} values in profiles for the 10 % nickel on silica catalysts compared to corresponding peaks observed for the 1 % nickel on silica catalysts. This difference in temperature between

catalysts of different metal content was more prominent for the M.T. and H.T. peaks.

4.1.2(c) T.P.R. of the Calcined Catalysts

The T.P.R. profiles for the calcined nickel on silica catalysts are shown in Figures 4.3 and 4.4 and the measured hydrogen uptake data during T.P.R. summarised in Table 4.4a. Additionally, for each T.P.R. profile, the hydrogen uptake per peak (expressed as a percentage of the total hydrogen uptake) is displayed in Table 4.4b. The L.T. and H.T. acronyms in this table refer to component peaks of the T.P.R. profiles with T_{\max} values at low and high temperatures, respectively, as described later in this section.

Table 4.4a

Hydrogen Uptake Data for Calcined Nickel on Silica Catalysts

Calcined Catalyst	Hydrogen Uptake ^{a,b}
10 % Ni/ICI silica	15.0 (17.5)
10 % Ni/Cab-O-Sil silica	16.7 (18.6)
10 % Ni/CS1030E silica	12.5 (18.6)
1 % Ni/ICI silica	1.9 (2.0)
1 % Ni/Cab-O-Sil silica	2.1 (2.9)
1 % Ni/CS1030E silica	2.1 (2.7)
1 % Ni/CS2040 (aq.) silica	1.6 (2.6)
1 % Ni/CS2040 (non-aq.) silica	1.6 (2.4)

a. Units: moles(g catalyst)⁻¹ x 10⁴.

b. The theoretical hydrogen uptake for 100 % reduction is given in brackets.

Table 4.4b

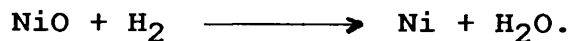
Fractional Hydrogen Uptake Per Identified Peak in the T.P.R.
Profiles for Calcined Nickel on Silica Catalysts

Calcined Catalyst	Percent H ₂ Uptake Per Peak	
	L.T.	H.T.
10 % Ni/ICI	53	47
10 % Ni/Cab-O-Sil ^a	93	7
10 % Ni/CS1030E ^a	79	21
1 % Ni/ICI	34	66
1 % Ni/Cab-O-Sil ^a	72	28
1 % Ni/CS1030E	40	60
1 % Ni/CS2040 (aq.)	100	--
1 % Ni/CS2040 (non-aq.) ^b	28	69

a. Shoulder present on low temperature side of L.T. peak.

b. Area of the peak at $T_{\max} = 1000$ K accounted for 3 % of the total hydrogen uptake.

The theoretical hydrogen uptake for each unreduced catalyst, shown in brackets in Table 4.4a, was calculated on the basis that the following stoichiometric reaction applies exclusively to the reduction of the calcined catalysts;



Three assumptions were made in using this equation to calculate the theoretical uptake of hydrogen by an unreduced calcined nickel on silica catalyst:

- i. The support did not adsorb hydrogen directly from the gas stream (due to impurities etc.);
- ii. Hydrogen spillover from the metal to the support did not occur or was negligible during T.P.R.;

iii. The only nickel species present in the unreduced calcined catalysts was nickel(II), e.g. nickel(III) was not present.

It is evident by inspection of the data presented in Table 4.4a that, in the majority of cases, total reduction of the nickel(II) oxide component of the unreduced calcined catalysts was not achieved during the T.P.R. experiments.

The temperature data for peak maxima observed in the T.P.R. profiles of the calcined 10 % nickel on silica catalysts (Figure 4.3) are presented in Table 4.5.

Table 4.5

T_{\max} Data for T.P.R. Profiles of Calcined 10 % Nickel on Silica Catalysts

Calcined Catalyst	T_{\max} (K)	
	L.T.	H.T.
Ni/ICI silica	650	839
Ni/Cab-O-Sil silica ^{a,b}	647	-
Ni/CS1030E silica ^b	657	789

a. Small, underlying H.T. peak observed with $T_{\max} =$ ca. 733 K.

b. Shoulder present on low temperature side of L.T. peak.

No general pattern was evident for the profiles of the calcined 10 % nickel on silica catalysts, in contrast to the T.P.R. profiles obtained for the uncalcined catalysts. Nevertheless, all the profiles shared a common L.T. peak with T_{\max} values in the temperature range 647 - 657 K. In addition, the profiles of 10 % nickel on Cab-O-Sil and CS1030E silicas displayed shoulders on the low temperature side of their respective L.T. peaks.

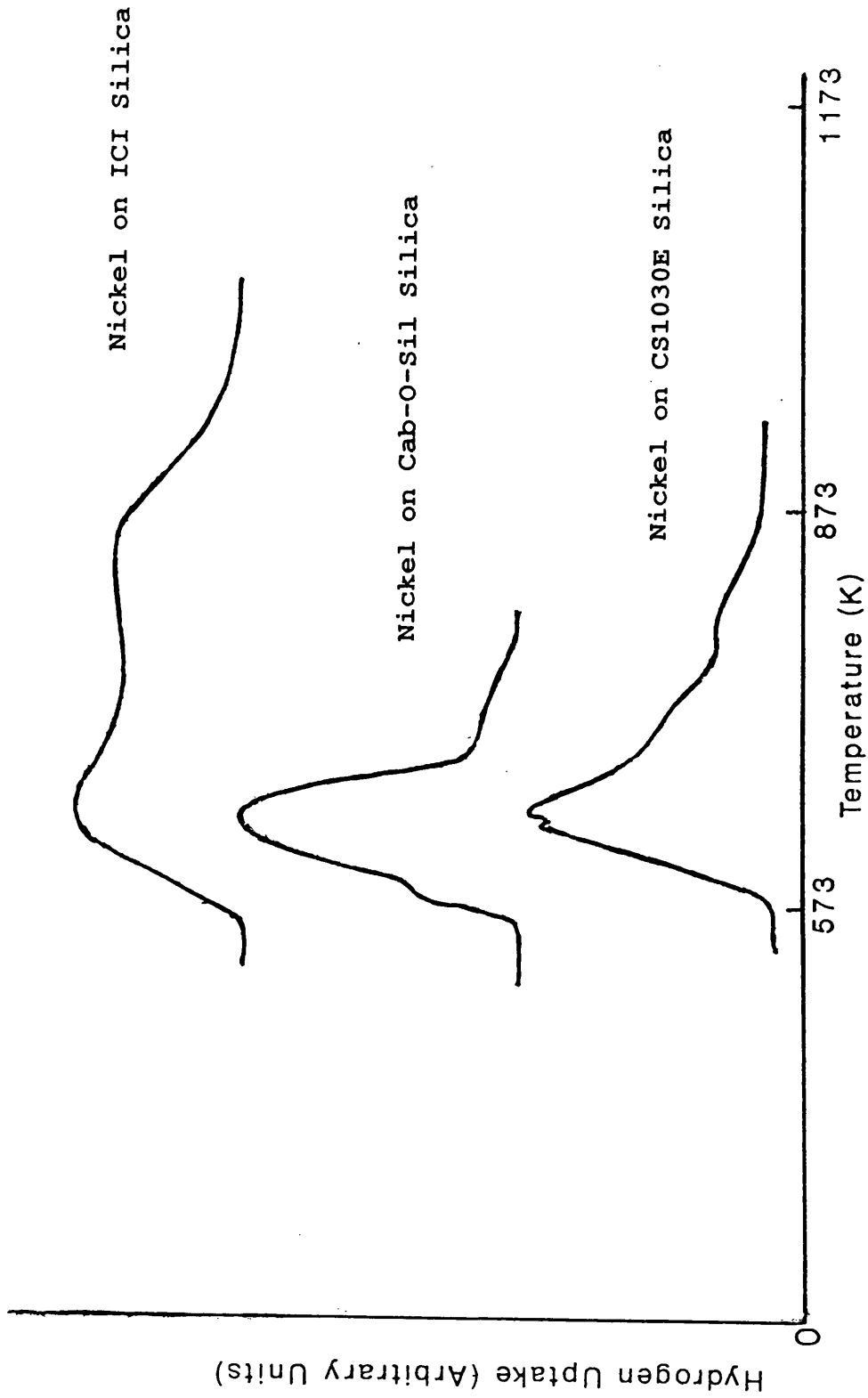


Fig. 4.3: T.P.R. Profiles of the Calcined 10 % w/w Nickel on Silica Catalysts

Significant H.T. peaks were also observed in the T.P.R. profiles of 10 % nickel on ICI silica ($T_{\max} = 839$ K) and CS1030E silica ($T_{\max} = 789$ K), where they were responsible for 47 % and 21 % of the respective total hydrogen uptakes observed for these unreduced catalysts. In the profile of 10 % nickel on Cab-O-Sil silica, a relatively small H.T. peak, 7 % of the total hydrogen uptake, underlaid the much larger L.T. peak; $T_{\max} = \text{ca. } 733$ K for the H.T. peak in this case.

T.P.R. data obtained for the calcined 1 % nickel on silica catalysts are presented in Table 4.6 and the T.P.R. profiles shown in Figure 4.4.

Table 4.6

T_{\max} Values for T.P.R. Profiles of Calcined 1 % Nickel on Silica Catalysts

Calcined Catalyst	T_{\max} (K)	
	L.T.	H.T.
Ni/ICI silica	635	708
Ni/Cab-O-Sil silica ^a	640	-
Ni/CS1030E silica	620	703
Ni/CS2040 (aq.) silica	618	-
Ni/CS2040 (non-aq.) silica ^b	603	736

a. Small, underlying H.T. peak observed with $T_{\max} = \text{ca. } 734$ K. A shoulder was also present on the low temperature side of the L.T. peak.

b. Small peak also present with $T_{\max} = 1000$ K.

The profiles of the calcined 1 % nickel on silica catalysts were similar to the T.P.R. profiles obtained for the calcined 10 % nickel on silica catalysts in that no

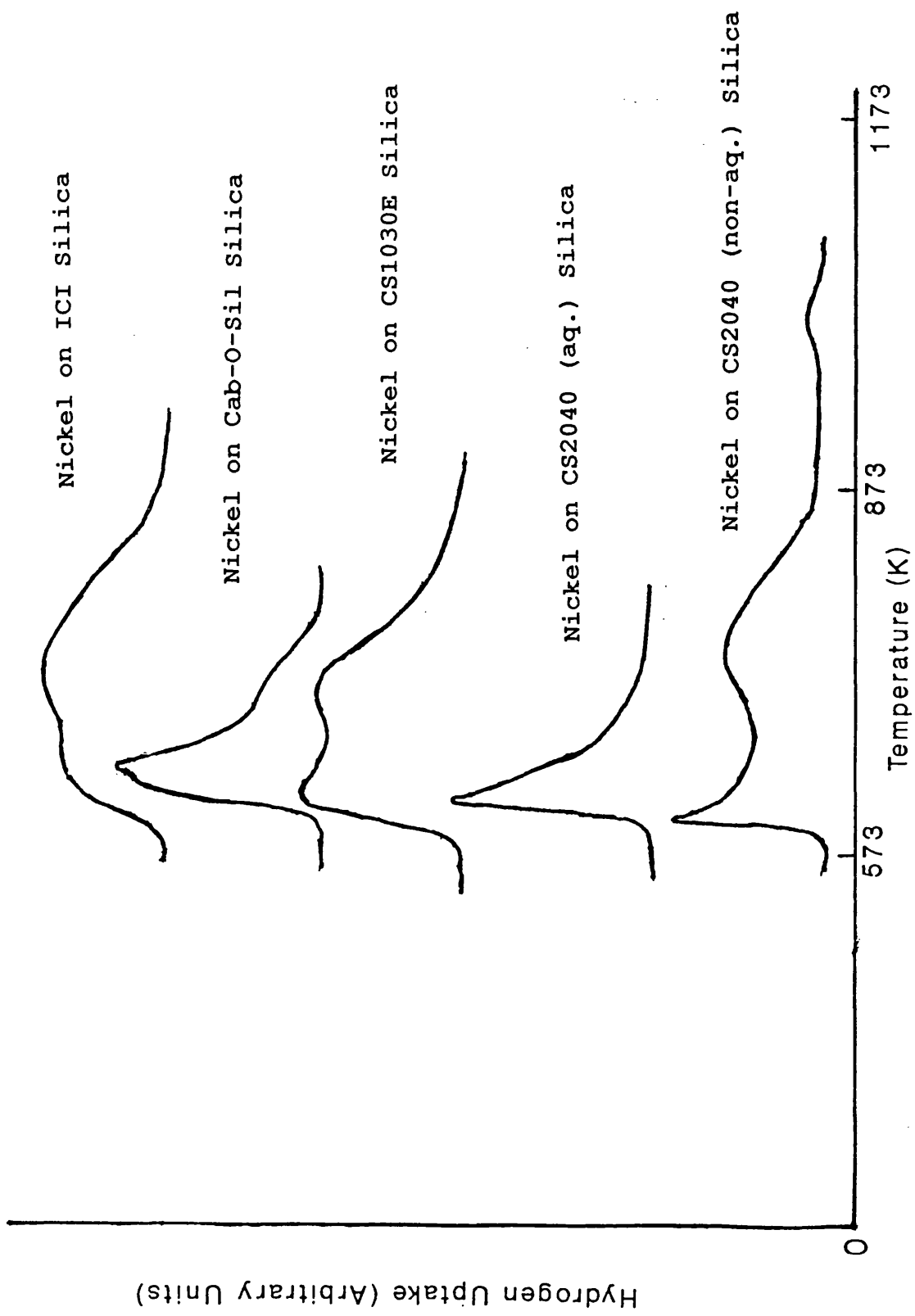


Fig. 4.4: T.P.R. Profiles of the Calcined 1 % w/w Nickel on Silica Catalysts

general pattern was evident. All the profiles, however, contained a common L.T. peak with T_{\max} values in the temperature interval 603 - 640 K. The T.P.R. profiles of 1 % nickel on ICI, CS1030E and CS2040 (non-aq.) silicas also exhibited large H.T. peaks (greater than 60 % of the total hydrogen uptake), with T_{\max} values in the temperature interval 703 - 736 K. Additionally, a small peak (3 % of the total hydrogen uptake and with $T_{\max} = 1000$ K) was present in the T.P.R. profile of 1 % nickel on CS2040 (non-aq.) silica. The profiles of 1 % nickel on CS2040 (aq.) and Cab-O-Sil silicas possessed, respectively, no H.T. peak and a relatively small H.T. peak (28 % of the total hydrogen uptake). The T.P.R. profile of 1 % nickel on Cab-O-Sil silica also displayed a shoulder on the low temperature side of the L.T. peak.

In summary, there was no general pattern discernible in the broad hydrogen uptake peaks observed in the T.P.R. profiles of the calcined nickel on silica catalysts. All the T.P.R. profiles shared, however, a common L.T. peak regardless of either the metal loading or the silica used as the support. The profiles of 1 % and 10 % nickel on Cab-O-Sil silica and 10 % nickel on CS1030E silica also displayed shoulders on the low temperature side of their respective L.T. peaks. The profiles of 1 % and 10 % nickel on ICI and CS1030E silicas all possessed relatively large H.T. peaks, as had the profile of 1 % nickel on CS2040 (non-aq.) silica. These H.T. peaks generally occurred at higher temperatures in the T.P.R. profiles of the 10 % nickel on silica catalysts relative to the 1 % nickel on silica catalysts.

Based on T.P.R. fingerprinting, the prepared calcined catalysts can be subdivided into two broad categories:

- i. catalysts which had a significant H.T. peak in their T.P.R. profiles;
- ii. catalysts which did not have a H.T. peak or possessed one of relatively small area in their profiles.

Nickel on ICI, CS1030E and CS2040 (non-aq.) silicas belonged to group (i), whereas nickel on Cab-O-Sil and CS2040 (aq.) silicas comprised group (ii).

4.2 Characterisation of the Reduced Catalysts

4.2.1 Carbon Monoxide Chemisorption

4.2.1(a) Carbon Monoxide Chemisorption in Hydrogen Carrier

Gas

The results of the experiment to determine the T.C.D. response to varying quantities of carbon monoxide are plotted in Figure 4.5. In this experiment, the mean of the detector response for three identical quantities of carbon monoxide in hydrogen carrier gas was determined for four distinct amounts of carbon monoxide [see Section 3.3.1(a)]. Figure 4.5 demonstrates that the T.C.D. response to carbon monoxide was linear in the region investigated. The detection limit for carbon monoxide in hydrogen carrier gas was estimated by drawing a best fit straight line through the calibration points using a least squares method. By extrapolating this line to zero detector response, the detection limit for carbon monoxide was estimated to be 3×10^{17} molecules.

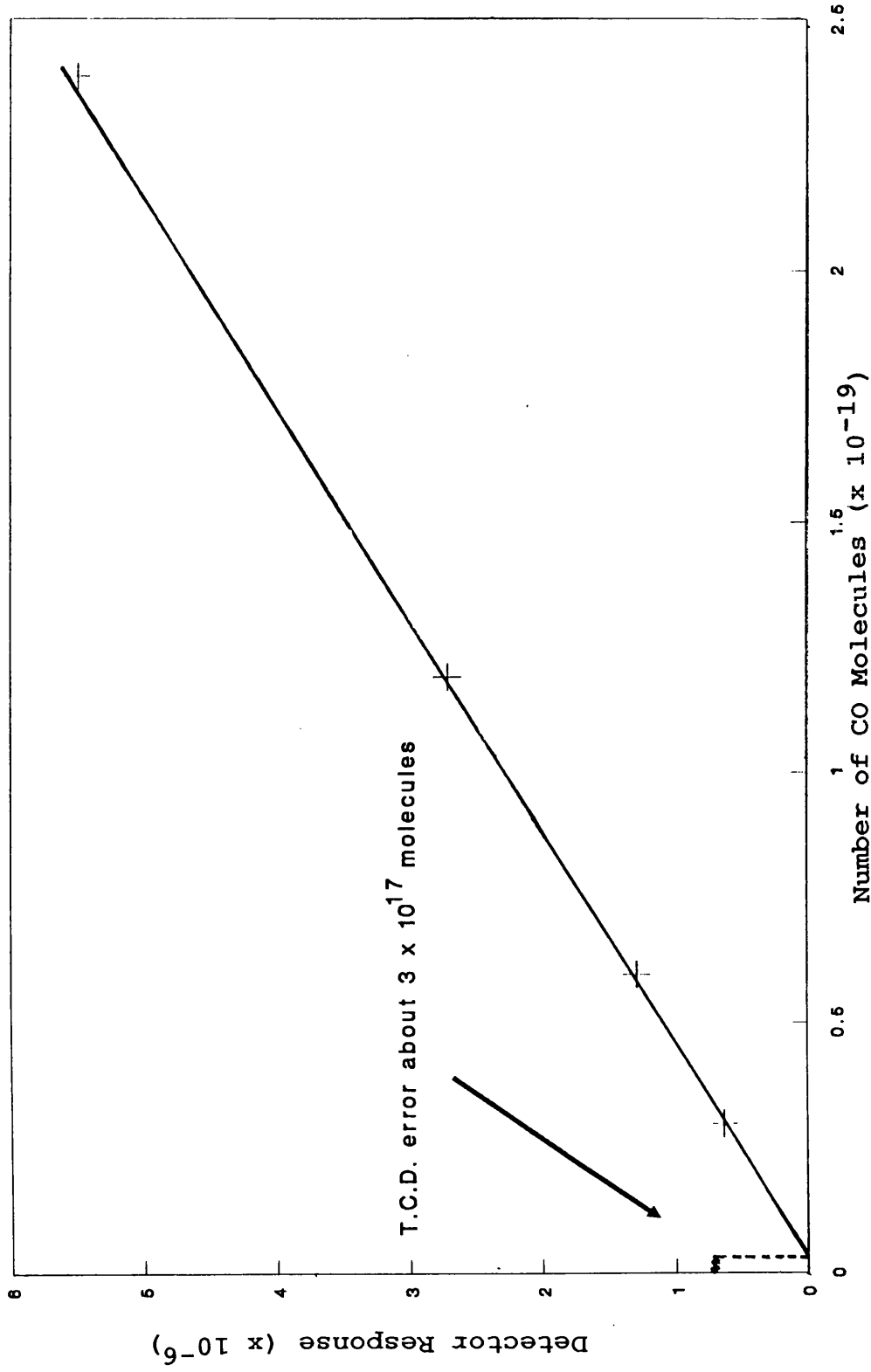


Fig. 4.5 T.C.D. Response Curve to Carbon Monoxide
Hydrogen Carrier Gas

The carbon monoxide chemisorption experiments were performed as described in Section 3.3.1(a) using a sample of each calcined catalyst which had been reduced in flowing hydrogen at 673 K using a standard procedure. After cooling the sample to 273 K, aliquots of carbon monoxide were pulsed into the stream of hydrogen carrier gas which was directed to flow through the reactor. Two adsorption experiments were performed using separate samples of each reduced catalyst.

The mass spectrometric analyses performed during the adsorption experiments on the eluted gases after the initial carbon monoxide pulses were introduced showed that, for all catalysts, the only m/e ratio which increased in intensity (in the region $m/e = 0$ to 50) was $m/e = 28$ (carbon monoxide). There was no evidence for the formation at 273 K of methane ($m/e = 16$), water ($m/e = 18$) or carbon dioxide ($m/e = 44$) during the adsorption of carbon monoxide on the catalysts in a hydrogen carrier gas. Hence, in the chemisorption experiments, the peak areas detected by the T.C.D. arose solely from unadsorbed carbon monoxide.

After saturation of each reduced catalyst had been achieved, i.e. when the respective peak areas for successive eluted pulses were equivalent ($\pm 2.5\%$), the peak areas of the last three eluted pulses of carbon monoxide were averaged and this value deemed to be equivalent to the detector response for the number of molecules in each pulse. By using this value, which was determined separately for each chemisorption experiment, the detected peak areas for the eluted pulses were then converted to the numbers of molecules of carbon monoxide eluted. These calculations

were straightforward as the amount of carbon monoxide present in a pulse was directly proportional to the peak area detected by the T.C.D. (see Figure 4.5, details given above). The difference between the number of carbon monoxide molecules detected in an eluted pulse and the number of molecules in the original aliquot gave the number of carbon monoxide molecules retained on the catalyst surface per pulse.

Adsorption isotherms for each catalyst were obtained by determining the total cumulative adsorption of carbon monoxide as a function of the total amount eluted (representative isotherms for the catalysts are given in Figures 4.6 to 4.13). For any particular catalyst, the number of carbon monoxide molecules adsorbed at saturation coverage under pulse-flow conditions corresponded to the number of molecules adsorbed in the plateau region of the adsorption isotherm plotted for the catalyst. The numbers of carbon monoxide molecules adsorbed at saturation coverage (expressed per gram of catalyst) are shown in Table 4.7. The data in Table 4.7 were obtained by averaging the results of the two experiments performed on separate samples of each reduced catalyst.

The number of surface nickel atoms present in each reduced catalyst sample was then calculated on the assumption that every chemisorbed carbon monoxide molecule bonded to two surface nickel atoms in a bridging configuration. As outlined in Section 1.4.1(a), the experimental evidence provided by other investigators indicates that carbon monoxide is bound predominantly in this form. From the numbers of surface nickel atoms

Fig. 4.6

Cumulative Amount of CO Adsorbed
Versus Cumulative Amount Eluted
10 % w/w Ni on ICI Silica

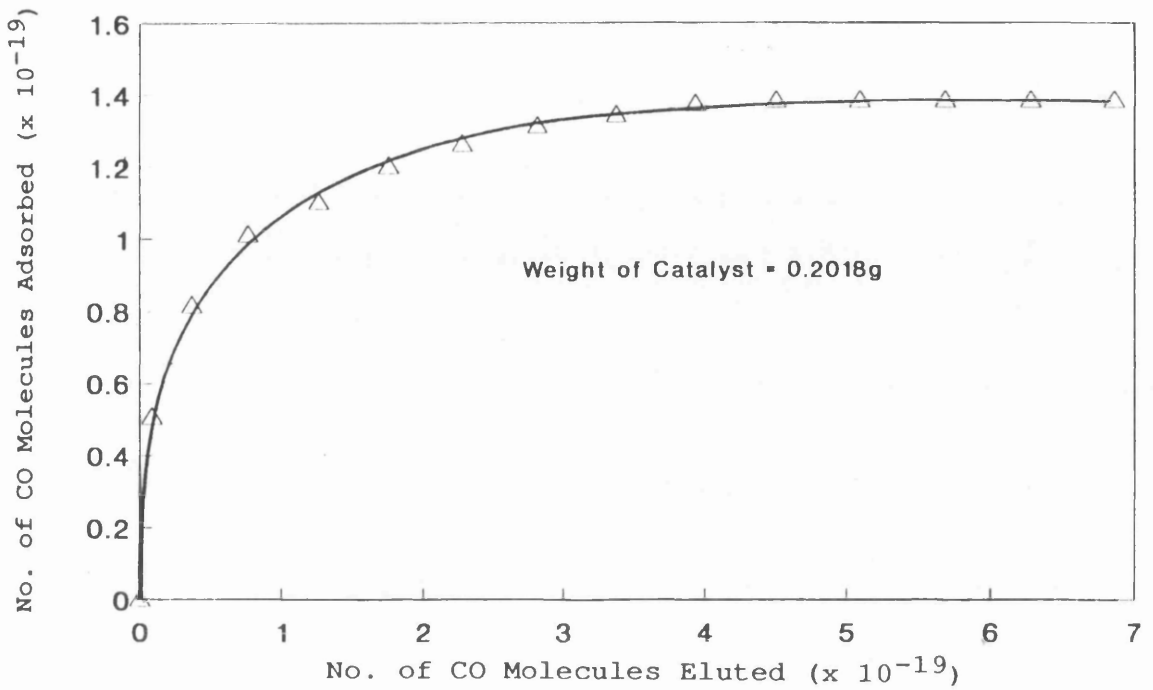


Fig. 4.7

Cumulative Amount of CO Adsorbed
Versus Cumulative Amount Eluted
10 % w/w Ni on Cab-O-Sil Silica

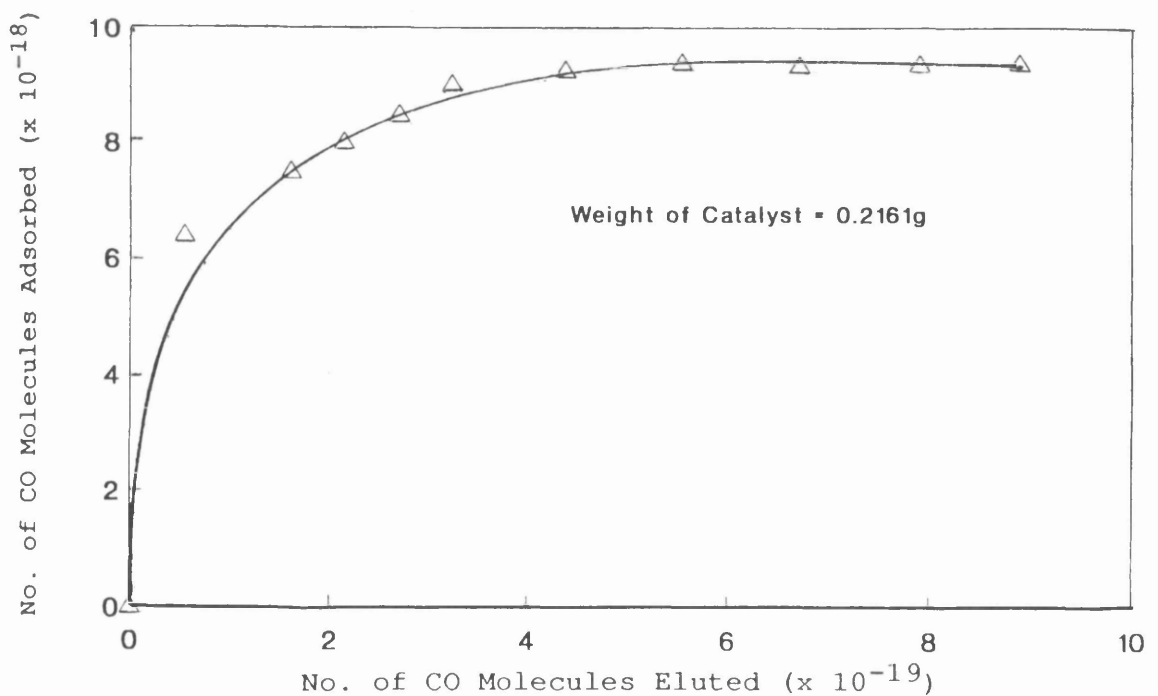


Fig. 4.8

Cumulative Amount of CO Adsorbed
Versus Cumulative Amount Eluted
10 % w/w Ni on CS1030E Silica

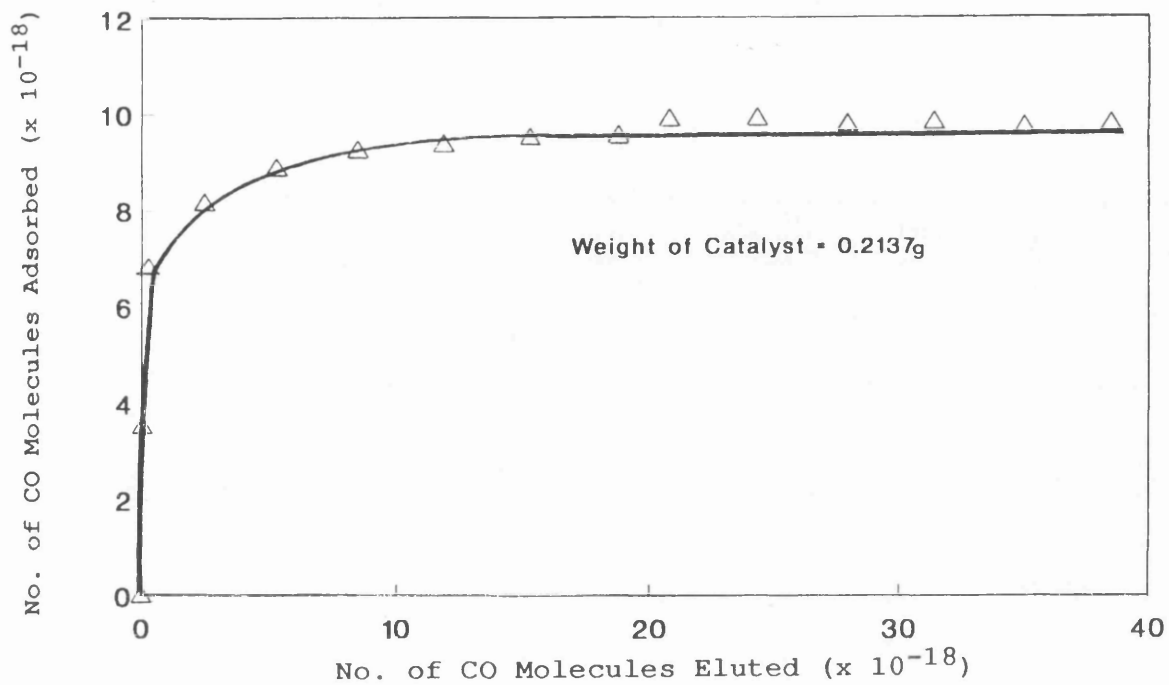


Fig. 4.9

Cumulative Amount of CO Adsorbed
Versus Cumulative Amount Eluted
1 % w/w Ni on ICI Silica

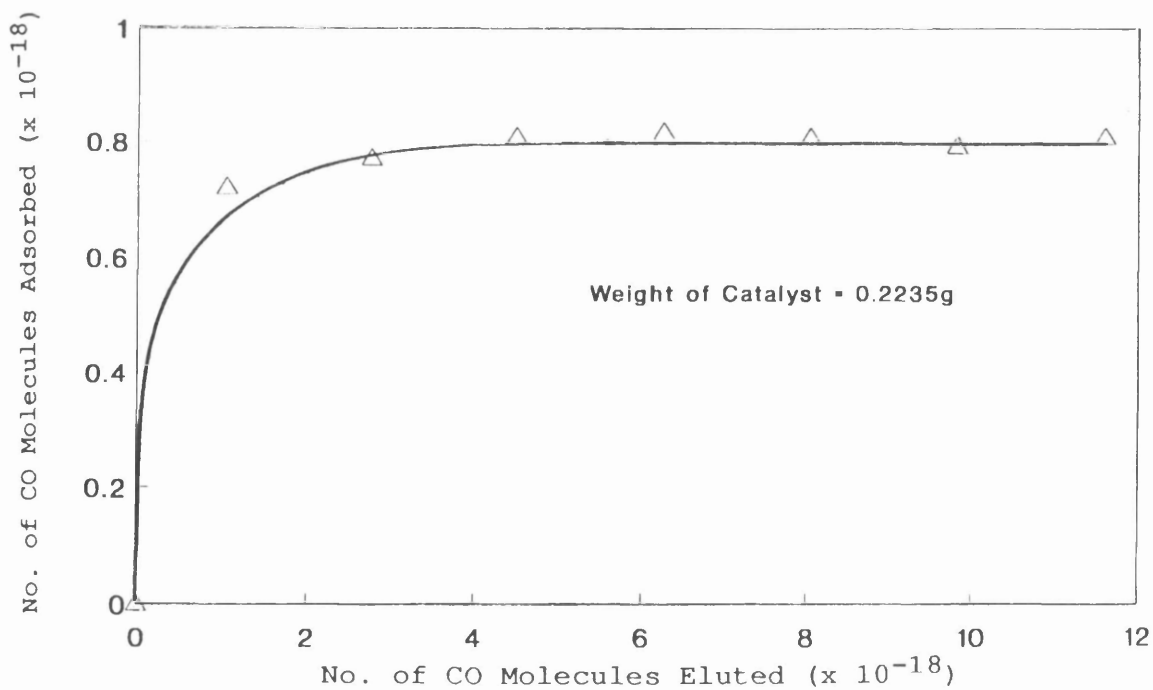


Fig. 4.10

Cumulative Amount of CO Adsorbed
Versus Cumulative Amount Eluted
1 % w/w Ni on Cab-O-Sil Silica

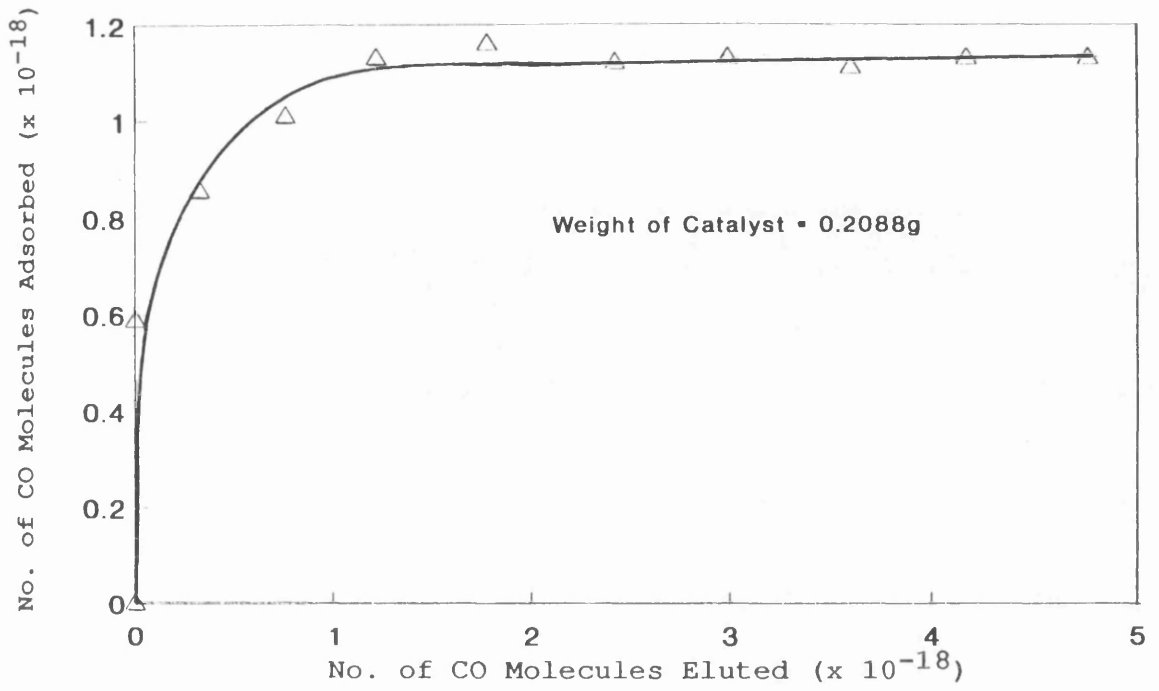


Fig. 4.11

Cumulative Amount of CO Adsorbed
Versus Cumulative Amount Eluted
1 % w/w Ni on CS1030E Silica

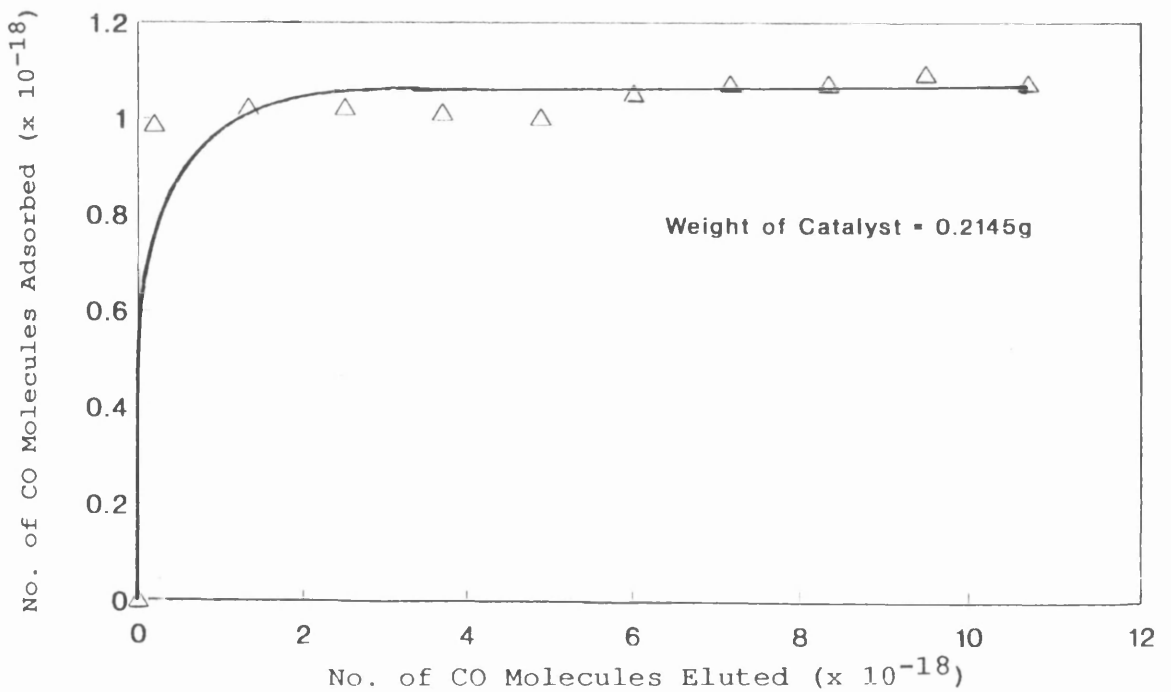


Fig. 4.12

Cumulative Amount of CO Adsorbed
Versus Cumulative Amount Eluted
1 % w/w Ni on CS2040 (aq.) Silica

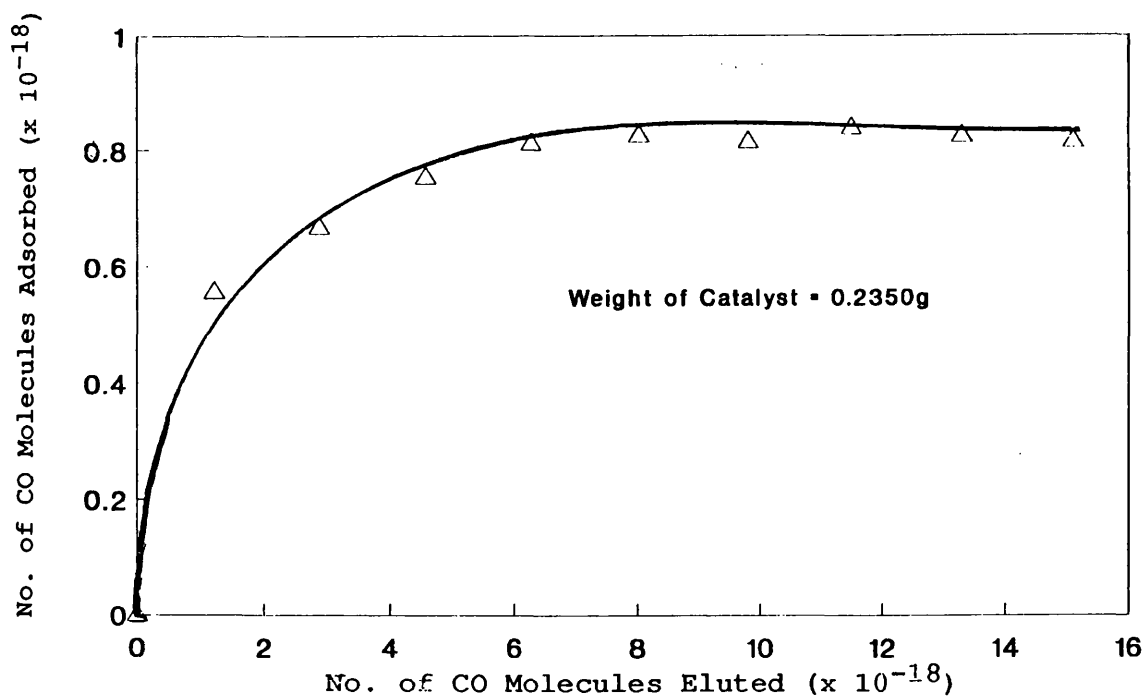
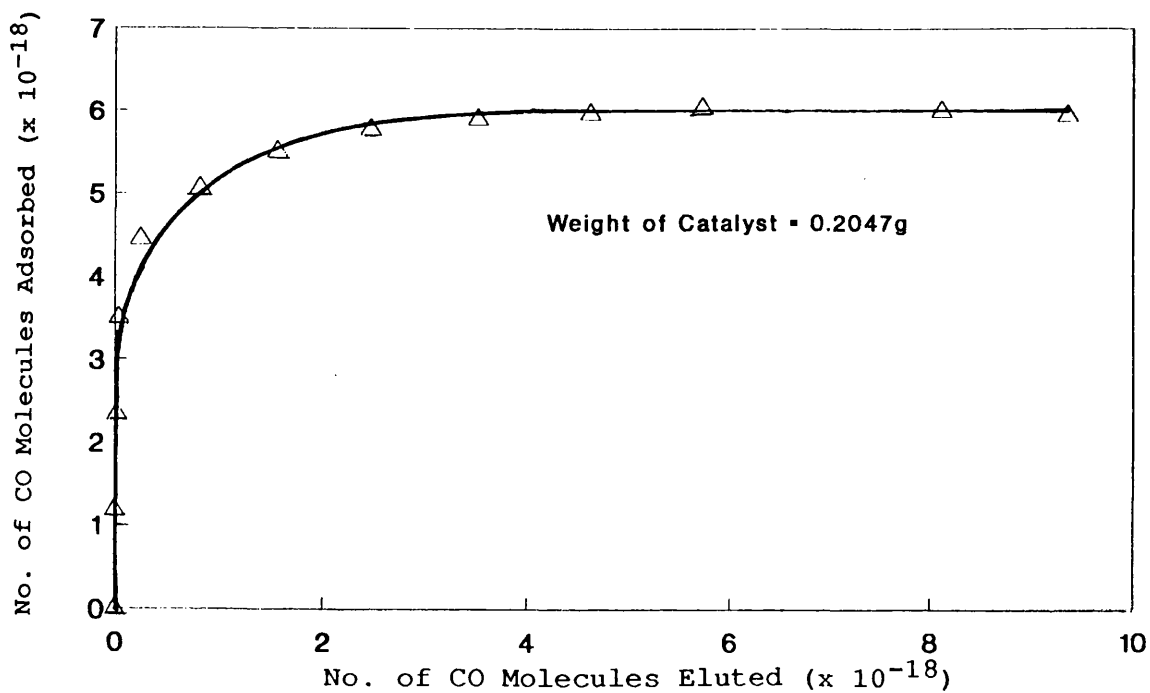


Fig. 4.13

Cumulative Amount of CO Adsorbed
Versus Cumulative Amount Eluted
1 % w/w Ni on CS2040 (non-aq.) Silica



determined, the dispersions (D), surface weighted average particle diameters (d_s) and nickel surface areas (S_{Ni}) of the catalysts were calculated using equations 1.1 (defined in Section 1.3.1), 1.6 (Section 1.3.2) and 1.11 (Section 1.3.3), respectively. These parameters are listed below in Table 4.8 and are in good agreement with the corresponding parameters obtained by T.E.M. analyses (Section 4.2.2).

Table 4.7

Averaged Carbon Monoxide Chemisorption Data for
Calcined Catalysts Reduced by the Flow Method

Expt. No.	Catalyst	Amount of CO Adsorbed ^a
1	10 % Ni/ICI	79
2	10 % Ni/Cab-O-Sil	33
3	10 % Ni/CS1030E	42
4	1 % Ni/ICI	6
5	1 % Ni/Cab-O-Sil	6
6	1 % Ni/CS1030E	4
7	1 % Ni/CS2040 (aq.)	4
8	1 % Ni/CS2040 (non-aq.)	30

a. Units: molecules(g catalyst)⁻¹ x 10⁻¹⁸.

4.2.1(b) Carbon Monoxide Chemisorption in Helium Carrier Gas

Prior to the chemisorption experiments described in the previous section, experiments were performed as detailed in Section 3.3.1(b) using helium as the carrier gas for the injections of carbon monoxide onto the catalysts. Various reduction procedures were used and are outlined in Table 3.1, Section 3.3.1(b). Carbon monoxide chemisorption

experiments were then performed on the reduced calcined catalysts in a flow of helium carrier gas at 273 K.

Table 4.8

Parameters Derived from Carbon Monoxide Chemisorption Data
For Catalysts Reduced by the Flow Method

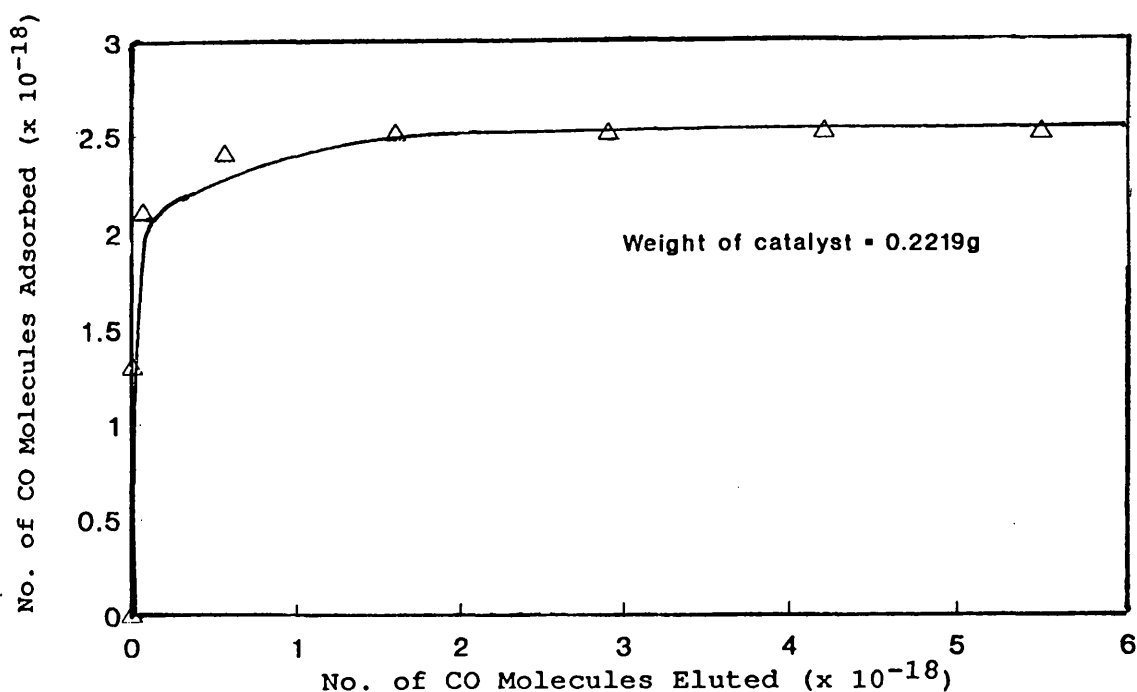
Expt. No.	Catalyst	D (%)	d_g (nm)	S_{Ni} [$m^2 (g Ni)^{-1}$]
1	10 % Ni/ICI	15	7	99
2	10 % Ni/Cab-O-Sil	6	17	40
3	10 % Ni/CS1030E	8	13	51
4	1 % Ni/ICI	9	11	61
5	1 % Ni/Cab-O-Sil	7	14	47
6	1 % Ni/CS1030E	5	22	31
7	1 % Ni/CS2040 (aq.)	5	20	33
8	1 % Ni/CS2040 (non-aq.)	42	2	283

The only catalyst reduction procedure found to result in a measurable adsorption of carbon monoxide was that described in experiment number 2, Table 3.1. In this experiment, a sample of the unreduced calcined 10 % nickel on ICI silica catalyst was heated at a constant rate ($\beta = 5$ K min.⁻¹) to 723 K in a stream of 6 % v/v hydrogen in argon. Immediately after the final temperature was attained, the gas stream through the catalyst bed was changed to pure hydrogen and the temperature maintained at 723 K for a further two hours. After this time the catalyst was flushed with helium at 723 K and then cooled under flowing helium to 273 K. Carbon monoxide was then pulsed through the catalyst bed using helium as the carrier gas. The

adsorption isotherm obtained for carbon monoxide chemisorption on this catalyst, plotted in the identical manner as described in Section 4.2.1(a), is shown in Figure 4.14.

Fig. 4.14

Cumulative Amount of CO Adsorbed
Versus Cumulative Amount Eluted
10 % Ni on ICI Silica (He Carrier Gas)



From this adsorption isotherm, the amount of carbon monoxide adsorbed by the catalyst to give saturation coverage under pulse-flow conditions was determined to be 1.1×10^{19} molecules(g catalyst) $^{-1}$. From equations 1.1, 1.6 and 1.11 (defined in Sections 1.3.1, 1.3.2 and 1.3.3, respectively); $D = 2\%$, $d_s = 47$ nm and $S_{Ni} = 14$ m 2 (g nickel) $^{-1}$, respectively. These parameters differ significantly from those obtained by carbon monoxide adsorption experiments on the reduced calcined 10 % nickel on ICI silica catalyst using hydrogen as the carrier gas, i.e. $D = 15\%$, $d_s = 7$ nm and $S_{Ni} = 99$ m 2 (g nickel) $^{-1}$. The

adsorption experiment using helium as the carrier gas, however, was performed using a sample of the 10 % nickel on ICI silica catalyst reduced under significantly different reduction conditions.

4.2.2 Transmission Electron Microscopic Analyses

Transmission electron micrographs have been recorded for all of the reduced 10 % nickel on silica catalysts and most of the reduced 1 % nickel on silica catalysts. As described in Section 3.3.2, calcined catalysts were reduced at 673 K in a flow of pure hydrogen using the identical procedure to that adopted as standard to reduce catalysts before the carbon monoxide chemisorption experiments in hydrogen carrier gas. Following reduction and cooling to ambient temperature, the reduced catalyst samples were passivated in a flow of oxygen in nitrogen gas.

Representative portions of typical micrographs recorded for the passivated catalyst samples are shown in Figures 4.15 to 4.20. In general, the micrographs exhibited a reasonable contrast between nickel particles and the silica supports, with the majority of particles being approximately spherical in shape. In areas of the supports free from nickel particles, the granular textures of the silicas were evident (9).

For the 1 % nickel on CS2040 (aq.) silica catalyst, the E.D.A.X. microanalysis on a supported particle revealed the presence of nickel metal (from the particle), silicon (from the support), oxygen (from the particle and the support), gold (from the microscope), copper (from the copper grid) and carbon (from the carbon film covering the

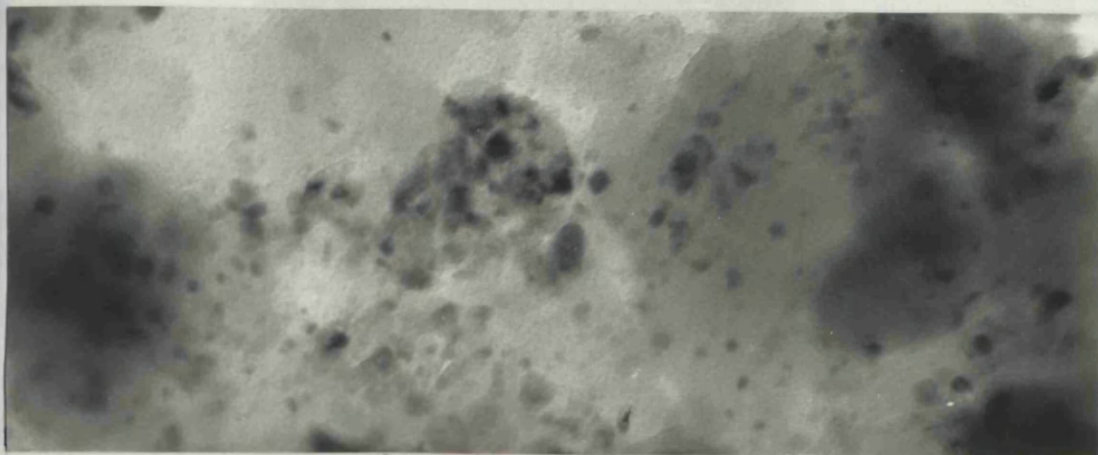


Fig. 4.15
10 % Nickel on ICI Silica
(x 360,000)



Fig. 4.16
10 % Nickel on Cab-O-Sil Silica
(x 300,000)

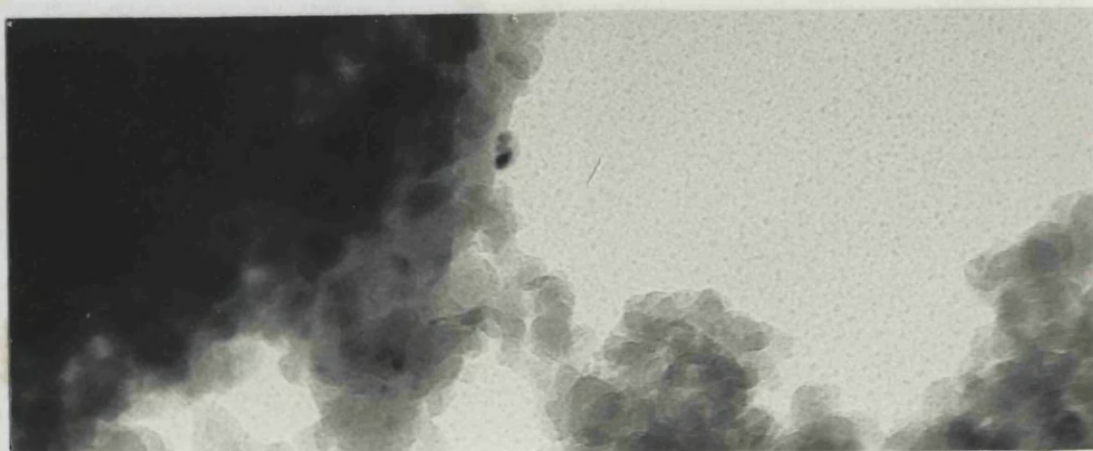


Fig. 4.17
10 % Nickel on CS1030E Silica
(x 360,000)

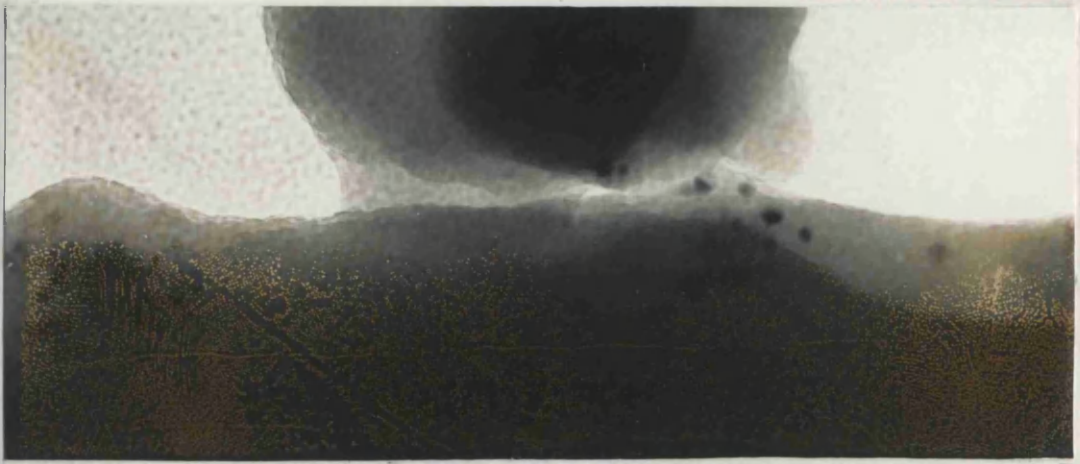


Fig. 4.18
1 % Nickel on ICI Silica
(x 360,000)



Fig. 4.19
1 % Nickel on CS2040
(aq.) Silica (x 294,000)

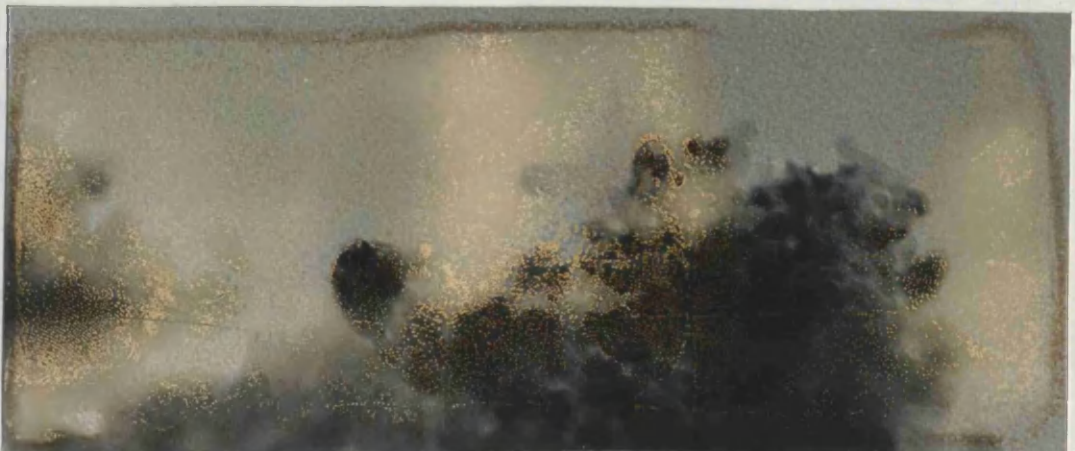


Fig. 4.20
1 % Nickel on CS2040
(non-aq.) Silica (x 360,000)

copper grid). No other elements were identified as being present.

For most catalysts examined by T.E.M., three separate particle size distributions were determined. If possible, each particle size distribution was based on one micrograph, but for some catalysts it was necessary to use two or three separate micrographs per particle size distribution to increase the number of particle diameters measured. For each particle size distribution, the diameters of between 125 to 287 particles were measured and the particle size distribution plotted in the form of a histogram using 1 nm size intervals (86). A cumulative particle size distribution histogram was also plotted for each catalyst utilising the combined data from the three separate particle size distributions determined for each catalyst. These cumulative particle size distribution histograms were found to be representative of the distribution of particle sizes in the catalysts as they were similar to their respective component histograms from which they were derived, i.e. in each case, the respective particle size distributions for the three separate areas of each catalyst were similar. The cumulative particle size distribution histograms are illustrated in Figures 4.21 to 4.26. The total numbers of particles measured are also given in the particle size distribution histograms.

Particle dimensions were evaluated according to the following criteria:

- i. Particular attention was given to particles located around the edges of the support where the difference in

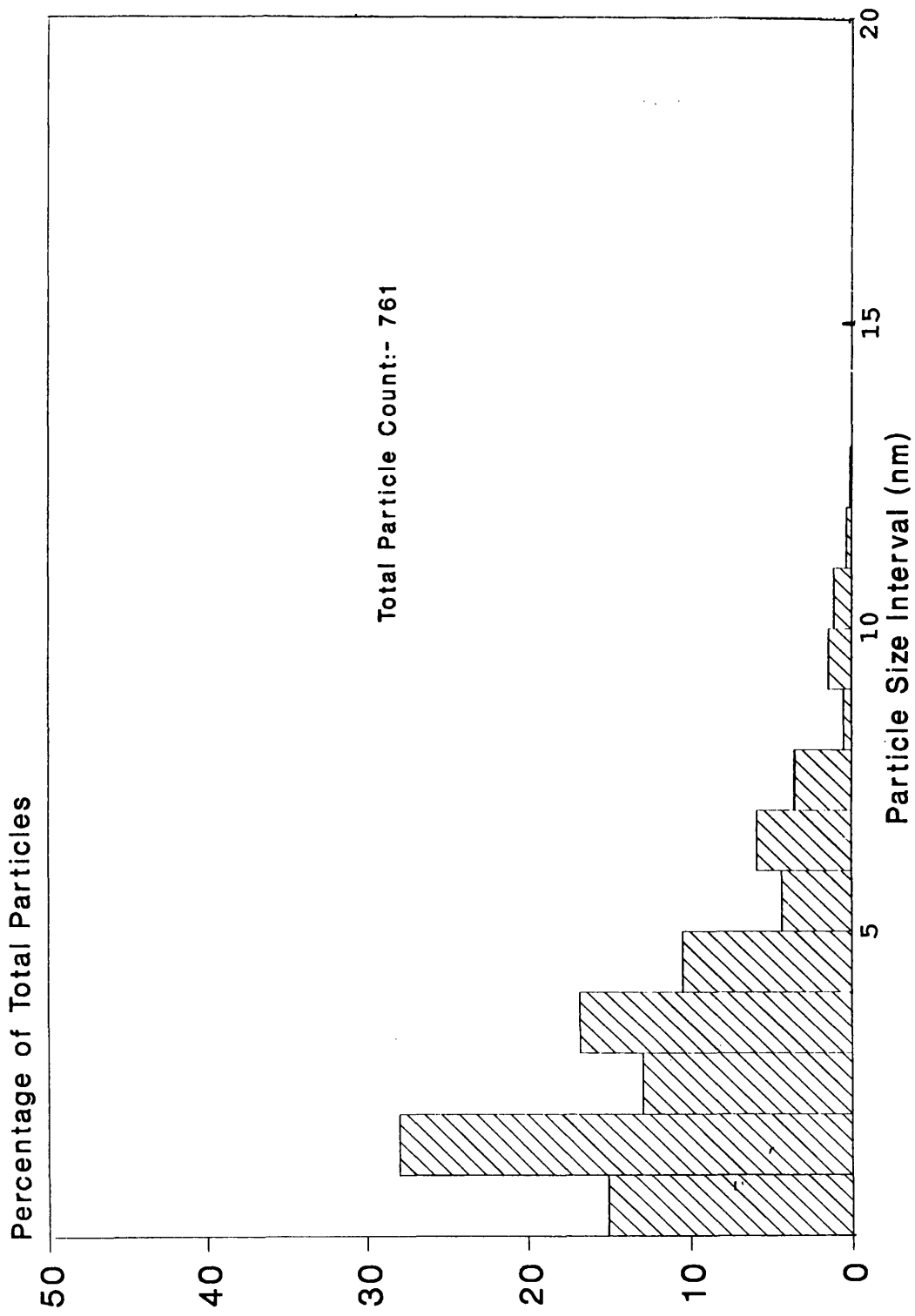


**Fig. 4.21 Combined Particle Size Distributions
10 % w/w Ni on ICI Silica**

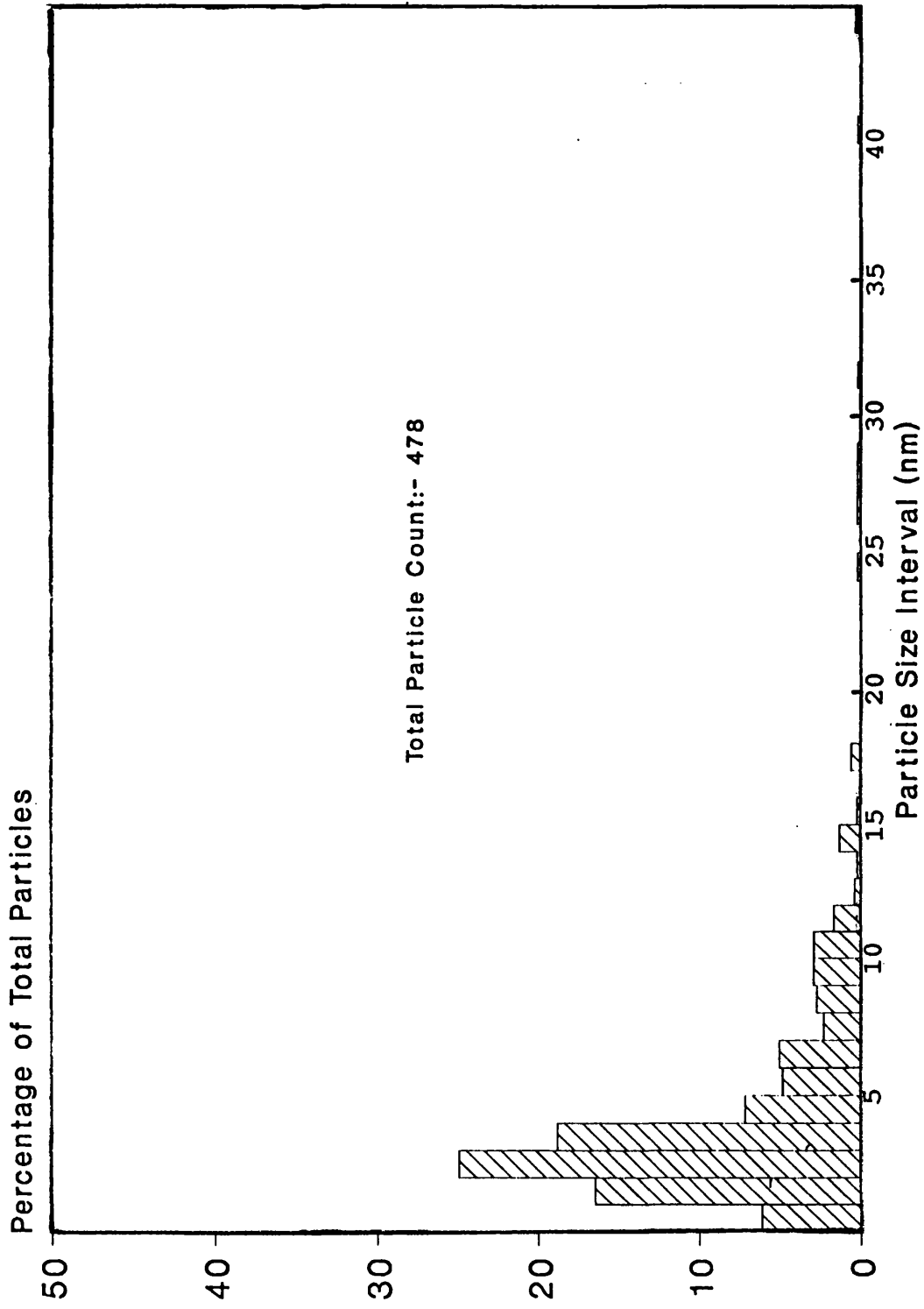


Fig. 4.22 Combined Particle Size Distributions
10 % w/w Ni on Cab-O-Sil Silica

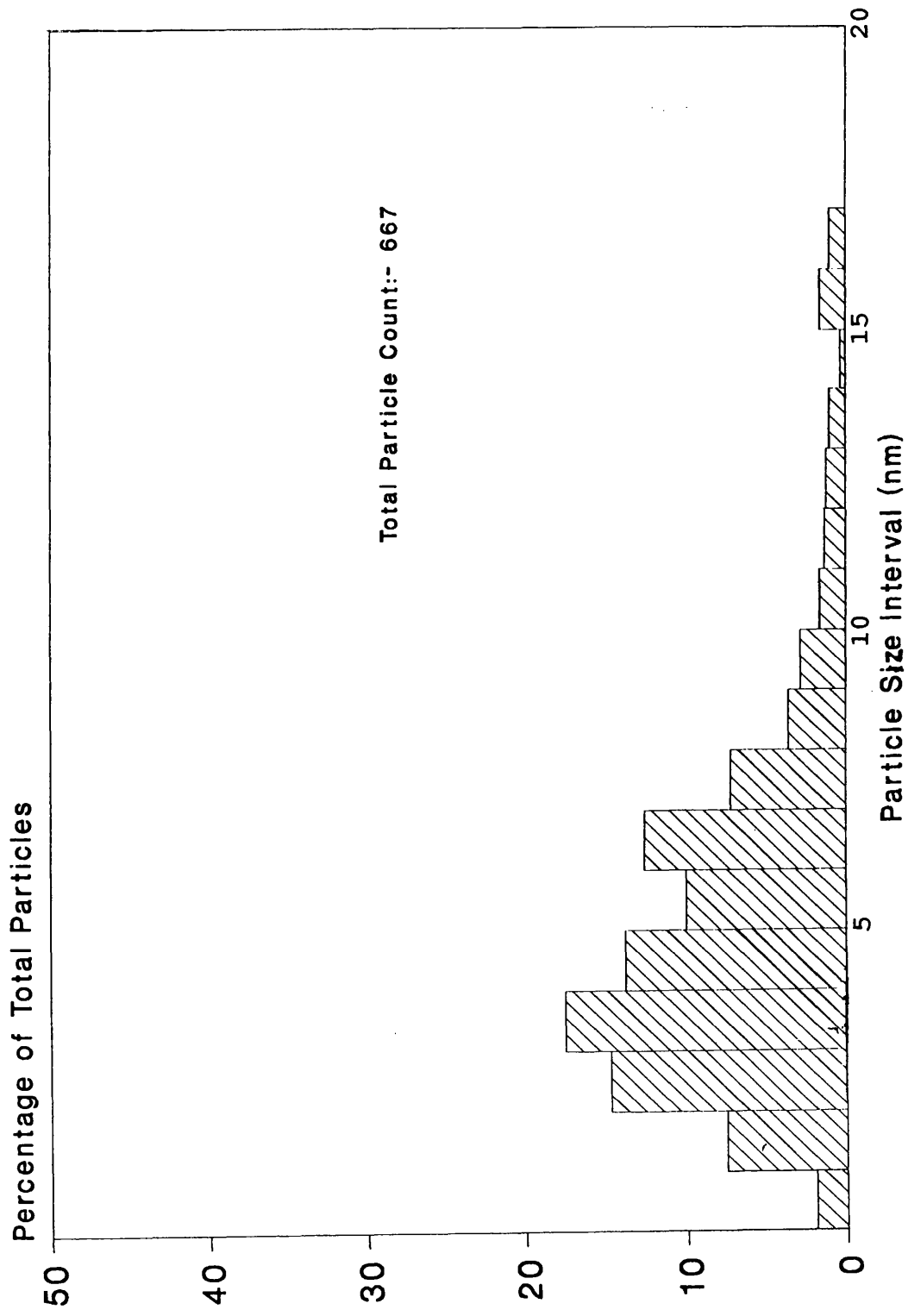


Fig. 4.23 Combined Particle Size Distributions
10 % w/w Ni on CS1030E Silica

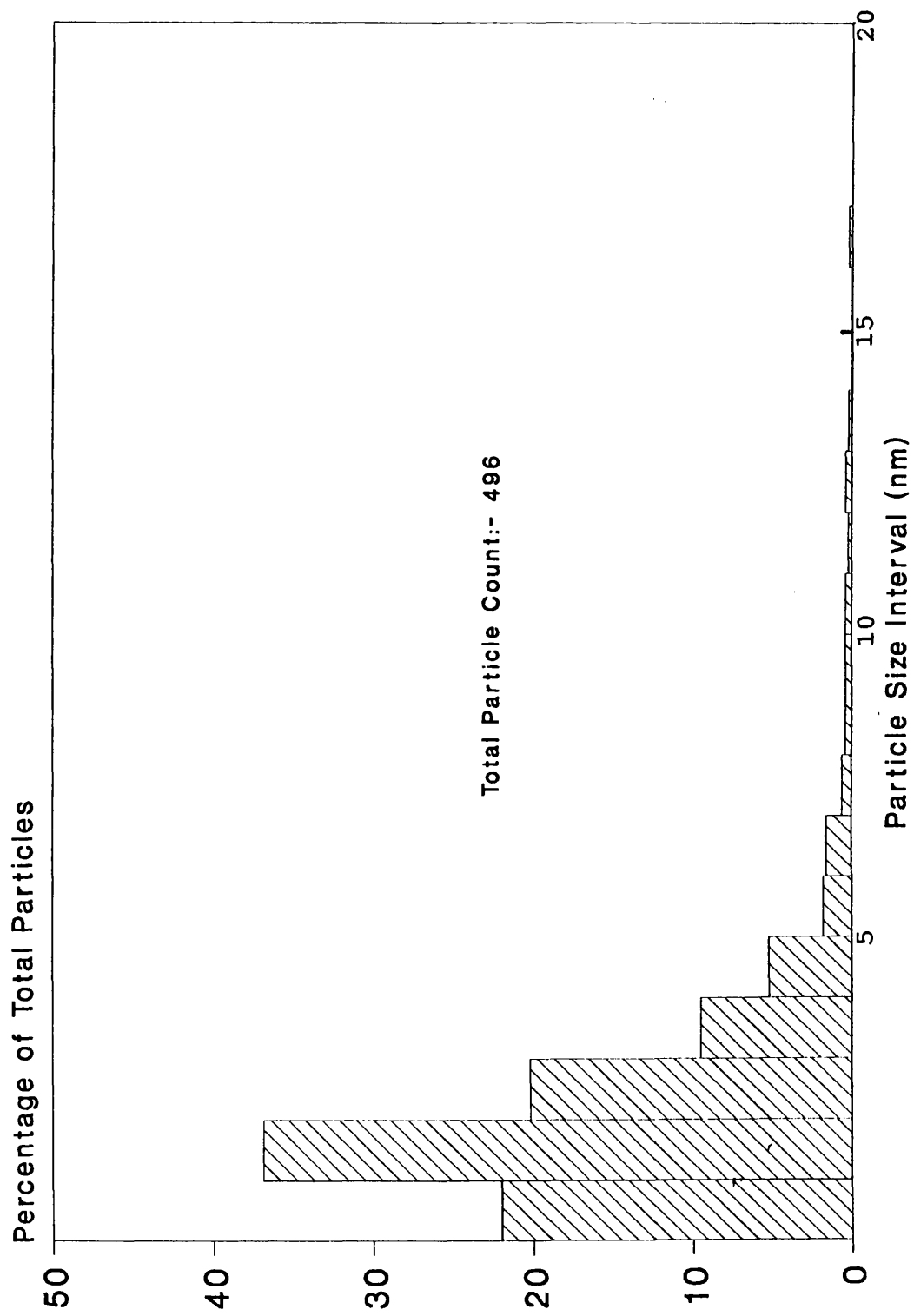


Fig. 4.24 Combined Particle Size Distributions
1 % w/w Ni on ICI Silica

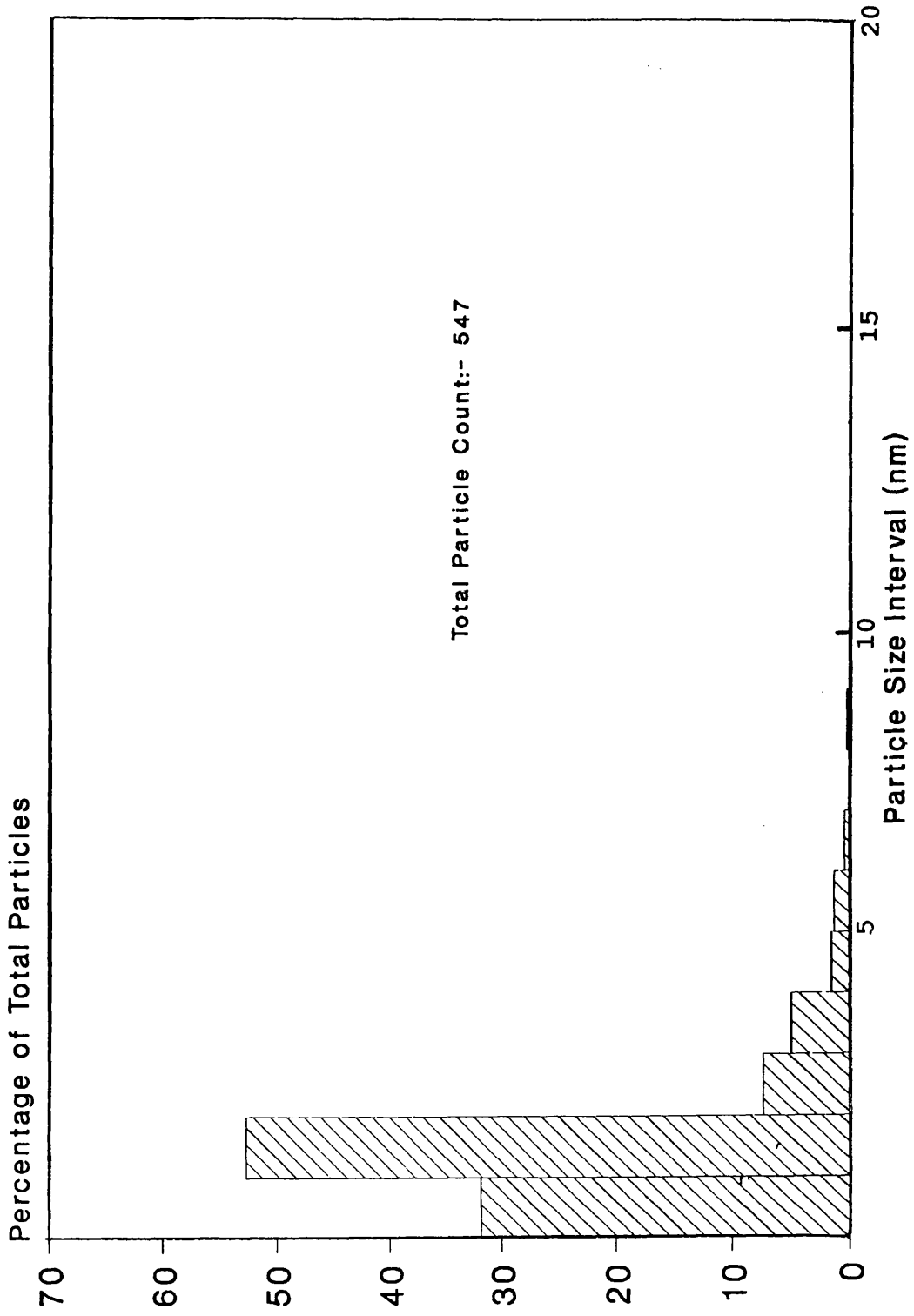


Fig. 4.25 Combined Particle Size Distributions
1 % w/w Ni on CS2040 Silica (aq.)

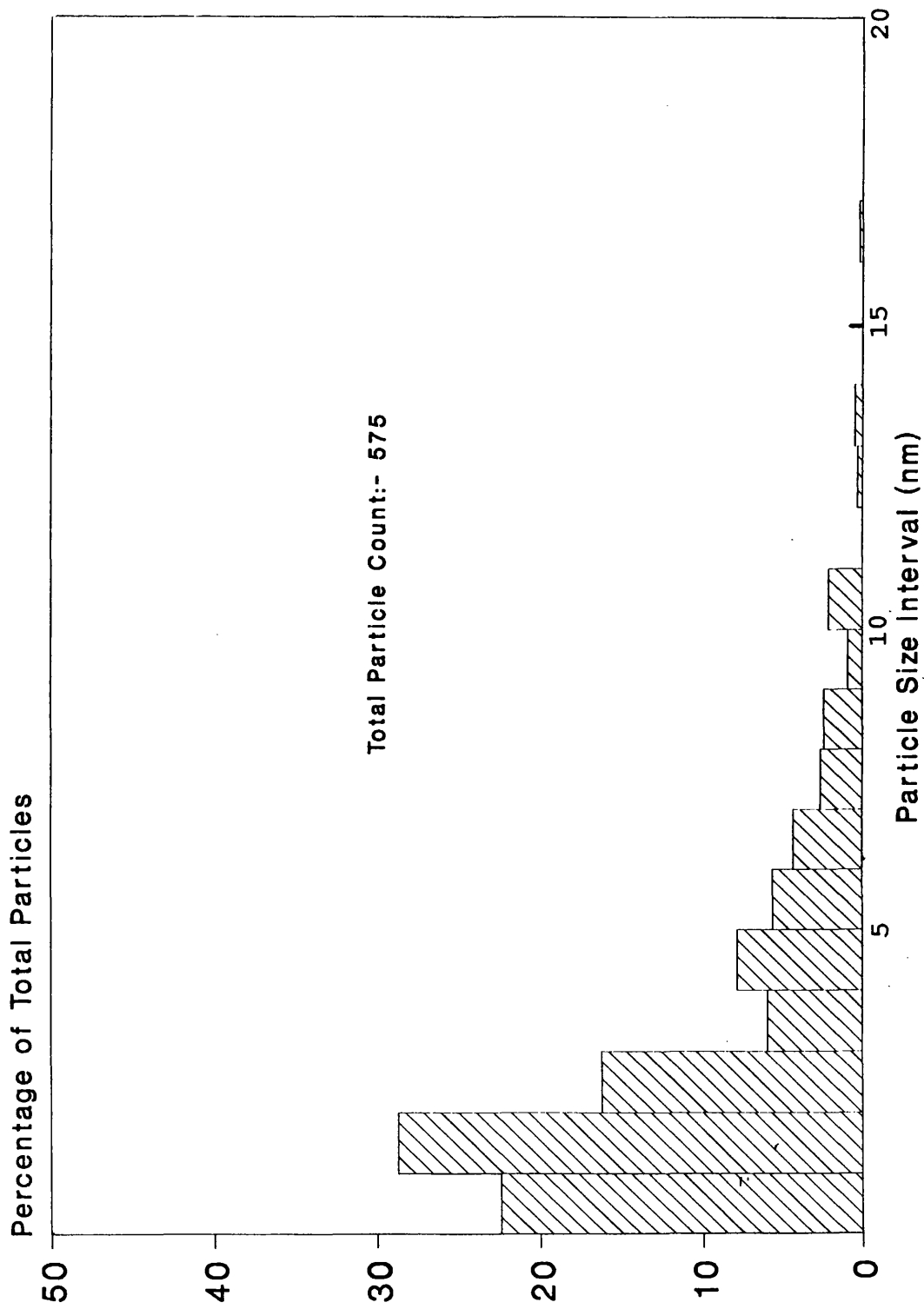


Fig. 4.26 Combined Particle Size Distributions
1 % w/w Ni on CS2040 Silica (non-aq.)

contrast between the support and nickel particles was greatest (23);

ii. The particle diameter was readily obtained for spherically shaped particles by direct measurement (23);

iii. In the case of elliptical or irregularly shaped particles, the mean of the largest and the smallest dimensions of the particle was calculated and the result quoted as the diameter (167).

The surface weighted average diameter (d_s) of each catalyst was calculated by applying expression 1.12 (defined in Section 1.4.2.) to the cumulative particle size distribution data. The d_s values for the catalysts are given, together with the respective values of nickel dispersion (D) and nickel surface area (S_{Ni}), in Table 4.9. D and S_{Ni} were calculated for each catalyst by rearranging equations 1.6 (Section 1.3.2) and 1.11 (Section 1.3.3), respectively.

Table 4.9

Parameters Derived from T.E.M. Data For Catalysts Reduced by the Flow Method

Catalyst	D (%)	d_s (nm)	S_{Ni} [$m^2/(g Ni)$]
10 % Ni on ICI	16	6	110
10 % Ni on Cab-O-Sil	5	19	36
10 % Ni on CS1030E	11	9	72
1 % Ni on ICI	15	7	100
1 % Ni on CS2040 (aq.)	32	3	210
1 % Ni on CS2040 (non-aq.)	13	8	90

Electron beam damage prevented measurements on 1% Ni on Cab-O-Sil and 1% Ni on CS1030E

A direct comparison of the data presented in the Table 4.9 can be made with the values for the corresponding parameters derived from the carbon monoxide chemisorption experiments listed in Table 4.8 (168). Such a comparison reveals that excellent agreement existed for data on the 10 % nickel on silica catalysts. The agreement between the two techniques was less satisfactory for the 1 % nickel on silica catalysts, notably for the catalysts prepared from the CS2040 silica. Similar differences between chemisorption and T.E.M. data can be found for nickel on silica catalysts in the literature (23, 169) and, in Section 5.1.3, explanations are proposed to why there were particularly large discrepancies between the two techniques for catalysts prepared from CS2040 silica.

4.3 Reaction Chemistry

In this section, subsections 4.3.1 and 4.3.2 detail the results obtained from testing the reduced catalysts by using ethene hydrogenation as a test reaction. By analysing the behaviour of the catalysts, it was possible to determine if any of the catalysts were behaving in an anomalous manner toward this reaction.

Section 4.3.1 describes the results obtained with respect to the deactivation behaviour over a series of hydrogenation reactions of the calcined catalysts reduced by the static technique (Section 3.4.1.1).

Section 4.3.2 details the results obtained from the single ethene hydrogenation reactions performed using the calcined catalysts reduced by the standard reduction technique in flowing hydrogen (Section 3.4.2.1).

4.3.1 Catalysts Reduced by the Static Method

The calcined catalysts were reduced at 723 K in the manner described in Section 3.4.1.1. After reduction and cooling to 273 K, up to six aliquots of a mixture of hydrogen and ethene were added successively to a reactor containing a sample of a reduced 10 % nickel on silica catalyst; the procedure for the reduced 1 % nickel on silica catalysts was slightly different, as described below. The pressure in the reaction vessel was then monitored for ca. 80 minutes after addition of each aliquot. Mass spectrometric analyses showed ethane to be the only product of reaction for all catalysts. The observed pressure change, therefore, after addition of an aliquot of the hydrogen and ethene mixture to the reactor was solely due to the consumption of hydrogen to form ethane. Hence the pressure change in the reactor was used to monitor the progress of each hydrogenation reaction.

A maximum of six hydrogenation reactions were performed using a sample of each 10 % nickel on silica catalyst. The experiments performed are listed in Table 4.10a. The reproducibility of the data was tested by duplicating two of the experiments and these are also listed in this table.

A small modification to the experimental procedure was introduced for the ethene hydrogenation studies performed using the reduced 1 % nickel on silica catalysts. For the first hydrogenation reaction performed using each 1 % nickel on silica catalyst, a relatively small amount of [¹⁸O]-carbon dioxide (ca. 1.25×10^{19} molecules) was added to the reactor with the aliquot of the hydrogen and ethene mixture. The progress of the reaction was then monitored as before.

Table 4.10a

Reactions Performed Using 10 % Nickel on Silica Catalysts
Reduced by the Static Method

Catalyst	Expt. No.	Initial Rate of 1st Hydrogenation Reaction ^a
Ni/ICI silica	1	3.7
Ni/Cab-O-Sil silica	2	5.7
Ni/Cab-O-Sil silica	2a ^b	1.3
Ni/CS1030E silica	3	6.1
Ni/CS1030E silica	3a ^b	5.6

a. Units: mol.s.⁻¹(g catalyst)⁻¹ x 10⁵.

b. Duplicate experiments.

As explained later in this section, mass spectrometric analysis of the condensable gases after the first hydrogenation reaction can quantify the amount of oxygen exchange between any exchangeable residual oxygen present on the surface of a catalyst and the added [¹⁸O]-carbon dioxide. Up to five further hydrogenation reactions were then performed in the normal way using each catalyst with no [¹⁸O]-carbon dioxide added to the reactor. The experiments performed are listed in Table 4.10b. The reproducibility of the data was tested by duplicating two of the experiments and these are also listed in this table.

In addition to listing the experiments performed, Tables 4.10a and 4.10b show the initial rates of the first hydrogenation reactions expressed in mol.s.⁻¹(g catalyst)⁻¹. The initial rate for each reaction was determined by drawing a tangent to the curve of a Δ(Pressure) versus time plot at

time equal to zero; the initial rate was equal to the gradient of this tangent. This method is illustrated in Figure 4.27 for the first hydrogenation reaction performed using 10 % nickel on ICI silica (experiment number 1, Table 4.10a). The initial rate expressed in moles per second per gram of catalyst was then calculated.

Table 4.10b

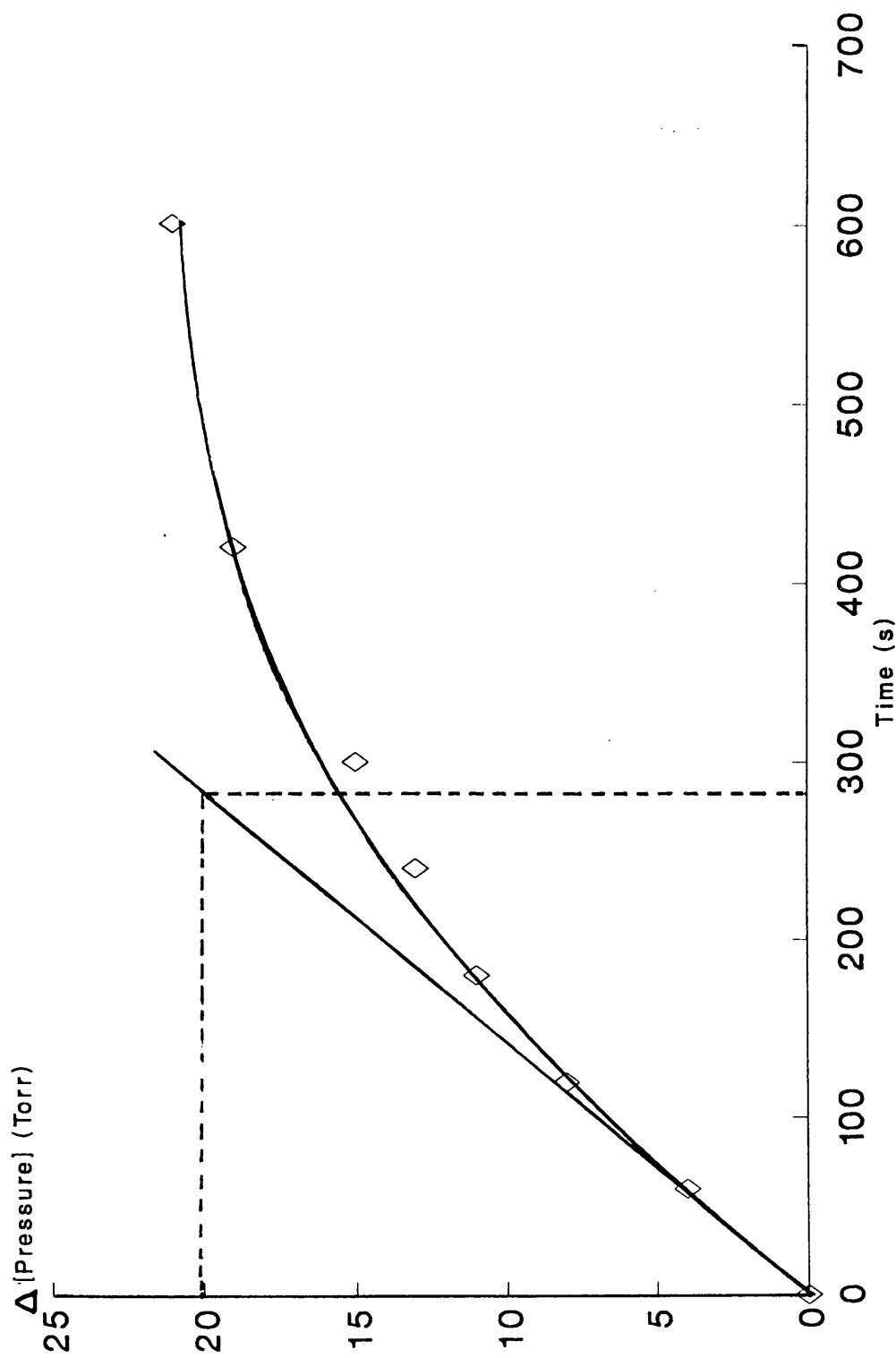
Reactions Performed Using 1 % Nickel on Silica Catalysts
Reduced by the Static Method

Catalyst	Expt. No.	Initial Rate of 1st Hydrogenation Reaction ^a
Ni/ICI silica	4	0.2
Ni/Cab-O-Sil silica	5	1.2
Ni/Cab-O-Sil silica	5a ^b	0.5
Ni/CS1030E silica	6	1.7
Ni/CS2040 (aq.) silica	7	0.7
Ni/CS2040 (aq.) silica	7a ^b	0.2
Ni/ICI silica (control)	8	0.0

a. Units: $\text{mol.s.}^{-1}(\text{g catalyst})^{-1} \times 10^5$.

b. Duplicate experiments.

Comparison of the duplicate experiments with their respective original experiments reveals that, in general, the reproducibility of the rate data was poor, i.e. experiment number 2 compared with 2a (Table 4.10a); 5 compared with 5a (Table 4.10b) and 7 compared with 7a (Table 4.10b). In addition, the oxidised 1 % nickel on ICI silica catalyst used in the control experiment (experiment number



Illustrated Example of Initial Rate
Calculation; 10 % Nickel on ICI Silica
First Hydrogenation Reaction

Fig. 4.27

8, Table 4.10b) was found to be completely inactive for ethene hydrogenation.

Despite the observed irreproducibility of the results, valuable information on the deactivation behaviours of the catalysts can be obtained by considering the experiments using the more active samples of the catalysts (experiment numbers 1, 2, 3, 4, 5, 6 and 7). If the initial rates for successive hydrogenation reactions are plotted against reaction number for these experiments, it can be seen that there was a gradual loss of catalytic activity, for all the catalysts generally, as the series of reactions progressed. These plots are illustrated for all the catalysts tested in Figures 4.28 and 4.29. The discontinuities in these curves, where the initial rate of reaction was faster for an ensuing reaction relative to that of the preceding reaction, corresponded with periods when the series of reactions were interrupted and the catalysts stored under hydrogen, e.g. overnight. The dotted lines in Figures 4.28 and 4.29 indicate when a catalyst was stored in such a way between successive reaction cycles.

As stated previously, during the first hydrogenation reaction using a reduced 1 % nickel on silica catalyst, a small amount of [^{18}O]-carbon dioxide (ca. 1.25×10^{19} molecules) was added to the reactor with the aliquot of the hydrogen and ethene mixture. These additions of [^{18}O]-carbon dioxide were made in order to investigate if residual (and exchangeable) oxygen was present on the surfaces of the catalysts after reduction. An identical procedure was also adopted for the sample of oxidised 1 % nickel on ICI silica used in the control experiment. It has been previously

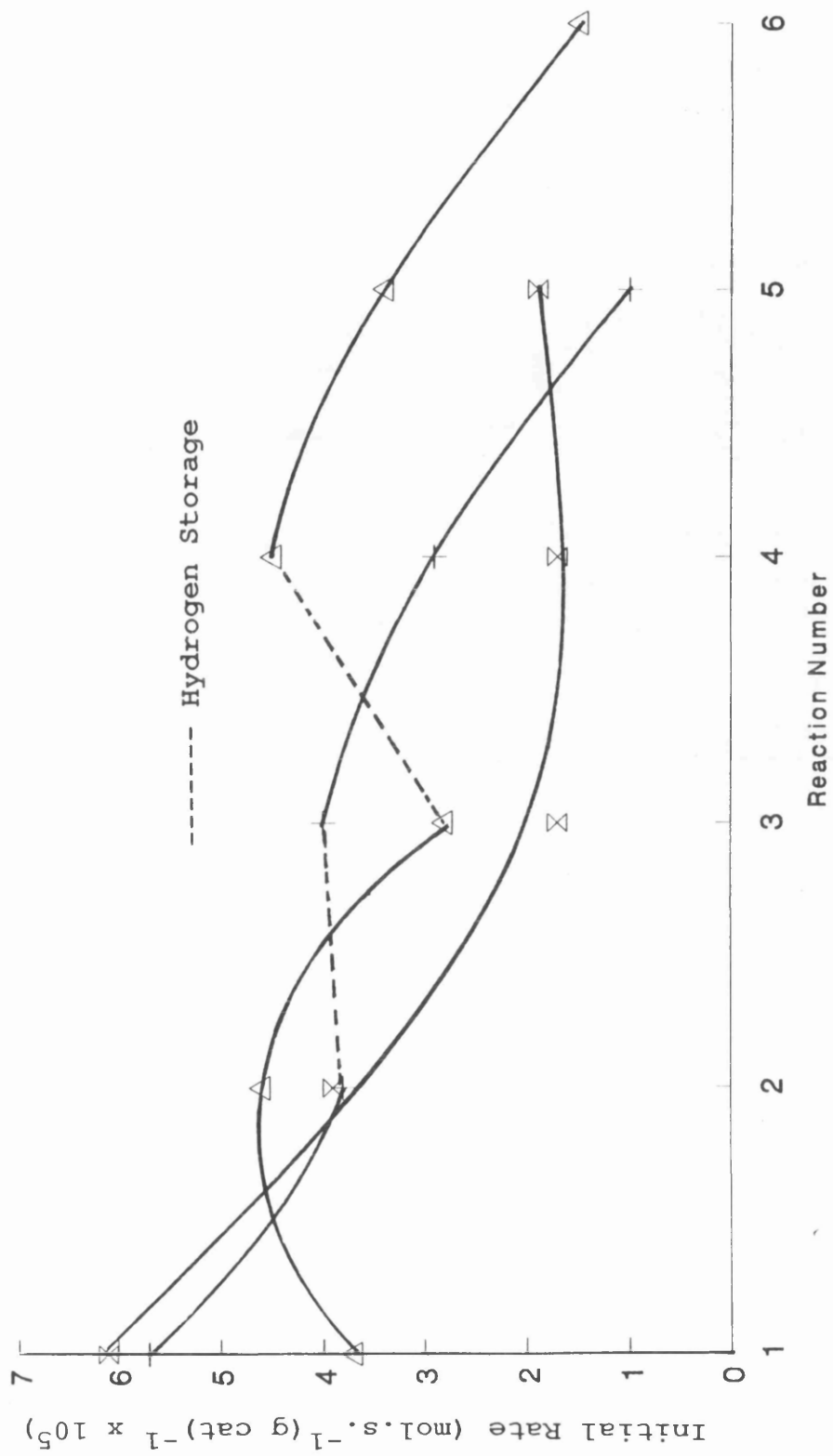


Fig. 4.28 Ethene Hydrogenations Performed on 10 % Nickel on Silica Catalysts

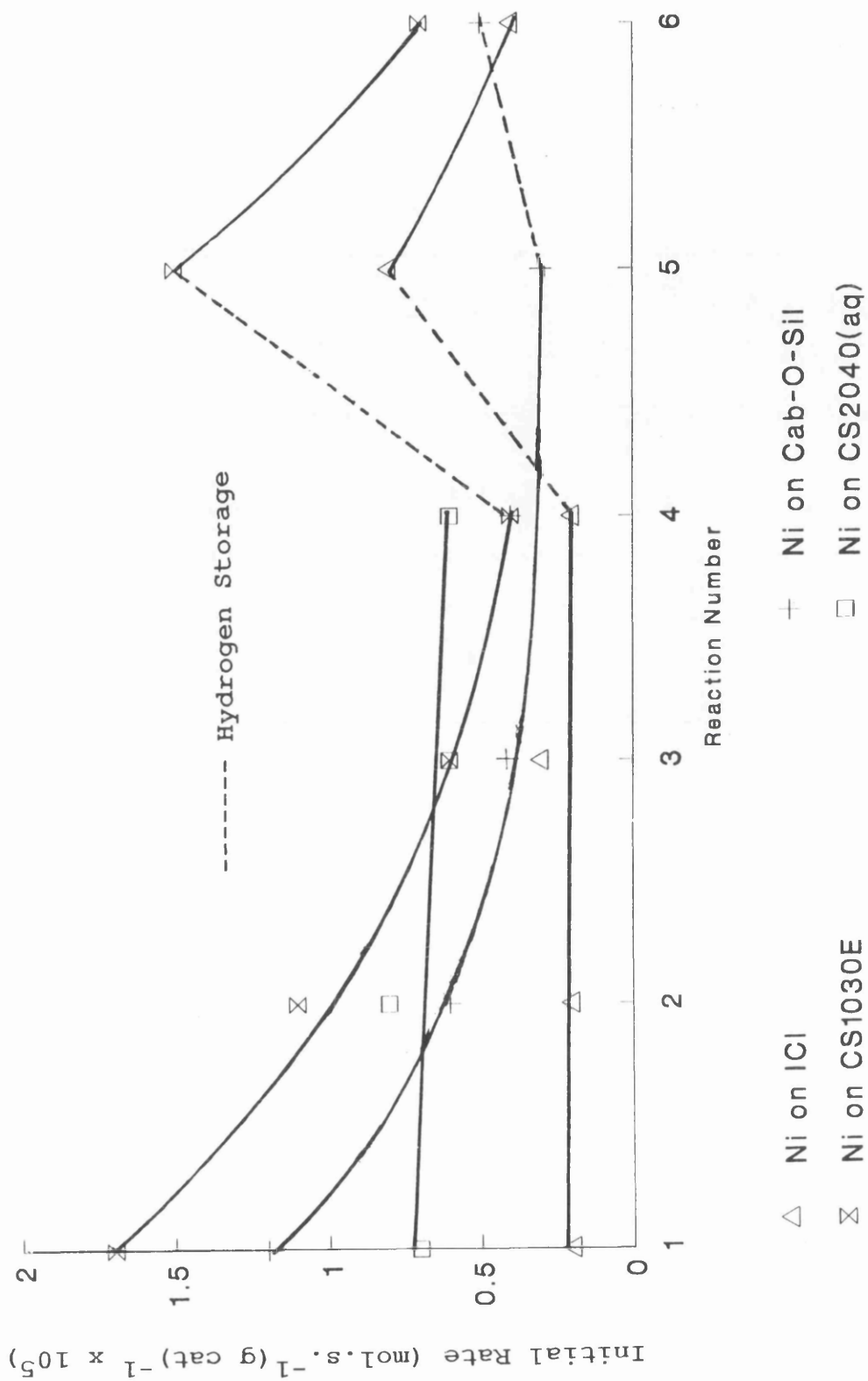


Fig. 4.29 Ethene Hydrogenations Performed on 1 % Nickel on Silica Catalysts

shown (163) that residual oxygen present on the metal surface of a silica-supported metal catalyst undergoes exchange with [^{18}O]-carbon dioxide. In this way, it is possible to detect and quantify exchangeable residual oxygen present on silica-supported metal catalysts after reduction.

Mass spectrometric analysis of the condensable gases recovered on completion of a reaction revealed that, for all samples, [^{16}O]-oxygen exchange had occurred between the catalysts and gas phase [^{18}O]-carbon dioxide. The results for this exchange, expressed in [^{16}O]-oxygen atoms (g catalyst) $^{-1}$, are given in Table 4.11. Mass spectrometry also demonstrated that gas phase [^{18}O]-carbon dioxide did not undergo any detectable [^{16}O]-oxygen exchange with pure silica at 273 K. Hence, oxygen exchange only occurred when nickel was present on the supports.

Table 4.11

Amount of [^{16}O]-Oxygen Exchange During the First Hydrogenation Reactions Using Catalysts Reduced by the Static Method

Catalyst	Expt. No.	No. of [^{16}O]-oxygen ^a Atoms Exchanged
1 % Ni/ICI	4	0.4
1 % Ni/Cab-O-Sil	5	2.3
1 % Ni/Cab-O-Sil	5 ^a ^b	18.5
1 % Ni/CS1030E	6	3.1
1 % Ni/CS2040 (aq.)	7	34.7
1 % Ni/CS2040 (aq.)	7 ^a ^b	7.0
1 % Ni/ICI (control)	8	23.5

a. Units: [^{16}O]-oxygen atoms (g catalyst) $^{-1}$ x 10^{-18} .

b. Duplicate experiments.

As a check on the ability of mass spectrometry to accurately quantify the amount of [^{16}O]-oxygen in a sample of [^{18}O]-carbon dioxide, the purity of the "as supplied" [^{18}O]-carbon dioxide was determined by mass spectrometry (details in Section 3.4.1.2). The analysis established the purity of the [^{18}O]-carbon dioxide to be 97.5 % atom [^{18}O]-oxygen (*cf.* manufacturer's analysis of 97 % atom [^{18}O]-oxygen).

Comparison of the original experiments with their respective duplicates indicates that the reproducibility of the [^{16}O]-oxygen exchange data was poor for catalysts reduced by the static method. Irreproducibility was also observed in the initial rate data for ethene hydrogenation between separate samples of the same catalyst reduced by the static method (Tables 4.10a and 4.10b).

4.3.2 Catalysts Reduced by the Flow Method

As an alternative method of reduction, the calcined catalysts were reduced by the standard procedure in flowing hydrogen gas at 673 K, as described in Section 3.4.2.1. A single ethene hydrogenation reaction using each reduced catalyst was then performed by adding an aliquot of a hydrogen and ethene mixture to the reactor and monitoring the pressure for 80 minutes. In each reaction, a small amount of [^{18}O]-carbon dioxide (ca. 1.08×10^{19} molecules) was also added to the reactor with the gas phase mixture of hydrogen and ethene. The condensable gases were then recovered and analysed by mass spectrometry after being in contact with the catalyst throughout the duration of the reaction. The initial rates, determined by the tangent

method (described in Section 4.3.1), and expressed in $\text{mol.s.}^{-1}(\text{g catalyst})^{-1}$, are listed in Table 4.12.

Table 4.12

Hydrogenation Reactions Performed Using Catalysts Reduced by
the Flow Method

Catalyst	Expt. No.	Initial Rate ^a
10 % Ni/ICI	1	3.7
10 % Ni/Cab-O-Sil	2	6.5
10 % Ni/Cab-O-Sil	2a ^b	7.8
10 % Ni/CS1030E	3	2.6
1 % Ni/ICI	4	3.9
1 % Ni/Cab-O-Sil	5	0.3
1 % Ni/CS1030E	6	0.6
1 % Ni/CS2040 (aq.)	7	0.7
1 % Ni/CS2040 (non-aq.)	8	1.6
1 % Ni/ICI (control)	9	0.0

a. Units: $\text{mol.s.}^{-1}(\text{g catalyst})^{-1} \times 10^5$.

b. Duplicate experiment.

The data given in Table 4.12 reveal that, contrary to the results for the catalysts reduced by the static method, the flow-reduced catalysts gave more reproducible rate data (experiment numbers 2 and 2a). Additionally, the oxidised 1 % nickel on ICI silica catalyst (experiment number 9) used in the control experiment was found to be completely inactive for the hydrogenation of ethene.

The reaction rates can be directly compared for the catalysts by additionally calculating the specific rates.

The specific rate is defined as the rate of reaction per unit area of metal surface (27, 67, 74). In this dissertation, the specific rates (listed in Table 4.13) were calculated on the basis of the S_{Ni} values (expressed in $m^2(g \text{ nickel})^{-1}$) determined from either the T.E.M. analyses or the carbon monoxide chemisorption experiments (Tables 4.9 and 4.8 in Sections 4.2.2 and 4.2.1(a), respectively).

Table 4.13

Specific Rates of Ethene Hydrogenation Performed Using Catalysts Reduced by the Flow Method

Catalyst	Expt. No.	Initial Specific Rate ^{a, b}	Initial Specific Rate ^{a, c}
10 % Ni/ICI	1	3.3	3.6
10 % Ni/Cab-O-Sil	2	16.6	14.9
10 % Ni/Cab-O-Sil	2a ^e	19.8	17.8
10 % Ni/CS1030E	3	3.3	4.7
1 % Ni/ICI	4	32.4	53.2
1 % Ni/Cab-O-Sil	5	-d	3.9
1 % Ni/CS1030E	6	-d	11.7
1 % Ni/CS2040 (aq.)	7	2.1	13.3
1 % Ni/CS2040 (non-aq.)	8	12.6	4.0
1 % Ni/ICI (control)	9	0.0	0.0

a. Units: $\text{mol.s.}^{-1}(\text{m}^2 \text{ nickel})^{-1} \times 10^6$.

b. Rate based on S_{Ni} values calculated from T.E.M. data (Table 4.9).

c. Rate based on S_{Ni} values calculated from carbon monoxide chemisorption data (Table 4.8).

d. T.E.M. data unavailable.

e. Duplicate experiment.

As previously stated, in each hydrogenation reaction, ca. 1.08×10^{19} molecules of $[^{18}\text{O}]$ -carbon dioxide were added to the reactor together with the aliquot of the hydrogen and ethene mixture. Mass spectrometric analyses of the condensable gases which had been in contact with the catalysts for 80 minutes revealed that $[^{16}\text{O}]$ -oxygen exchange had occurred for all samples. The amounts of $[^{16}\text{O}]$ -oxygen exchange are shown for the catalysts in Table 4.14a.

Table 4.14a

Amount of $[^{16}\text{O}]$ -oxygen Exchange Expressed per Gram of Catalyst For Catalysts Reduced by the Flow Method

Catalyst	Expt. No.	No. of Atoms of $[^{16}\text{O}]$ -oxygen Exchanged ^a
10 % Ni/ICI	1	41.1
10 % Ni/Cab-O-Sil	2	42.6
10 % Ni/Cab-O-Sil	2a ^b	33.1
10 % Ni/CS1030E	3	44.4
1 % Ni/ICI	4	8.9
1 % Ni/Cab-O-Sil	5	11.4
1 % Ni/CS1030E	6	2.7
1 % Ni/CS2040 (aq.)	7	3.7
1 % Ni/CS2040 (non-aq.)	8	5.2
1 % Ni/ICI (control)	9	15.1

a. Units: $[^{16}\text{O}]$ -oxygen atoms (g catalyst)⁻¹ $\times 10^{-18}$.

b. Duplicate experiment.

Since the metallic surface areas of the flow-reduced catalysts have been determined, the amount of exchangeable

[¹⁶O]-oxygen can also be expressed as a function of the surface area of nickel. This is shown for the catalysts in Table 4.14b.

Table 4.14b

Amount of [¹⁶O]-oxygen Exchange Expressed per m² of Nickel
For Catalysts Reduced by the Flow Method

Catalyst	Expt. No.	No. of ^{a, b} [¹⁶ O]-O Atoms Exchanged	No. of ^{a, c} [¹⁶ O]-O Atoms Exchanged
10 % Ni/ICI	1	3.6	4.0
10 % Ni/Cab-O-Sil	2	10.9	9.8
10 % Ni/Cab-O-Sil	2a ^e	8.4	7.6
10 % Ni/CS1030E	3	5.7	8.0
1 % Ni/ICI	4	7.5	12.2
1 % Ni/Cab-O-Sil	5	- ^d	14.3
1 % Ni/CS1030E	6	- ^d	5.5
1 % Ni/CS2040 (aq.)	7	1.2	7.5
1 % Ni/CS2040 (non-aq.)	8	4.2	1.3
1 % Ni/ICI (control)	9	12.6	20.7

- a. Units: [¹⁶O]-oxygen atoms(m² nickel)⁻¹ x 10⁻¹⁸.
b. Exchange data based on S_{Ni} values calculated from T.E.M. data (Table 4.9).
c. Exchange data based on S_{Ni} values calculated from carbon monoxide chemisorption data (Table 4.8).
d. T.E.M. data unavailable.
e. Duplicate experiment.

Comparison of both the rate and [¹⁶O]-oxygen exchange data between the two duplicate experiments, numbers 2 and 2a, reveals that the data obtained for the catalysts reduced

by the flow method were more reproducible than those obtained for the catalysts reduced by the static method.

CHAPTER FIVE

CHAPTER FIVE

DISCUSSION

The experimental results detailed in Chapter Four have been correlated with data generated by the Cambridge and Surrey research groups and discussed with reference to previous literature reports.

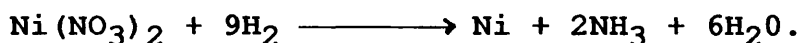
5.1 The Influence of the Support on the Nature of the Deposited Nickel Precursor States and the Resultant Nickel Particles Formed Upon Reduction

In the following two subsections the probable nature of the nickel metal precursors existing on the supports is described for the uncalcined and calcined catalysts in their unreduced states. In Section 5.1.3 a description is given of how, for the calcined catalysts, the nature of the nickel metal precursors deposited on the supports affect the resulting nickel dispersions of the reduced catalysts. A summary of the above material is presented in Section 5.1.4, where models for the nature of the supported nickel metal precursors before and after calcination are proposed. The types of nickel particles formed after calcination and subsequent reduction are also discussed.

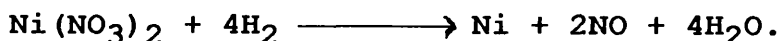
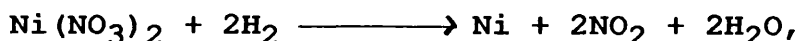
5.1.1 Uncalcined Catalysts

Examination of the T.P.R. profiles for the uncalcined catalysts illustrated in Figures 4.1 and 4.2 reveals that, for all the catalysts, a common pattern consisting of three peaks was obtained: a sharp L.T. peak followed by two broader peaks which occurred at somewhat higher temperature (i.e. the M.T. and H.T. peaks). Comparison of these T.P.R.

profiles with others reported in the literature is difficult as the number of T.P.R. studies of uncalcined catalysts is limited (5, 9, 85, 90, 91). This is probably due to the interpretation of T.P.R. profiles for silica-supported nickel salts being further complicated by reduction of the nickel(II) counter-ion, e.g. nitrate, occurring during T.P.R. experiments (90, 91). The resultant hydrogen uptake in a T.P.R. experiment, therefore, is generally higher than that calculated on the basis of the amount of nickel(II) cations alone. For example, one mole of nickel nitrate may require up to nine moles of hydrogen for complete reduction (28):



Other reduction reactions are also possible (28):



The T.P.R. profiles of the uncalcined catalysts obtained in the present study (Figures 4.1 and 4.2) were very similar to that obtained for silica-supported nickel nitrate by Burch and Flambard (5). These workers associated the large, sharp L.T. peak observed in their profile ($T_{\text{max}} = 590 \text{ K}$) with the reduction of nickel oxide. A very broad and poorly resolved peak was also observed with $T_{\text{max}} = \text{ca. } 700 \text{ K}$. The authors proposed that this peak was due to the reduction of the same species responsible for the high temperature peak in the T.P.R. profile of supported nickel oxide (see Section 5.1.2). Montes et al. (9) did not hypothesize as to the nature of any specific nickel species responsible for the reduction peaks in their T.P.R.

profile obtained for silica-supported nickel nitrate. They simply noted that the main reduction peak occurred at a lower temperature than the reduction of bulk nickel oxide. This feature was also observed in the present study where the T_{\max} values for the L.T. peaks of the uncalcined catalysts were in the range 528 - 573 K (cf. unsupported nickel oxide where $T_{\max} = 641$ K for the main reduction peak).

An explanation as to the nature of the species responsible for the sharp L.T. peaks obtained in the T.P.R. profiles can be proposed by considering several studies in the literature (17, 97, 101). These workers studied the thermal decomposition of both unsupported and silica-supported nickel nitrate and found that the process was a complex multi-stage reaction with steps occurring at various temperatures. Interestingly, it was found that the temperatures for all stages of decomposition were significantly lower for the supported nickel nitrate relative to the corresponding stages for unsupported nickel nitrate. Decomposition of the supported nickel nitrate to form nickel oxide was complete by ca. 573 K (97, 101). This temperature was very similar to the T_{\max} values for the L.T. peaks in the T.P.R. profiles of the uncalcined catalysts and it is proposed that reduction of the decomposition products of the nitrate ions caused these uptakes of hydrogen.

The nature of the species responsible for the M.T. reduction peaks in the T.P.R. profiles, T_{\max} values in the range 617 - 717 K, is thought to have been nickel oxide which formed after the decomposition and reduction of the

nitrate ions. This assignment has been made on the basis that the temperatures at which the M.T. peaks appeared were similar to that observed for the reduction of unsupported nickel oxide ($T_{\max} = 641$ K, main reduction peak). Moreover, the T_{\max} values for the M.T. peaks were similar to the T_{\max} values for the low temperature peaks in the profiles of the calcined catalysts obtained under identical T.P.R. conditions; these low temperature peaks were assigned to the reduction of large particles of nickel oxide (see Section 5.1.2 for details).

The nature of the species which reduced and caused the H.T. peaks in the profiles is unclear. It is known (5, 170) that uncalcined catalysts, prepared by the impregnation of silica with an acidic solution of nickel nitrate followed by drying, predominantly consist of crystallites of nickel nitrate hexahydrate deposited on the silica. In addition, a small amount of ion-exchange occurs between the nickel(II) cations and the protons of the silanol groups on the silica surface. Reduction of such an ion-exchanged species of nickel could account for the H.T. peaks observed in the T.P.R. profiles as uncalcined catalysts prepared by ion-exchange are known to contain metal precursors which are very resistant to reduction (5, 88).

To summarise, assignments can be made as to the nature of the species which led to the three reduction peaks observed in the T.P.R. profiles of the uncalcined catalysts. These assignments are as follows: the L.T. peak was due to the reduction of decomposition products of the nitrate ions. The M.T. peak was due to the reduction of nickel oxide particles left after the nitrate ions were decomposed and

reduced. The H.T. peak was due to the reduction of nickel which had undergone ion-exchange with protons from the silanol groups on the silica surface. Since all three of these peaks were common to each T.P.R. profile, independent of metal loading or silica used as the support, it is apparent that the uncalcined catalysts in their unreduced states all contained the same species of nickel metal precursors in approximately similar proportions.

5.1.2 Calcined Catalysts

In contrast to the T.P.R. profiles obtained for the uncalcined catalysts (discussed in the previous section), profiles obtained for the calcined catalysts displayed no common pattern. Unlike the case of uncalcined catalysts, however, comparison of the profiles illustrated in Figures 4.3 and 4.4 with similar profiles in the literature is facilitated by the many T.P.R. experiments reported using silica-supported nickel oxide samples (9, 85, 90, 91, 97, 100, 101, 171). Many of these studies show very similar results to those obtained here.

In agreement with a study by Mile et al. (101), it was observed in the present study that pure silica did not undergo reduction under the conditions of the T.P.R. experiments. It was further observed in both the present study and many other studies (9, 18, 85, 90, 91, 93 - 98, 100, 101, 171) that unsupported nickel oxide undergoes reduction when heated at a constant rate in hydrogen at a substantially lower temperature and within a much narrower temperature range than silica-supported nickel oxide. The T.P.R. profile of unsupported nickel oxide obtained in the

current study consisted of a shoulder ($T_{\max} = 596$ K) on the low temperature side of the major nickel oxide reduction peak ($T_{\max} = 641$ K). Similar shoulders have been observed in T.P.R. profiles of both unsupported and silica-supported nickel oxide and have been attributed to the reduction of traces of nickel(III) oxide in the nickel(II) oxide (97, 101, 171), although it is not known whether the peak is due to the partial reduction of nickel(III) to give nickel(II) or complete reduction to nickel(0) (171). The relative size of this peak has been shown to vary widely between different samples of unsupported or supported nickel(II) oxide and is sometimes absent from the profile altogether (97, 101, 171), although its occurrence or non-occurrence does not affect the rest of the profile. Hence the shoulders observed on the low temperature side of the L.T. peaks in the T.P.R. profiles of the unsupported nickel oxide, the calcined nickel on Cab-O-Sil silica catalysts and the calcined 10 % nickel on CS1030E silica catalyst are assigned to the reduction of small amounts of nickel(III) oxide. As mentioned above, the absence of this peak in the other T.P.R. profiles was not significant.

All the profiles possessed common L.T. peaks, with T_{\max} values in the range 603 - 657 K, similar to those observed by Mile and co-workers (97, 101, 171) and others (9, 100) and attributed by them to the reduction of large particles of nickel oxide with little or no interaction with the support (hereafter known as the L.T. species). This assignation of the L.T. species is further substantiated by the similarity of the T_{\max} values of the L.T. peaks to that

of 641 K observed for the reduction of unsupported nickel oxide.

The assignation of the species responsible for the significant H.T. peaks (hereafter referred to as the H.T. species) observed in the profiles of the calcined nickel on ICI, CS1030E and CS2040 (non-aq.) silica catalysts is more problematic. No obvious correlation existed between the amount of the H.T. species present in the unreduced calcined catalysts (Table 4.4b) with either the BET surface areas, the average pore diameters or the pore volumes of the catalysts (listed in Table 4.1, Section 4.1.1). Similar H.T. peaks have also been observed in many other studies on silica-supported nickel oxide samples (9, 90, 97, 100, 101, 171).

Two models have been proposed in the literature to describe the nature of the species whose reduction is responsible for the H.T. peaks. The first model, referred to as the two-particle size model, has been proposed by several researchers to explain observations that a portion of silica-supported nickel oxide is of low relative reducibility (18, 88, 172). The model proposed in these studies is that an unreduced calcined catalyst consists of two sizes of nickel oxide particles. The larger particles of nickel oxide (the L.T. species) undergo reduction at a low temperature similar to bulk nickel oxide, whereas the smaller particles (the H.T. species) undergo reduction at substantially higher temperatures. As previously discussed in Section 1.5.1, Roman and Delmon (18) attributed the decrease in reducibility to the lack of nucleation sites for nickel oxide reduction on the smaller particles. This

model can also explain the lack of X.R.D. evidence for the presence of bulk nickel hydrosilicate (11, 18, 88, 99 - 101), which some investigators have proposed to be the H.T. species (see below). However, the possibility that a very small proportion of the supported nickel in silica-supported nickel oxide is in the form of thin layers of amorphous nickel hydrosilicate on the surface of the support cannot be dismissed. In fact, Roman and Delmon (18) remarked that a small proportion of the supported nickel in their calcined 18.9 % nickel on silica catalyst, which was prepared by impregnation, was "unreducible" under the reduction conditions used in their study. They suggested that this small amount of nickel was in the form of amorphous nickel hydrosilicate.

The second model commonly advanced to account for the H.T. peak is that it is the result of the reduction of nickel hydrosilicate. It is well known that unreduced catalysts prepared by co-precipitation, deposition-precipitation and ion-exchange methods contain an often sizable proportion of nickel hydrosilicate which reduces only at high temperature (5, 6, 8 - 10, 72, 85, 88, 95, 103, 104). Little direct evidence exists, however, for the presence of nickel hydrosilicate in unreduced catalysts prepared by impregnation. Certainly, in the present study, T.E.M. analyses of the reduced catalysts provided no evidence for the presence of layers of nickel hydrosilicate on the surfaces of the supports. Such layers of nickel hydrosilicate have been detected by T.E.M. for both reduced and unreduced catalysts prepared by deposition-precipitation (9, 10). A further argument against nickel hydrosilicate

being the species whose reduction was responsible for the H.T. peak is supplied by Mile and co-workers (101, 171). They observed that under the T.P.R. conditions used in their studies, prepared nickel hydrosilicate began to reduce slowly at temperatures exceeding ca. 823 K, whereas the H.T. species observed in their T.P.R. profiles of nickel oxide on silica was completely reduced by 823 K.

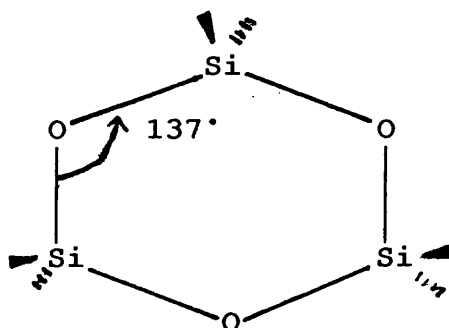
A third model to describe the nature of the H.T. species is suggested by this work. This model is based on the interaction of supported nickel oxide with the fundamental structure of the silica support. It is therefore necessary initially to consider the nature of the supports themselves.

As discussed in Appendix B, the Cambridge group has characterised the pure silica supports by neutron diffraction and ^{29}Si MAS NMR spectroscopy - and also the reduced 1 % nickel on ICI silica catalyst by small angle neutron scattering (S.A.N.S.). The characterisation studies revealed that the silica supports consisted of varying populations of cyclic species, containing from three to ten silicon atoms plus an equal number of associated bridging oxygen atoms. The distribution of the high energy (strained) three-fold siloxane rings, i.e. rings containing three [Si-O-] units, varied significantly between the different silicas.

Figure 5.1 shows a structural diagram of a three-fold siloxane ring displaying a strained Si-O-Si bond angle of 137° [cf. $145 - 147^\circ$ for a typically unstrained Si-O-Si bond angle in silica (161)]. These three-fold siloxane rings contribute the majority of the metastable energy within

silica structures (161, 173) and hence silicas which contain a large proportion of these rings in their structures are high in metastable energy.

Figure 5.1
A Three-fold Siloxane
Ring



The distributions of three-fold siloxane rings in the supports, quantified by the neutron diffraction experiments, are shown in Table 5.1 (see Appendix B for details on the diffraction experiments). The data in Table 5.1 were calculated by assuming that all the three-fold siloxane rings within the silica networks were at the surface, an assumption known to be valid (174). Lineshape analyses of the ^{29}Si MAS NMR spectra recorded for the silicas also agree qualitatively with the determined distributions of the three-fold siloxane rings (ref. 161 and Appendix B).

From the results listed below in Table 5.1 it can be seen that the metastable energies of the supports descended in the order ICI silica > CS2040 (non-aq.) silica > CS2040 (aq.) silica > Cab-O-Sil silica. Considering now the T.P.R. experiments, it was shown that the calcined nickel on ICI and CS2040 (non-aq.) silica catalysts contained significant amounts of the H.T. nickel species whereas the calcined nickel on Cab-O-Sil and CS2040 (aq.) silica catalysts contained only small amounts of the H.T. species. Hence, calcined catalysts prepared from silicas with high metastable energies, i.e. large proportions of three-fold

siloxane rings in their structures, contained significant amounts of the H.T. nickel species.

Table 5.1

The Distribution of Three-fold Siloxane Rings on the Surfaces of the Supports

Support ^a	% Three-fold Siloxane Rings
ICI	40 - 50
Cab-O-Sil	0 - 5
CS2040 (non-aq.) ^b	30 - 35
CS2040 (aq.) ^c	< 20

a. No data available on CS1030E silica.

b. Before treatment in water.

c. After treatment in water.

It is reasonable to suggest that an interaction occurred in a calcined catalyst between a portion of the supported nickel oxide and the three-fold siloxane rings on the surface of the support to form the H.T. nickel species; three-fold siloxane rings are highly strained and so relatively unstable (173). Calcined catalysts prepared from supports with large proportions of three-fold siloxane rings would therefore contain large amounts of the H.T. species as was observed. The interaction between the nickel oxide and the three-fold siloxane rings would have probably released the strain energy of the silica to form a unique nickel environment giving rise to the H.T. reduction peak. A suggested mechanism by which nickel oxide could interact with a three-fold siloxane ring to release strain energy is illustrated in Figure 5.2.

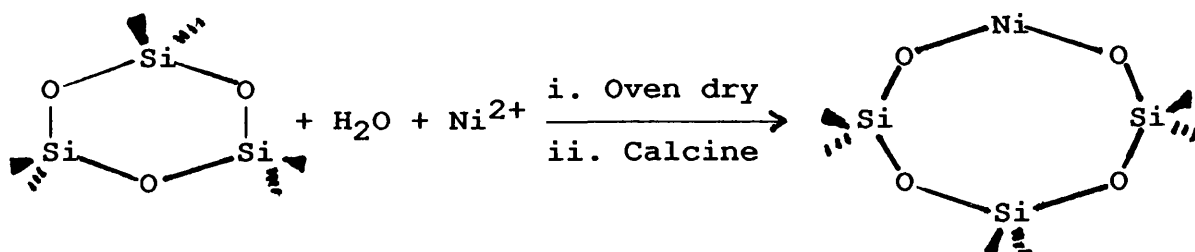


Figure 5.2 Possible Interaction Between Nickel Oxide and a Three-fold Siloxane Ring

In this proposed model one (or more) Ni-O units insert into a three-fold siloxane ring thereby releasing the strain energy. The inclusion of a metal-oxygen unit into a siloxane ring has already been demonstrated for aluminium (175).

A process involving ring opening such as the one proposed in Figure 5.2 is likely to be an activated process since a Si-O bond must be broken to allow insertion. Any ring opening process would, therefore, be liable to occur during, but not before, calcination as this was when the catalysts were subjected to the highest temperature (723 K). Mile *et al.* (171) noted that calcination led to the formation of very strong interactions between supported nickel oxide and silica leading to particles which were virtually immobile and possibly anchored to the support.

The ring species formed by insertion of a Ni-O unit or units could have then acted as nucleation centres for further growth of nickel oxide particles on the surface of the silica during calcination. These particles would be anchored to the support and would be expected to be thermally stable toward sintering as described by Mile *et al.* (171). As discussed below, these particles may behave differently with respect to reduction compared to nickel

oxide particles which were simply deposited on the silica surface (i.e. the L.T. species).

Further evidence that certain specific sites on the support may be responsible for the formation of the H.T. species can be found in the studies of Mile and co-workers (101, 171). In these studies it was discovered that a thirty-fold increase in the nickel loading on Gasil 35 silica resulted in an over forty-fold increase in the amount of the L.T. species of nickel in the calcined catalyst. In contrast, only a very modest increase (approximately two-fold) in the amount of the H.T. species occurred. This indicated that there were specific sites on the support which interacted with nickel to form the H.T. species and that the number of these sites was limited. This would be the case if the sites were three-fold siloxane rings on the surface of the silica.

The above phenomenon was also observed in the present study where the relative proportion of the H.T. to the L.T. peak was higher, in all cases, for the calcined 1 % nickel on silica catalysts compared to the calcined 10 % nickel on silica catalysts prepared from the same silica (Tables 4.4b and 5.2). The data in Table 5.2, below, clearly show that while the increase in the size of the L.T. peak was proportionate with the increase in metal loading for all the supports, the increase in the size of the H.T. peak was significantly smaller than the total increase in the metal loading. The LT_{10} and HT_{10} designations in this table refer to the amounts of hydrogen taken up by the L.T. and H.T. species in the calcined 10 % nickel on silica catalysts, respectively. Similarly, LT_1 and HT_1 refer to

the hydrogen uptakes for the various species in the calcined 1 % nickel on silica catalysts.

Table 5.2

Relative Increases in Hydrogen Uptake by the L.T. and H.T. Species on Increasing the Nickel Loading on the Supports

Calcined Catalyst	Actual Hydrogen Uptake ^a		Ratio of Peaks for the Supports	
	LT Peak	HT Peak	LT ₁₀ /LT ₁	HT ₁₀ /HT ₁
10 % Ni/ICI	8.0	7.0	12.3	5.6
1 % Ni/ICI	0.6	1.3
10 % Ni/Cab-O-Sil	15.6	1.2	10.3	2.0
1 % Ni/Cab-O-Sil	1.5	0.6
10 % Ni/CS1030E	9.9	2.6	11.8	2.1
1 % Ni/CS1030E	0.8	1.3		

a. Units: moles (g catalyst)⁻¹ x 10⁴.

The data in Table 5.2 also show that the relative increase in the size of the H.T. peak was larger on increasing the metal loading on the ICI silica than on either the CS1030E or Cab-O-Sil silicas. This indicated that there were relatively more sites available on the surface of the ICI silica for interacting with the nickel to produce the H.T. species. This is consistent with the neutron diffraction analyses of the silicas, Table 5.1, where a higher proportion of three-fold siloxane rings were shown to exist on the surface of the ICI silica.

Considering now the calcined catalysts prepared from the CS2040 silica, it can be seen from the data in Table 5.1 that, after treatment in water, the proportion of three-fold

siloxane rings in the water-unstable CS2040 silica was decreased considerably. The surface morphology of this silica was also radically altered after exposure to water (e.g. the average pore diameter decreased from 20.8 to 11.5 nm, see Table B1, Appendix B). Hence, there was no significant H.T. peak observed in the T.P.R. profile of the calcined catalyst prepared using this silica by the aqueous impregnation method (Figure 4.4). In contrast, the calcined catalyst prepared by non-aqueous impregnation of the CS2040 silica, a preparative method which maintains the high energy surface of the support (176), displayed a large H.T. peak in its T.P.R. profile (Figure 4.4). A peak occurring at a very high temperature was also observed in this profile ($T_{\max} = 1000$ K). The reduction of the species responsible for this peak began at a temperature of ca. 900 K, which was similar to the temperature of greater than 823 K determined by Mile and co-workers (101, 171) to be required for the initiation of reduction of bulk nickel hydrosilicate. For this particular unreduced catalyst, therefore, it was possible that a small amount of the supported nickel was in the form of nickel hydrosilicate (ca. 3 % of the nickel as determined by T.P.R. - Section 4.1.2(c), Table 4.4b). Hence this calcined catalyst displayed a spectrum of nickel metal precursor interaction with the support: the L.T. species which interacted only weakly or not at all with the support, the H.T. species which interacted in an intermediary manner with the support and the probable nickel hydrosilicate species which interacted strongly with the support. This finding is in agreement with the observation of Roman and Delmon (18) and

other workers (88) that three types of nickel metal precursor can be present in silica-supported nickel oxide samples prepared by impregnation, each type behaving differently with respect to reduction.

The observation that only nickel oxide is usually detected in unreduced calcined catalysts prepared by impregnation (9, 11, 17, 18, 85, 88, 89, 96, 97, 99, 100, 101) can be explained by the ring insertion model. The amount of nickel incorporated into the three-fold siloxane rings would be very limited and in a non-crystalline form and would, therefore, be invisible to techniques such as X.R.D. Therefore, only the nickel oxide particles of the L.T. and H.T. species would be detected. Furthermore, the presence of nickel hydrosilicate is limited to unreduced catalysts prepared by specific methods, e.g. co-precipitation or possibly the non-aqueous impregnation of CS2040 silica as demonstrated in this study, but as a general rule it is not present in unreduced catalysts prepared by impregnation. Even where nickel hydrosilicate may be present, e.g. in the exceptional case of the calcined nickel on CS2040 (non-aq.) silica catalyst, techniques such as X.R.D. may still not detect its presence. Mile *et al.* (101) stated that if the amount of nickel hydrosilicate in a catalyst is very small and present in thin amorphous layers on the support surface, then well defined X.R.D. reflections for this compound will be absent.

The ring insertion model for the nature of the H.T. species also accounts for some observations in the literature. Increasing the temperature and/or the time of the calcination stage increases the relative proportion of

the H.T. species to the L.T. species as determined by T.P.R. (97, 101, 171). This observation can be accounted for by considering that a longer or a higher temperature calcination stage would promote the reaction of nickel oxide with three-fold siloxane rings. Under more severe calcination conditions, the number of three-fold siloxane ring sites would also be increased in the support as it is known (160, 174, 175, 177) that three-fold siloxane rings can be formed during heat treatment of silica by the endothermic (174) condensation of vicinal silanol groups (see Figure 5.3). Both the promotion of the nickel oxide reaction with the three-fold siloxane rings and the increased proportion of these rings in the silica would lead to the observed increase in the amount of the H.T. species in the calcined catalyst.

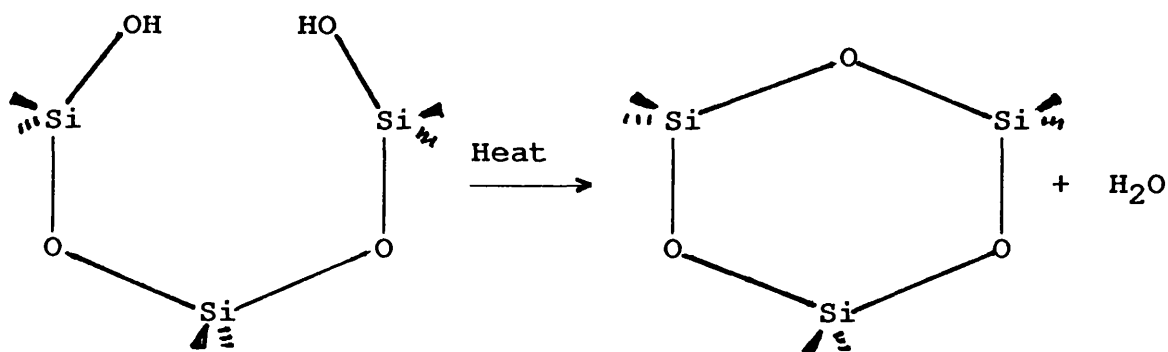


Figure 5.3 Condensation of Vicinal Silanol Groups to Form a Three-fold Siloxane Ring.

Direct evidence substantiating the hypothesis of Ni-O unit insertion into three-fold siloxane rings to form the H.T. species has been provided by the Cambridge group using ^{29}Si MAS NMR spectroscopy (178). Experiments were performed on two 1 % nickel on silica catalysts; nickel on ICI silica and nickel on Cab-O-Sil silica. These catalysts

were prepared by reducing the relevant calcined catalysts at 723 K. The reduced catalysts were then analysed by ^{29}Si MAS NMR spectroscopy. A signal at a chemical shift (relative to TMS) of ca. -114 ppm was detected for the nickel on ICI silica (*cf.* ca. -110 ppm in pure silica). The position of this signal was indicative of a Si-O-Ni bonding arrangement which would be expected to be present if the proposed nature of the H.T. species was correct.

Reduction of the nickel oxide moieties contained in a three-fold siloxane ring to yield nickel metal plus a reformed three-fold siloxane ring would be energetically unfavourable as a three-fold siloxane ring is of very high energy. It was, therefore, likely that the Ni-O inserted ring structures remained intact while the attached nickel oxide particles underwent reduction and hence the NMR signal indicating the Si-O-Ni bond was detected in the reduced catalyst (178). No equivalent signal was detected for the reduced nickel on Cab-O-Sil silica catalyst and hence little or no Si-O-Ni bonding arrangements were present in this catalyst.

As well as increasing the proportion of the H.T. species in calcined catalysts, increasing the temperature of the calcination stage promotes better nickel dispersion in reduced catalysts (101, 171). The diminution in the resultant nickel particle size of the reduced catalyst combined with the increase in the amount of the H.T. species present in the calcined catalyst suggests that the H.T. nickel species was in the form of small particles. This is because nickel particles are generally similar in size to the nickel oxide particles from which they are derived upon

reduction under moderate conditions (29). Considering these small particles to be nickel oxide which had nucleated on the Ni-O inserted three-fold siloxane rings, the explanation suggested by Roman and Delmon (18) for a form of nickel oxide which is unusually difficult to reduce could be applicable, i.e. small particles of nickel oxide are more difficult to reduce because nucleation sites for reduction are limited by either:

- i. the nickel oxide domains being too thin or;
- ii. the absence of suitable special nucleus forming sites.

The dispersion of nickel on a silica support may thus be governed by the energetics of the support, i.e. the amount of three-fold siloxane rings within the silica network, and not, for example, the BET surface area of the support. In fact, a significant decrease in nickel dispersion is not generally observed when a catalyst is prepared from a relatively low surface area silica compared to one prepared from a high surface area silica (95).

Further evidence as to the size and nature of particles of the L.T. and H.T. species was provided by the sintering study performed by the Cambridge group using reduced nickel on ICI silica (details in Appendix B). Samples of the calcined 1 % nickel on ICI silica catalyst were reduced at 723 K and then further heated in flowing hydrogen at temperatures ranging from 723 - 1223 K. During heating the nickel particle sizes of the samples were determined by S.A.N.S. Analyses of the S.A.N.S. data suggested that a bimodal distribution of nickel particle sizes (1 - 2 nm and 20 - 40 nm diameters) existed for this catalyst with the smaller particles resistant to sintering up to ca. 1023 K.

The larger particles were free to migrate on the surface at all temperatures studied. This suggests that the thermally stable smaller particles were anchored to the support and the proposed ring insertion model for the H.T. species could account for this. It was probable that the two types of nickel particle identified by S.A.N.S. as being present in this particular catalyst were each formed by the reduction of either the L.T. or H.T. species of nickel oxide contained in the calcined catalyst. Upon reduction of a nickel oxide particle associated with a Ni-O inserted ring species, the inserted nickel oxide moiety or moieties would have served as an anchorage point for the newly-formed nickel particle. Thus, reduction of the H.T. species of nickel oxide probably gave the small, thermally stable nickel particles. On the other hand, reduction of the L.T. species of nickel oxide, which was not anchored to the support, gave the larger, thermally unstable nickel particles.

Some interesting observations which seem to further substantiate the proposed nature of the H.T. species were made by Guo, Arai and Nishiyama (84). They found that precalcination of a silica support at temperatures between 673 and 1123 K before aqueous impregnation of the support with a nickel nitrate solution greatly improved the resulting nickel dispersion in the reduced catalyst; the maximal nickel dispersion was achieved when catalysts were prepared from supports which were precalcined at temperatures between 923 and 1023 K. Guo et al. also found that rehydration of a heat treated support by immersion in water at 343 K for several days before impregnation decreased the resultant nickel dispersion. T.E.M. analyses

showed that after calcination of the samples of supported nickel nitrate prepared from heat treated supports, the particles of nickel oxide were better dispersed than those particles for calcined catalysts prepared from the support without heat treatment.

The phenomena observed by Guo *et al.* are readily explicable by the concentration of three-fold siloxane rings being increased by thermal treatment of the silica as discussed earlier. The Cambridge group found that the maximum number of three-fold siloxane rings were formed on the supports after dehydroxylation at ca. 923 K (Appendix B); this temperature was comparable to the support precalcination temperatures (923 - 1023 K) discovered by Guo *et al.* (84) to maximise the resultant nickel dispersions for catalysts prepared from thermally treated supports. Upon impregnation and calcination, therefore, a larger proportion of the H.T. species of nickel oxide was formed for catalysts prepared from heat treated supports relative to those prepared from the untreated silica support. Thus the average nickel oxide particle size was observed to be smaller by T.E.M. and the resultant nickel dispersion increased for reduced catalysts prepared using precalcined supports.

Guo *et al.* also observed that the resultant nickel dispersion of a reduced catalyst prepared from a rehydrated heat treated support was reduced relative to a catalyst prepared from a support that had only been heat treated. Rehydrating a heat treated support before impregnation would reverse the reaction illustrated in Figure 5.3. In consequence, the concentration of three-fold siloxane rings

on the surface of the support would be decreased and hence the amount of the H.T. species ultimately formed would be diminished. Accordingly, upon reduction, the nickel dispersion was found to be less for a catalyst prepared from a rehydrated heat treated support relative to catalysts prepared from supports that had only been heat treated.

The question which now needs to be addressed is why the nickel oxide particles associated with the H.T. species were apparently smaller than the nickel oxide particles of the L.T. species. To do this it is necessary to consider the processes that occurred during each stage of preparation of the calcined catalysts, i.e. the impregnation, drying and calcination stages.

As previously stated in Section 5.1.1, an uncalcined catalyst in the unreduced state, prepared by impregnation of a silica with an acidic solution of nickel nitrate followed by drying, consists predominantly of crystallites of nickel nitrate hexahydrate deposited on the surface of the support. A small amount of ion-exchange may also occur between nickel(II) ions and surface silanol groups. The calcination stage, performed in the present study at a temperature of 723 K, then completely decomposes the nickel nitrate crystallites to nickel oxide (thermal decomposition of silica-supported nickel nitrate is complete by ca. 573 K - Section 5.1.1).

Two explanations can be invoked to account for the dispersion of nickel oxide particles after the calcination stage:

Firstly, it is known that during thermal decomposition of crystallites of supported nickel nitrate hexahydrate, the

crystallites liquefy by dissolution in their own water of crystallisation (9, 97). A similar argument to the idea of dynamic wettability of the support proposed by Guo *et al.* (84) can then be applied. It is proposed that droplets of this semi-decomposed hydrated nickel nitrate were more easily split or shrunk on more hydrophobic silica surfaces. Silicas with large distributions of three-fold siloxane rings on their surfaces are relatively hydrophobic in nature (160) due to lack of silanol groups. Hence predominantly small droplets of liquid will have formed on such hydrophobic surfaces before insertion of nickel oxide moieties into the siloxane rings. Small nickel oxide particles would have been formed upon complete decomposition of these droplets with the main nucleation sites for nickel oxide growth being nickel oxide moieties inserted into three-fold siloxane rings on the silica surface, *i.e.* the H.T. species. Consequently, a high degree of nickel oxide dispersion was achieved.

For less hydrophobic surfaces, *i.e.* silicas with a small proportion of three-fold siloxane rings, mainly large droplets of liquid will have formed giving rise to large particles of nickel oxide. These particles simply nucleate as the liquid dries and have no interaction with the support (10), *i.e.* the L.T. species.

Secondly, an alternative explanation is that during decomposition of the nickel nitrate crystallites, nickel oxide particle nucleation was initiated on the surface of the support. Additional decomposition then led to further particle growth on the nucleation sites. Particles which had grown on nickel oxide moieties incorporated into three-

fold siloxane rings, i.e. H.T. species, would be immobile and so the particle size would depend only on the amount of nickel oxide deposited from the decomposing nickel nitrate. In the case of nickel oxide particles which had no anchorage point on the surface, i.e. L.T. species, further particle growth may have occurred through a process of sintering (28, 89, 95, 96, 171) as well as further deposition of nickel oxide from the decomposing nickel nitrate. Hence the L.T. species consisted of larger particles of nickel oxide relative to the H.T. species.

To summarise, in this study four different nickel species with differing reducibilities have been identified. The first nickel metal precursor reduced at low temperature and was, on the basis of literature evidence, a small amount of nickel(III) oxide in the supported nickel(II) oxide. The second metal precursor, the L.T. species, reduced at a slightly higher temperature and has been identified as large particles of nickel oxide with little or no interaction with the support. The third metal precursor, the H.T. species, is proposed to have been small and difficult-to-reduce particles of nickel oxide which were anchored to the support via an interaction with the strained three-fold siloxane rings on the silica surface. The fourth species appears to be very exceptional and its presence limited to only one of the unreduced catalysts prepared in this study. This species is proposed to have been nickel hydrosilicate, as its temperature of reduction was similar to that of synthesised nickel hydrosilicate.

5.1.3 The Influence of the Support on the Average Nickel Particle Size

The observation that the H.T. species was probably nickel oxide in the form of small, sinter-resistant particles anchored to the support implies that reduction of a calcined catalyst with a higher proportion of this species will give a catalyst with a smaller average particle size than reduction of a calcined catalyst with a lower proportion. In Table 5.3 the proportions of the hydrogen uptakes (expressed as percentages) due to the reduction of the H.T. species in the calcined catalysts during T.P.R. are contrasted with the determined d_s values for the reduced catalysts.

Table 5.3

Comparison of the d_s Values of the Reduced Catalysts with Hydrogen Uptakes due to the Reduction of the H.T. Species During T.P.R. of the Calcined Catalysts

Calcined Catalyst	% H ₂ Uptake by H.T. Species ^a	d_s (nm) ^b
10 % Ni/ICI	47	7
10 % Ni/Cab-O-Sil	7	17
1 % Ni/ICI	66	11
1 % Ni/Cab-O-Sil	28	14
1 % Ni/CS2040 (aq.)	0	20
1 % Ni/CS2040 (non-aq.)	69	2

a. Determined by T.P.R. of the calcined catalysts.

b. Determined by carbon monoxide chemisorption for the catalysts reduced at 673 K under a flow of hydrogen using the standard conditions [Section 3.3.1(a)].

The average nickel particle sizes determined by carbon monoxide chemisorption for the catalysts reduced using the standard conditions demonstrated that, for the 10 % nickel on silica catalysts, reduction of a calcined catalyst with a greater proportion of the H.T. species did indeed lead to a reduced catalyst with a smaller average particle size. The average nickel particle sizes increased in the order nickel/ICI silica < nickel/Cab-O-Sil silica, while the proportion of the H.T. species in the unreduced calcined catalysts was greater for the nickel oxide on ICI silica than for the nickel oxide on Cab-O-Sil silica.

Considering now the reduced 1 % nickel on silica catalysts, the average particle sizes, based on carbon monoxide chemisorption, increased in the order nickel/CS2040 (non-aq.) silica < nickel/ICI silica < nickel/Cab-O-Sil silica < nickel/CS2040 (aq.) silica. The proportions of the H.T. species in the unreduced calcined catalysts were found to decrease in the order nickel oxide/CS2040 (non-aq.) silica > nickel oxide/ICI silica > nickel oxide/Cab-O-Sil silica > nickel oxide/CS2040 (aq.) silica. Thus, for catalysts with either 1 % or 10 % nickel loading, the average particle sizes of the reduced catalysts decreased as the proportions of the H.T. species increased in the unreduced calcined catalysts. It should be noted that the reduced 1 % nickel on CS2040 (aq.) silica catalyst probably had a much smaller actual average particle size than that determined by the chemisorption experiment. As discussed below this catalyst may represent a special case.

The results of Mile *et al.* (101) also clearly demonstrated a relationship between the proportion of the

H.T. species in an unreduced calcined catalyst and the average nickel particle size upon catalyst reduction.

The d_g values obtained in the present study by T.E.M. analyses of the reduced and passivated catalysts (Table 4.9, Section 4.2.2) followed the same order for the 10 % nickel on silica catalysts as described above. For the 1 % nickel on silica catalysts, the ascending order of the d_g values for the catalysts was nickel/CS2040 (aq.) silica < nickel/CS2040 (non-aq.) silica \approx nickel/ICI silica (the d_g value for the 1 % nickel on Cab-O-Sil silica catalyst was not determined). There were, however, large discrepancies between the d_g values determined by carbon monoxide chemisorption and T.E.M. analyses for the two catalysts prepared from the CS2040 silica. Possible explanations for these discrepancies are given later in this section.

As stated earlier, it was probable that the reduced catalysts contained two types of nickel particle, each derived from one of the two species of nickel oxide in the unreduced calcined catalysts. By analysing the particle size distributions obtained by T.E.M. for the reduced catalysts, it should be possible to identify these particles as the two types of particle widely varied in their sizes. Catalysts prepared by reducing calcined catalysts which contained large proportions of the L.T. species would be expected to contain large particles of nickel (20 - 40 nm in diameter). On the other hand, catalysts prepared by reducing calcined catalysts which contained large proportions of the H.T. species would be expected to contain predominantly small particles of nickel (1 - 2 nm in diameter).

The nickel particle size distribution determined by T.E.M. analysis of the reduced 1 % nickel on ICI silica catalyst (Figure 4.24) established that the majority of nickel particle diameters were in the 1 - 2 nm class (cf. 1 - 2 nm for the size of nickel particles proposed to be derived from the H.T. nickel species). Some particles were also identified by T.E.M. to be in the 16 - 17 nm class (cf. 20 - 40 nm for the size of particles proposed to be derived from the L.T. nickel species). Hence, the data from the T.E.M. analysis agreed qualitatively with the S.A.N.S. data for this catalyst, i.e. the majority of the particles were in the smaller particle diameter class (1 - 2 nm) while some were much larger in size. The ICI support had a large distribution of three-fold siloxane rings on its surface (40 - 50 %), and consequently the major form of nickel oxide in the unreduced calcined catalyst was the H.T. species (66 % of the hydrogen uptake during T.P.R.). Hence, the reduced nickel particles supported on this silica would be expected to be derived mainly from the H.T. species of nickel oxide.

For the reduced 10 % nickel on ICI silica catalyst T.E.M. analysis demonstrated that the majority of particles were in the size range 1 - 2 nm (Figure 4.21). This size range was identical to the size range of the particles proposed to be formed upon reduction of the H.T. nickel species. Hence, again, for this particular support most of the particles were apparently formed by reduction of the H.T. species of nickel oxide.

Moreover, the T.E.M. analysis of the reduced 10 % nickel on Cab-O-Sil silica catalyst (Figure 4.22) established that particles with diameters of up to 45 nm

were present in this catalyst (cf. 20 - 40 nm for the size of particles proposed to be formed upon reduction of the L.T. nickel oxide species). In fact, the average nickel particle size for this catalyst was 19 nm (which was close to the lower limit of 20 nm proposed for particles derived from the L.T. nickel oxide species). Cab-O-Sil silica is a support of low surface energy, i.e. it contains only a small proportion of three-fold siloxane rings, and hence the calcined catalyst prepared from this support contained mainly the L.T. species of nickel oxide (93 % of hydrogen uptake during T.P.R.). Reduction of this catalyst therefore led to the formation of large particles of nickel.

Based on the T.E.M. analyses, the trend of increased nickel dispersion with higher support metastable energy was apparently reversed for the reduced 1 % nickel on CS2040 silica catalysts, where the average particle sizes were determined to be 8 and 3 nm for the catalysts prepared by the non-aqueous and aqueous methods (Figures 4.26 and 4.25), respectively. There were, however, particularly large discrepancies for both these catalysts between the average particle sizes determined by T.E.M. and those determined by carbon monoxide chemisorption.

The question which now must be posed is why there was such an apparent discrepancy between the respective d_g values determined by T.E.M. and chemisorption methods for each of the reduced catalysts prepared from the CS2040 silica.

The value of the average particle size determined for the reduced nickel on CS2040 (aq.) silica catalyst from carbon monoxide chemisorption experiments undoubtedly

reflected the drastic change in the silica surface morphology during the preparation of this catalyst. Contraction of the average pore diameter of the support occurred for this catalyst during the drying and calcination stages (Section 4.1.1) and it was possible for large numbers of particles of unreduced nickel species to have been partially or completely encapsulated by the support, i.e. by being trapped down collapsed and semi-collapsed pores. The observation that the calcined nickel on CS2040 (aq.) silica catalyst had the lowest estimated reducibility under T.P.R. conditions, see Table 5.4, indicated that some of the unreduced nickel was inaccessible even to reduction gases.

Table 5.4

Estimated Percentage Reduction of the Calcined Catalysts
During T.P.R.

Calcined Catalyst	Percentage Reduction ^a
10 % Ni/ICI	86
10 % Ni/Cab-O-Sil	90
10 % Ni/CS1030E	67
1 % Ni/ICI	95
1 % Ni/Cab-O-Sil	72
1 % Ni/CS1030E	78
1 % Ni/CS2040 (aq.)	62
1 % Ni/CS2040 (non-aq.)	67

a. The values given in this table were calculated on the basis of the hydrogen uptake data obtained during the T.P.R. experiments. Hydrogen spillover and support reduction effects were assumed to be negligible.

The particles of nickel metal precursor species trapped down collapsed pores will have been small as the encapsulation of these particles would have prevented further particle growth by a sintering mechanism or by further deposition of nickel oxide from decomposing nickel nitrate crystallites. The particles of nickel metal precursor may also have fragmented during the encapsulation process. Hence after reduction, a large number of small crystallites of unreduced nickel metal precursor may have been trapped in collapsed pores.

Further sintering of the support may have also occurred during the reduction of the calcined catalyst as water, which is known to promote the sintering of silica (160), was formed during the reduction of the supported nickel oxide. This further sintering of the support may have additionally increased the amount of nickel encapsulated in the support (more details below). Encapsulation of nickel in silica by pore collapse has been observed before (11). Hence, for the reduced catalyst, carbon monoxide chemisorption experiments led to a large d_s value being determined as only a limited amount of the total nickel in the catalyst was accessible to the carbon monoxide adsorbate, indicative of poor dispersion, i.e. large particles.

The T.E.M. data for the reduced nickel on CS2040 (aq.) silica catalyst indicated that no large particles were present and in fact no particles over 9 nm in diameter were observed, with the majority of particles being between 1 - 2 nm in diameter (Figure 4.25). The T.P.R. experiments indicated that little or no H.T. species was present in the unreduced calcined form of this catalyst (Figure 4.4). It

was, therefore, probable that during reduction, large particles of the L.T. species of nickel oxide which had not been fragmented and subsequently encapsulated (and hence were accessible to the hydrogen) released considerable amounts of water into the support immediately surrounding the particles. This water would have caused further sintering of the support in the vicinities of the particles which may have in turn led to the fragmentation and possible encapsulation of the newly-formed nickel particles.

In addition to detecting nickel particles on the surface of the support, therefore, T.E.M. analysis of the reduced 1 % nickel on CS2040 (aq.) silica catalyst would have detected the encapsulated and fragmented particles of unreduced and reduced nickel; both of which would have been small in diameter. Hence T.E.M. analysis of this catalyst led to a value for d_g that was much smaller compared to that determined by carbon monoxide chemisorption. The value of d_g determined by carbon monoxide chemisorption is more useful in a catalytic sense as nickel particles, whether reduced or unreduced, which are occluded by the support will take no part in a catalytic reaction (16, 21).

The position of the reduced 1 % nickel on CS2040 (aq.) silica catalyst as the catalyst with the largest d_g value in the above list of the d_g values for the 1 % nickel catalysts (determined by carbon monoxide chemisorption) was perhaps fortuitous. This catalyst probably represents a special case where the particle size was not so much determined by the energetics of the support, but by the drastic changes in silica morphology during the preparation and activation stages.

The smaller discrepancy between the d_s values determined from T.E.M. and chemisorption methods for the reduced 1 % nickel on CS2040 (non-aq.) silica catalyst can be explained by the fact that this catalyst had the smallest d_s value of all the catalysts as determined by carbon monoxide chemisorption. Mustard and Bartholomew (13) observed that reduction of a calcined 2.7 % nickel on silica catalyst gave a very fine dispersion of nickel. The d_s value as determined by chemisorption for the reduced catalyst was much smaller than that determined from T.E.M. and the authors accounted for this by the presence of thin electron transparent particles on the surface of the support. A similar observation was made for nickel on silica catalysts by Montes and co-workers (9).

The d_s value for the reduced nickel on CS2040 (non-aq.) silica catalyst as determined by carbon monoxide chemisorption was 2 nm. Hence there was likely to be a significant proportion of extremely small particles which were invisible to T.E.M. analysis. This would be especially true after the passivation treatment where the majority of a very small nickel particle would have been converted to nickel oxide (9), which gives less of a contrast between the particle and the support. Larger particles would have remained mainly as nickel with a thin covering of nickel oxide after passivation (9) and therefore would exhibit good contrast with the support.

In conclusion, for both the reduced catalysts prepared from CS2040 silica, the most useful values of d_s were determined by carbon monoxide chemisorption and not by T.E.M. The agreement between d_s values determined by the

two methods for all the other catalysts was satisfactory. The d_g values determined for the catalysts by carbon monoxide chemisorption, shown in Table 5.3, followed an inverse order to that of the surface energies of the silicas for both the 1 % and 10 % nickel loadings, i.e. nickel on CS2040 (non-aq.) and ICI silicas had smaller average particle sizes than nickel on Cab-O-Sil or CS2040 (aq.) silicas. An apparent discrepancy arose, however, with the reduced 1 % nickel on CS2040 (non-aq.) silica catalyst; it had a smaller average particle diameter than the reduced 1 % nickel on ICI silica catalyst despite the ICI silica possessing higher surface energy. This can be explained by recalling that the neutron diffraction experiments, Appendix B, quantified the concentration of three-fold siloxane rings in silicas that had not been in contact with water after manufacture, except for the aqueously treated and dried CS2040 silica (designated CS2040 (aq.) in Table 5.1). During aqueous impregnation of the ICI silica, some of the three-fold siloxane rings would slowly react with water and hence lower the surface energy of the support. This could not happen during the non-aqueous impregnation of CS2040 silica and so effectively more three-fold siloxane ring sites may have been available to interact with nickel on this silica relative to the aqueously impregnated ICI silica. The excellent metal dispersion obtained by a non-aqueous impregnation technique may not be limited to CS2040 silica: there are reported cases in the literature (179) of catalysts prepared by non-aqueous impregnation methods which have far superior metal dispersions compared to analogous catalysts prepared by aqueous methods.

To summarise, therefore, the data in Table 5.3 combined with the data from the S.A.N.S. experiments demonstrated that reduction of calcined catalysts which contained large proportions of the H.T. species of nickel oxide, i.e. catalysts prepared from supports with high surface energies, led to reduced catalysts with good and relatively thermally stable nickel dispersions. Conversely, reduction of calcined catalysts which contained large proportions of the L.T. species of nickel oxide, i.e. catalysts prepared from supports with low surface energies, led to reduced catalysts with poor and thermally unstable nickel dispersions.

5.1.4 General Conclusions on the Nature of Nickel Metal Precursors in Uncalcined and Calcined Catalysts

From this work conclusions can be made regarding the nature of nickel metal precursors contained in the uncalcined catalysts in their unreduced states. For these catalysts, nickel nitrate hexahydrate crystallites were the predominant form of nickel metal precursor on the silicas. A small proportion of the supported nickel was in the form of a reduction-resistant species, the probable nature of which was ion-exchanged nickel(II) ions.

If an uncalcined catalyst was calcined, the following two extremes could arise dependent on the nature of the silica support.

i. For a calcined catalyst prepared from a silica of low surface energy, the nickel metal precursor was predominantly in the form of large particles of nickel oxide which had little or no interaction with the support. Reduction of catalysts of this nature led to reduced catalysts with large

nickel particles, i.e. poor nickel dispersions, which readily underwent sintering at low temperatures.

ii. For a calcined catalyst prepared from a silica of high surface energy, two forms of nickel metal precursor were generally present. One form was large particles of nickel oxide as described above, which was the minor form on such a support. The other form, which predominated on supports of high surface energy, was small particles of nickel oxide which probably interacted with three-fold siloxane rings possibly in the manner shown in Figure 5.2. Reduction of the nickel oxide in the form of large particles led to large nickel particles as previously stated. Reduction of the nickel oxide species which interacted with the support occurred at higher temperature and led to the formation of small particles of nickel which were thermally stable.

These two situations represent extreme cases and for unreduced calcined catalysts prepared from supports of intermediate surface energy, the relative proportions of the H.T. to the L.T. species of nickel oxide will vary. In these cases, the proportion of the H.T. to the L.T. species will be greater for unreduced catalysts prepared from supports of higher surface energy relative to those prepared from supports of lower surface energy.

In addition to the two forms of nickel oxide species, unreduced calcined catalysts can contain a third form of nickel metal precursor which is very easily reduced. This species is thought to be small amounts of nickel(III) ions present in the supported nickel(II) oxide particles.

In exceptional cases, a fourth form of nickel metal precursor which is extremely difficult to reduce may be

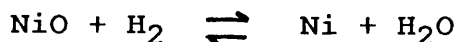
present in unreduced calcined catalysts prepared by impregnation. It is proposed that this species is nickel hydrosilicate.

From the above, it can be seen that the energetics of a silica support can affect the nature of the deposited nickel metal precursors after calcination and, consequently, the nature of the supported metal in the reduced catalyst.

5.2 Reaction Chemistry

Before considering the reaction chemistry of the reduced catalysts, it is necessary to explain why the procedures for the reduction of the calcined catalysts in the present study were adopted. It was established from the T.P.R. experiments that a temperature of 673 K or greater would be sufficient to reduce the calcined catalysts, as the H.T. peaks in the profiles of the catalysts had begun by these temperatures - except for the small amount of the very reduction-resistant species of nickel (probably nickel hydrosilicate) in the calcined 1 % nickel on CS2040 (non-aq.) silica catalyst. If adequate time was allowed, therefore, for the calcined catalysts to reduce at temperatures of 673 K or higher then complete, or at least a high degree, of reduction of the L.T. and H.T. nickel precursor species would be achieved.

To promote a higher degree of reduction, pure hydrogen was used as the reduction gas rather than the 6 % v/v hydrogen in argon used in T.P.R. experiments. By using pure hydrogen the following equilibrium reaction could be displaced to the right (95):



Evidence that the use of pure hydrogen as the reduction gas would increase the degree of catalyst reduction was furnished by the reduction and chemisorption experiments outlined in Table 3.1, Section 3.3.1(b). Out of all the experiments listed in this table, only catalyst reduction using pure hydrogen (experiment number 2) resulted in a measurable amount of chemisorption - see Section 4.2.1(b).

Two reduction procedures were utilised in this study to reduce the calcined catalysts for catalysing ethene hydrogenation. The first procedure was performed by adding a series of aliquots of hydrogen to a sealed and heated reactor containing a sample of a calcined catalyst, i.e. static reduction. The second procedure was performed by heating a sample of a calcined catalyst in a flow of hydrogen, i.e. flow reduction.

The static reduction procedure was performed at 723 K and is described in Section 3.4.1.1. Several changes of the hydrogen atmosphere above each catalyst sample were made during reduction to ensure that water vapour formed by the reduction process was removed from the vicinity of the catalyst samples. Efficacious removal of water vapour is known to increase the degree of catalyst reduction (8, 95). As shown by the data in Tables 4.10a and 4.10b, the static reduction procedure did produce catalysts that catalysed the hydrogenation of ethene. Repetition of several of these experiments demonstrated that the reproducibility of the catalysts reduced in this manner was poor, as the initial rates of the first ethene hydrogenation reactions varied significantly for samples of the same catalyst reduced in separate reductions. The irreproducibility of the samples

was further substantiated, for the 1 % nickel on silica catalysts, by the [^{18}O]-carbon dioxide isotope exchange data (Table 4.11).

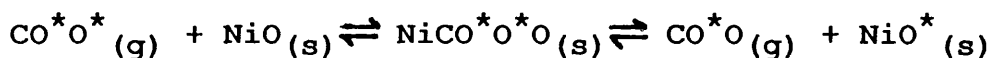
In summary, the static method of catalyst reduction gave rise to irreproducible samples. This was perhaps not surprising, as similar irreproducibility for samples of catalysts prepared by impregnation has been noted before (8). The irreproducibility may have arisen due to the critical importance of the partial pressure of water on both the degree of reduction and the particle size of nickel in a catalyst (9, 29, 95). These two parameters are crucial in determining the reaction rate and the amount of oxygen present on the surface of a catalyst. Complete control must be exercised, therefore, over the length of time each hydrogen aliquot is in contact with the catalyst and also the length of time of the evacuation stage together with the efficiency of the evacuation. Although tight control was maintained over such variables during the static reduction procedure, slight variations may have arisen between separate reductions of samples of the same calcined catalyst leading to differing partial pressures of water in contact with the samples during reduction. This could have led to substantial differences in the degree of reduction and the average particle size between samples. Such a problem is not encountered for catalyst reduction utilising flowing hydrogen, provided that the gas flow is sufficient to remove water vapour as it is formed (8, 95).

The important conclusion which can be drawn from this work is that, despite the presence of residual oxygen on the surface of the nickel after the reduction sequence, the

supported nickel was still able to catalyse the hydrogenation of ethene (Tables 4.10a and 4.10b). The amount of exchangeable oxygen varied by a factor of about eighty between the active catalysts (Table 4.11), but such wide variation is not unusual, similar variations having been found in other studies (163). As might be intuitively expected, the statically-reduced and deliberately oxidised sample of the 1 % nickel on ICI silica catalyst used in the control experiment (experiment number 8, Table 4.11) generated a very large amount of [^{16}O]-oxygen exchange on a per gram of catalyst basis (second only to experiment number 7, Table 4.11). The control sample was also inactive for ethene hydrogenation as no pressure change occurred after admission of the ethene and hydrogen mixture to the reactor. This was indicative of the absence of any metallic surface in the oxidised catalyst. Mass spectrometric analysis of the ethene, hydrogen and [^{18}O]-carbon dioxide mixture in contact with the control sample for 80 minutes also confirmed no ethene hydrogenation had occurred. In addition, no dimerisation of the ethene to gas phase C_4 hydrocarbons occurred at a temperature of 273 K, in agreement with the observation of Lapinski and Ekerdt (169).

To understand why the fully oxidised sample of catalyst in the control experiment exchanged a smaller amount of oxygen with [^{18}O]-carbon dioxide gas than a partially reduced catalyst, it is important to consider how the oxygen exchange process occurred. In agreement with other studies (71, 163), it was found that no oxygen exchange occurred between pure silica and [^{18}O]-carbon dioxide. Hence, oxygen exchange occurred only on the metal surfaces of the

catalysts between residual oxygen and the added carbon dioxide, with no exchange with oxygen from the supports. Carbon dioxide chemisorption, itself, has been found to be weak and reversible on fully reduced or partially reduced samples of nickel oxide on silica (71). If residual oxygen is present on the metal surface of a catalyst, and [^{18}O]-carbon dioxide is added, then exchange has been demonstrated to occur between this oxygen and the reversibly adsorbed [^{18}O]-carbon dioxide (71, 163). Connor and Bennett (71) proposed that an adsorbed carbonate-type intermediate was formed by carbon dioxide adsorbing on a strongly held surface oxygen (probably O^{2-}), i.e. formation of surface nickel carbonate occurs;



where O^* represents an [^{18}O]-oxygen atom. The formation of the surface nickel carbonate was found to be reversible in nature and so oxygen exchange can occur.

From the above description of the oxygen exchange mechanism, it can be seen that it was a process that occurred purely on the metal surface. Hence the amount of exchange was not only governed by the total amount of oxygen associated with the nickel component of the catalyst, but also by the amount of oxygen on the metal surface. The amount of oxygen exchange, therefore, may have depended on two factors;

- i. The dispersion of the nickel.
- ii. The reducibility of the nickel metal precursor species in the unreduced calcined catalyst.

To decide which of the above factors had the greater potential influence on the amount of exchangeable oxygen,

consider the case of a poorly reduced catalyst with a poor dispersion (i.e. large particles). On contact with this catalyst, only a small amount of [^{16}O]-oxygen will be exchanged into the [^{18}O]-carbon dioxide as the gas is in contact with only a relatively small overall particle surface area, most of the oxygen being present in the bulk of the particles and not exchangeable. On the other hand, with a well dispersed catalyst with a high degree of reduction, where the metal component of the catalyst contains only a relatively small amount of oxygen, a large proportion of this oxygen will be located at the surface of the particles and may be exchangeable. A comparatively large amount of oxygen exchange, therefore, may occur with this catalyst. Hence the major factor governing the potential amount of oxygen available for exchange will have been the metal dispersion and not the actual oxygen content of the metal component. Therefore, it was possible to achieve a greater amount of oxygen exchange using a partially reduced catalyst, e.g. experiment number 7, Table 4.11, relative to a fully oxidised catalyst, e.g. experiment number 8, Table 4.11.

No data are available for the dispersions of nickel in the statically-reduced catalysts but it seems likely, on the basis of the above argument, that the 1 % nickel on CS2040 (aq.) silica catalyst (experiment number 7) was better dispersed than the oxidised 1 % nickel on ICI silica catalyst used in the control experiment (experiment number 8). However, the reproducibility of all the catalysts reduced by static reduction was poor, as another sample of the 1 % nickel on CS2040 (aq.) silica catalyst reduced in

the identical manner (experiment number 7a) gave only about 20 % of the amount of exchange observed for the original experiment.

Further complication arises from the observation of Jackson, Robertson and Willis (163), that although substantial oxygen exchange occurred when [^{18}O]-carbon dioxide was used as a probe for residual oxygen on the surface of copper on silica catalysts, the majority of the metal surface of each catalyst was covered by a non-exchangeable oxygen species. Similarly, the amount of oxygen exchange observed between a supported nickel catalyst and [^{18}O]-carbon dioxide could be comparatively small relative to the total amount of residual oxygen present on the metal surface of the catalyst. Thus the amount of oxygen exchange was only quantitative with respect to the amount of exchangeable oxygen species located on the metal surface but not necessarily quantitative with respect to the total amount of oxygen present. Indeed, it is shown later in this section, by the oxygen exchange results for the oxidised catalyst used in the control experiment for the flow-reduced catalysts (where the d_g values are known for the catalysts), that all the oxygen present on the nickel surface of a catalyst was not exchangeable.

Direct comparison of the initial rates for the first hydrogenation reactions performed using the statically-reduced catalysts was not possible, since a proper comparison can only be made using specific rate data, i.e. the rate of reaction per m^2 of nickel. Qualitatively, however, the rate of reaction per gram of catalyst was generally greater for the 10 % nickel on silica catalysts

compared to the 1 % nickel on silica catalysts. This was not unexpected as the amount of metal surface area per gram of catalyst for the 10 % nickel on silica catalysts may have been larger. This can be seen by consideration of the hypothetical cases of two moderately dispersed catalysts: a 10 % nickel on silica catalyst and a 1 % nickel on silica catalyst with d_s values of 20 and 5 nm, respectively. The S_{Ni} values for these two catalysts, calculated using expression 1.11 (defined in Section 1.3.3), are 34 and 135 $m^2(g \text{ nickel})^{-1}$, respectively. Hence on a per gram of catalyst basis, the 10 % nickel on silica catalyst has a larger metal surface area than the 1 % nickel on silica catalyst, i.e. $S_{Ni} = 3.4$ and $1.3 m^2(g \text{ catalyst})^{-1}$, respectively.

No apparent correlation existed between the rate data for the initial hydrogenation reactions performed using the 1 % nickel on silica catalysts (Table 4.10b) and the amounts of exchangeable oxygen on the metal surfaces of these catalysts (Table 4.11). This is illustrated by comparing experiment numbers 4 and 5 in these tables, where the ethene hydrogenation rates for the first reactions were 0.2×10^{-5} and $1.2 \times 10^{-5} \text{ mol.s.}^{-1}(g \text{ catalyst})^{-1}$, respectively, whilst the amounts of exchangeable oxygen for these catalysts were 0.4×10^{18} and $2.3 \times 10^{18} \text{ atoms}(g \text{ catalyst})^{-1}$, respectively. The catalyst sample used in experiment number 4, therefore, had less exchangeable oxygen and catalysed ethene hydrogenation at a slower rate than the catalyst sample used in experiment number 5. On the other hand, comparison of experiment numbers 5a and 6 shows that the initial hydrogenation rates using these catalysts were 0.5×10^{-5}

and $1.7 \times 10^{-5} \text{ mol.s.}^{-1}(\text{g catalyst})^{-1}$, respectively, whilst the amounts of exchangeable oxygen were 18.5×10^{18} and $3.1 \times 10^{18} \text{ atoms}(\text{g catalyst})^{-1}$, respectively. Hence, in this latter case, the catalyst with the lower amount of exchangeable oxygen catalysed the hydrogenation of ethene faster than the catalyst with the larger amount. The metal surface areas of the catalysts reduced by the static method, however, were not determined and hence the specific rates of hydrogenation per m^2 of nickel were unknown. A direct comparison between the specific rates of hydrogenation for the different catalysts was therefore impossible. In addition, the oxygen exchange data were quantitative with respect to the amounts of exchangeable oxygen on the metal surfaces of the catalysts and not the total amounts of oxygen present.

Regarding the behaviour of the statically-reduced catalysts over a series of hydrogenation reactions, Figures 4.28 and 4.29 demonstrate that, for both the 1 % and 10 % nickel on silica catalysts, the rate of hydrogenation generally decreased with successive reaction. Whilst the curves showing this decrease in rate between successive hydrogenation reactions were not smooth, the discontinuities corresponded to periods when the catalysts were stored under hydrogen (e.g. overnight). Periods when the catalysts were stored in such a way between successive reactions are indicated by the dotted lines in Figures 4.28 and 4.29. It is apparent that this method of storage led to a partial reactivation of the catalysts. Analogous increases in the reaction rate have previously been observed after similar storage procedures for olefin hydrogenation catalysts (180).

It is well known that the deactivation of reduced supported metal catalysts during ethene hydrogenation is primarily due to the formation of carbonaceous residues on the metal surfaces of the catalysts (98, 181, 182). These carbonaceous residues are overlayers of adsorbed hydrocarbon species which are deficient in hydrogen and which form by the dissociative adsorption of ethene on the metal surfaces. The effect of the formation and subsequent build-up of such an overlayer is to decrease the rate at which the hydrogenation reaction occurs. Carbonaceous residue formation is, in its earlier stages, partially reversible by hydrogenation (29, 98, 181).

In the present study the steady deactivation of the catalysts as the hydrogenation cycles progressed can be ascribed to the formation and subsequent build-up of carbonaceous overlayers on the metal surfaces of the catalysts. After periods of storage under hydrogen, the catalysts regained some of their former activity due to the partial hydrogenation of these carbonaceous overlayers. Thus the catalysts which were reduced by the static method apparently behaved in the expected manner toward ethene hydrogenation and were not anomalous with respect to their deactivation behaviours.

The second reduction procedure utilised in this study employed a flow of hydrogen gas to reduce the catalysts and is described in Section 3.3.1(a). The reduction was performed at a temperature of 673 K, which was lower than the temperature used in the static reduction procedure, but which was equivalent to that used in the reduction procedure adopted by the other research groups involved in this study.

In contrast to the catalysts reduced by the static method, the initial rates of ethene hydrogenation per gram of catalyst obtained using catalysts reduced by flowing hydrogen were reproducible (Table 4.12). The reproducibility of the catalyst samples was confirmed by the oxygen exchange data presented in Table 4.14a. The values of d_s , D and S_{Ni} for the flow-reduced catalysts were also determined using carbon monoxide chemisorption and T.E.M. techniques (Tables 4.8 and 4.9, respectively). This allowed both the specific rate data for the ethene hydrogenation reactions and the amounts of exchangeable oxygen per m^2 of nickel to be calculated for the catalysts.

Comparison of the initial rates per gram of catalyst for the first hydrogenation reactions performed using the flow-reduced calcined catalysts with their counterparts reduced by the static method shows that the flow method produced more active catalysts. This indicated that the flow reduction technique was more efficient at producing a higher degree of reduction than the static reduction technique as highlighted earlier in this section. Additionally, the efficient removal of water vapour is known to prevent sintering and favour the formation of small nickel particles (8, 9, 16, 29, 95).

As in the case of the catalysts reduced by the static procedure, the presence of residual oxygen on the metal surfaces of the flow-reduced catalysts was confirmed by using [^{18}O]-carbon dioxide as a surface probe for oxygen (Table 4.14a). The amounts of exchangeable oxygen per m^2 of nickel were also calculated and are shown in Table 4.14b. Examining the figures in this table, it can be seen that the

oxidised 1 % nickel on ICI silica catalyst used in the control experiment (experiment number 9), and which was catalytically inactive, had the largest amount of exchangeable oxygen per m^2 of nickel.

Similar to the observation of Jackson et al. (163) for copper on silica catalysts, the control experiment demonstrated that all the residual oxygen present on the nickel surfaces of the catalysts was not exchangeable. If the d_s value of 7 nm derived from the T.E.M. data (Table 4.9) for the catalyst used in the control experiment was considered to reflect the actual size of the nickel particles on the surface of the support more accurately than the d_s value from the chemisorption experiments (see below for details), then the proportion of oxygen which was exchangeable can be calculated in the following way:-

The data derived from the T.E.M. analyses, Table 4.9, showed that for the flow-reduced 1.2 % w/w nickel on ICI silica catalyst used in the control experiment, $S_{\text{Ni}} = 100 \text{ m}^2 (\text{g nickel})^{-1}$.

Hence;

$$\begin{aligned} S_{\text{Ni}} &= 1.2/100 (\text{g nickel})/(\text{g catalyst}) \times 100 \text{ m}^2/(\text{g nickel}) \\ &= 1.2 \text{ m}^2(\text{g catalyst})^{-1} \end{aligned}$$

Since the average cross-sectional area of a nickel atom is $6.5 \times 10^{-20} \text{ m}^2$ (Section 1.3.2), the total number of surface nickel atoms, N_s , was;

$$N_s = 1.2/6.5 \times 10^{-20} = 1.85 \times 10^{19} \text{ Ni atoms (g catalyst)}^{-1}$$

If the metal surface of the catalyst was assumed to be fully oxidised and each surface nickel atom associated with an oxygen atom, i.e. monolayer coverage, then there were $1.85 \times 10^{19} \text{ O atoms (g catalyst)}^{-1}$.

Experimentally, 1.51×10^{19} O atoms (g catalyst)⁻¹ were exchanged in the control experiment, i.e. 82 ($\pm 12^a$) % of the oxygen monolayer capacity of the catalyst. Hence, this calculation shows that approximately 82 % of the oxygen present on the metal surface of the catalyst used in control experiment was exchangeable. This calculation, therefore, demonstrates that all the oxygen on the surfaces of the catalysts was not exchangeable.

The presence of residual oxygen on all the flow-reduced catalysts led to discrepancies between the d_g values obtained from T.E.M. analyses (Table 4.9) and those obtained from the carbon monoxide chemisorption experiments (Table 4.8). The d_g values obtained from T.E.M. analyses were generally smaller than those obtained from carbon monoxide chemisorption experiments - the 1 % nickel on CS2040 (non-aq.) silica catalyst was a special exception as discussed earlier. T.E.M. analysis is known frequently to give an accurate value for the actual average size of the supported particles in a catalyst (16), but the presence of oxygen, not all of which was exchangeable, on the supported particles in the catalysts in the present study meant that some of the metal surface was unavailable for carbon monoxide chemisorption. Hence the d_g values for the catalysts determined from carbon monoxide chemisorption data were generally larger reflecting, in a catalytic sense, the effective average particle sizes.

Unless otherwise specified, in the following discussion on the rates of ethene hydrogenation by the catalysts

a. Error calculated by assuming an error of 10 % for the S_{Ni} value determined by T.E.M. (13).

reduced by flowing hydrogen, the specific rates referred to will be restricted to those calculated using the carbon monoxide chemisorption data. Carbon monoxide chemisorption will only have detected surface nickel atoms which were capable of adsorption and hence could catalyse ethene hydrogenation. Thus the carbon monoxide chemisorption data were more relevant in a catalytic sense.

The reduced 10 % nickel on silica catalysts had a generally higher rate of reaction per gram of catalyst compared to the reduced 1 % nickel on silica catalysts (Table 4.12). This was due to the 10 % nickel on silica catalysts possessing a larger nickel surface area on a per gram of catalyst basis than the 1 % nickel on silica catalysts: the S_{Ni} values were in the ranges 4.4 - 10.2 and 0.5 - 4.0 $m^2(g \text{ catalyst})^{-1}$ for the 10 % and 1 % nickel on silica catalysts, respectively. Direct comparison of the reaction rates for all the catalysts can also be made using the specific rate data (Table 4.13). Examination of this data shows that the specific rates ranged from 3.6×10^{-6} to $53.2 \times 10^{-6} \text{ mol.s.}^{-1}(m^2 \text{ nickel})^{-1}$.

According to the classification proposed by Boudart (14) ethene hydrogenation is a surface insensitive (or facile) reaction. This means that the specific reaction rate, i.e. the rate expressed per unit surface area of the active phase (in this case nickel metal), is expected to change little with the size of the particles, type of support or method of catalyst preparation (12, 14, 16). The specific rates of reaction for surface insensitive reactions are ordinarily found to vary within a factor of ten (12).

The specific rates of reaction in this study, Table 4.13, varied to a slightly greater extent than the factor of ten expected for a surface insensitive reaction. By substituting the specific rate calculated from the T.E.M. data for the reduced 1 % nickel on ICI silica catalyst (experiment number 4 in Table 4.13) instead of the rate calculated from the carbon monoxide chemisorption experiments, it is found that the specific rates now varied within a factor of ten - the rates range from 3.6×10^{-6} to $32.4 \times 10^{-6} \text{ mol.s.}^{-1}(\text{m}^2 \text{ nickel})^{-1}$. Hence the specific rate calculated from the carbon monoxide chemisorption data for this catalyst may be inaccurate.

In fact, with the exception of the specific rate for the 1 % nickel on ICI silica catalyst, the specific rates varied to within about a factor of four and were in the range 3.6×10^{-6} to $14.9 \times 10^{-6} \text{ mol.s.}^{-1}(\text{m}^2 \text{ nickel})^{-1}$. This variation was very similar to the factor of three obtained by Crawford, Roberts and Kemball (183) for the specific rates of ethene hydrogenation reactions performed using sintered nickel films of varying average particle sizes.

For the series of catalysts studied, no obvious correlations were observed between the relatively small variations in the specific rate of reaction and either the support, the average particle size or the amount of exchangeable oxygen per m^2 of nickel. For example, for the 10 % nickel on silica catalysts, the specific rate with respect to the catalyst support increased in the order ICI silica < CS1030E silica < Cab-O-Sil silica. For the 1 % nickel on silica catalysts, the corresponding order was

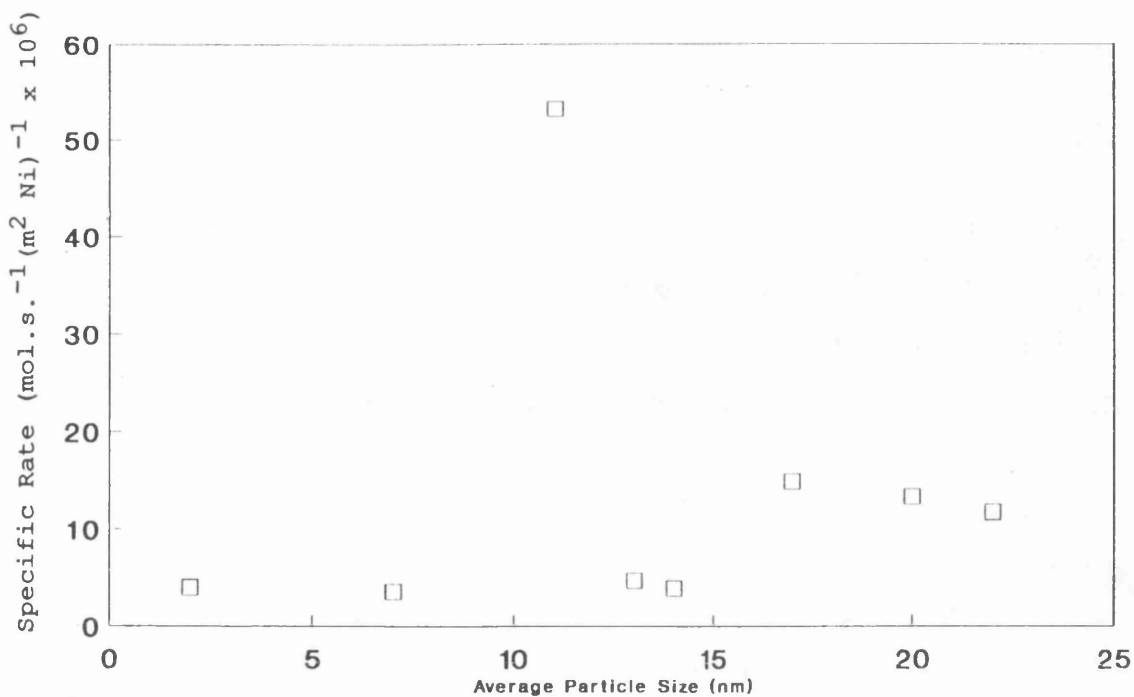
reversed, i.e. Cab-O-Sil silica < CS1030E silica < ICI silica. In addition, Figures 5.4 and 5.5 confirm that no apparent correlation existed between the specific rate and either the average particle size or the amount of exchangeable oxygen per m^2 of nickel. Similar results for surface insensitive reactions were obtained by Aguinaga and co-workers (12) when they plotted the specific rate against average particle size. The result that the amount of exchangeable oxygen did not affect the specific rate meant that the oxygen on the metal surfaces of the catalysts was only operating as a site-blocking poison: i.e. despite large variations in the amount of exchangeable oxygen per m^2 of nickel between the catalysts no correlation was evident with the rate of reaction per m^2 of nickel.

Two explanations for the observed variations in the specific rates are possible;

- i. The variations in the specific rates between catalysts could have arisen due to rapid (a few milliseconds) formation of surface carbonaceous overlayers (184). Thus the actual working surfaces of the catalysts may have developed only after deactivation of some of the active sites (16). The initial metal surface areas determined for the catalysts, therefore, may not have accurately represented the active surface areas, even in a proportional manner, since the rates of formation of carbonaceous overlayers may also vary with particle size (16).
- ii. The second possibility is that reactive growth of the particle size occurred during the reaction and this again led to the effective metal surface areas of the catalysts

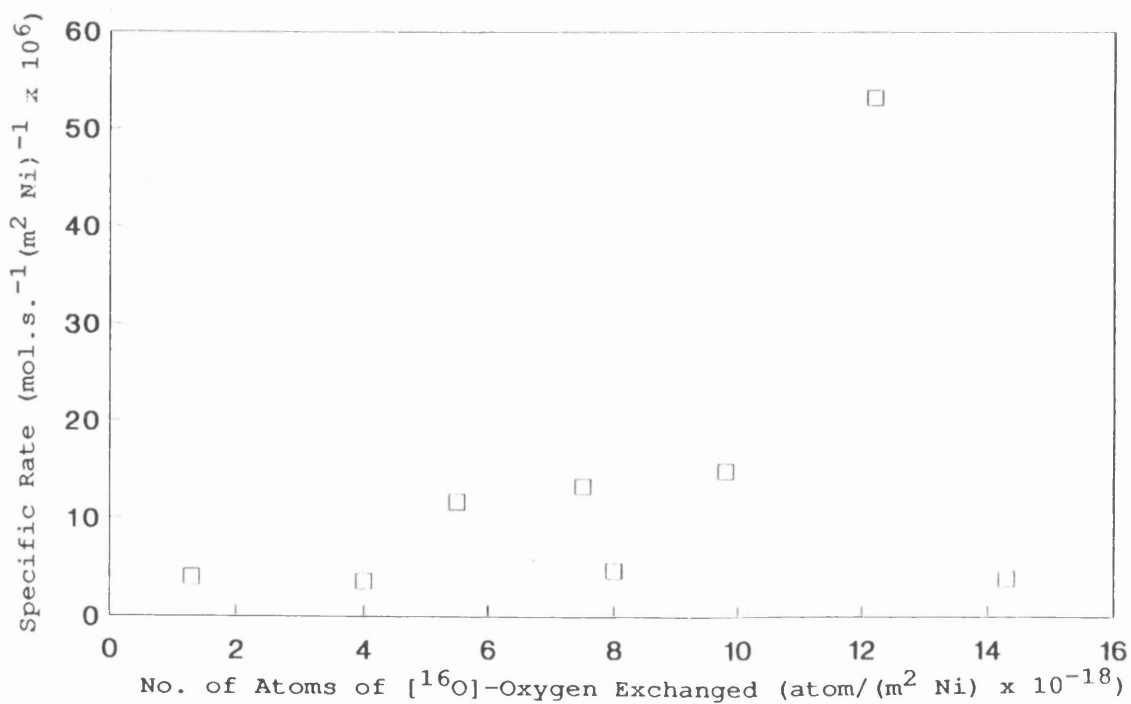
Fig. 5.4

Average Particle Size Versus the Specific Rate of Ethene Hydrogenation



All data calculated using carbon monoxide chemisorption results.

Fig. 5.5 Amount of Exchangeable Oxygen Versus the Specific Rate of Ethene Hydrogenation



All data calculated using carbon monoxide chemisorption results.

during reaction differing from those measured prior to reaction (16, 25, 29, 183).

Both these processes, which may occur simultaneously, would have led to variations in the calculated specific rates between catalysts. These variations would be relatively small compared to the variations in the specific rates observed for surface sensitive reactions (12).

In summary, it was apparent that ethene hydrogenation is a surface insensitive reaction, in agreement with the literature (12, 14, 183), with the specific rate unaffected by the average particle size and the type of silica used as the support. Furthermore, the specific rate appeared to be unaffected by the presence of varying amounts of exchangeable oxygen per m^2 of nickel, unless the surface was fully oxidised (i.e. the control experiment, data in Tables 4.13 and 4.14b) where the reaction was completely inhibited.

In addition, it is known from the studies performed using catalysts reduced by the static procedure, that the catalysts underwent a process of deactivation during a series of ethene hydrogenation reactions. Partial restoration of catalytic activities occurred after storage of the catalysts under hydrogen. The reduced catalysts, therefore, displayed no anomalous behaviour with respect to ethene hydrogenation and hence the use of this as a test reaction has shown the catalysts not to have been atypical in their behaviour, at least with respect toward ethene hydrogenation. Additionally, the uncalcined and calcined catalysts in their unreduced states have been shown, by the use of T.P.R., to have behaved similarly toward reduction in

hydrogen as other analogous unreduced catalysts reported in the literature (Sections 5.1.1 and 5.1.2).

It has been established by the use of a simple test reaction and T.P.R., that the catalysts in their reduced and unreduced states behaved in the expected manner toward ethene hydrogenation and reduction. Hence, the catalysts used in this study appear to have been typical with respect to other catalysts reported in the literature (5, 12, 101, 180, 183). Accordingly, the conclusions reached in Sections 5.1.3 and 5.1.4 concerning the nature of the supported nickel metal precursors and supported nickel in these catalysts can be extrapolated generally to nickel on silica catalysts prepared by impregnation.

In the above discussion it has been shown that the rate of ethene hydrogenation was dependent on the nickel surface area only and not on the nature of the support, in accordance with the literature (12, 14). In contrast, the Surrey group (Prof. J. R. Jones *et al.*) have identified a reaction where the nature of the support was thought to play an important role by interacting directly with the reactants and products of the reaction. A brief summary of the findings of the Surrey group is given in Appendix C. Further details are described elsewhere (185).

5.3 General Summary

In conclusion, the work described in this thesis together with data produced by the Cambridge and Surrey research centres has shown how the nature of a silica support can influence;

- i. The nature and reducibility of the supported nickel metal precursor species in an unreduced calcined catalyst.
- ii. The dispersion and nature of the supported nickel particles derived from these nickel precursor species upon reduction.
- iii. The rate of certain chemical reactions by interaction with the products and/or the reactants of these reactions.

In the course of the work described in this thesis, a clear and complete interpretation of the T.P.R. profiles obtained for uncalcined nickel on silica catalysts has been proposed. A critical reassessment of the literature interpretation of T.P.R. profiles of silica-supported nickel oxide samples has led, in conjunction with the data produced in this study and by the Cambridge and Surrey groups, to the development of a model for a type of nickel metal precursor/support interaction which causes the nickel metal precursor to reduce only at high temperature. By applying this model, it has been possible to explain other observations previously reported in the literature. The nature and behaviour of the different types of nickel particle formed on reduction of the calcined catalysts has also been described.

The use of a simple test reaction, ethene hydrogenation, has shown that the reduced calcined catalysts were active for ethene hydrogenation and that deactivation of the catalysts occurred over an extended series of ethene hydrogenation reactions. Partial reactivation of the catalysts also occurred after storage of the catalysts under hydrogen. The specific rate data for ethene hydrogenation calculated for all the catalysts has shown that this

reaction was surface insensitive; all these observations were consistent with the literature (12, 14, 180). This, in conjunction with the results of the T.P.R. experiments, has shown the reduced and unreduced catalysts not to be anomalous, at least with respect to their behaviour toward ethene hydrogenation and their T.P.R. characteristics. Hence, the conclusions reached in the present study, for the catalysts, regarding the nature of the supported nickel metal precursor species and supported nickel metal are generally applicable to nickel on silica catalysts prepared by impregnation.

Through the work described in this thesis, therefore, an understanding has been gained into how the fundamental structure of silica supports affect the structure and behaviour of unreduced and reduced silica-supported nickel catalysts.

APPENDICES

Appendix A - Silica Support DataA1. ICI Silica Support (186)

This is a high purity "in house" silica prepared by acidification of a sodium silicate solution. Sodium silicate solution ($400 \text{ gl}^{-1} \text{ SiO}_2$) was acidified with 4 molar sulphuric acid and a solution of oxalic acid (10 gl^{-1}) in 1 molar sulphuric acid. The purpose of the oxalic acid treatment was to complex cationic impurities such as iron, aluminium and titanium ions and therefore prevent them from precipitating. The silica sol formed after acidification of the sodium silicate solution was allowed to gel for 10 minutes and then left overnight to shrink. The liquor exuded from the gel was then drained and the gel chopped before drying in a domestic microwave oven. Following this procedure, residual water was reduced by 80 % and the gel had shrunk to one third its original volume.

The gel was then extracted with one aliquot of water, three of 1 molar sulphuric acid and finally two of water before the silica was dried to constant weight, again in the microwave oven.

The impurities determined by ICP-AES are:

Fe	< 1 ppm
Ti	< 1 ppm
Al	< 3 ppm
Na	< 10 ppm

A2. Cab-O-Sil M-5 Silica Support (187)

Cab-O-Sil is produced by flame hydrolysis of silicon tetrachloride in a hydrogen/oxygen flame at around 2070 K. This gives a colloidal silica of high purity and zero porosity which differs markedly from silicas produced by the silica gel route. The particle size is very small (7 - 15 nm), however individual particles do not exist as separate entities because they fuse to form aggregates with chain-like structures.

The typical properties of Cab-O-Sil M-5 are:

Surface Area (m^2g^{-1})	200
Density (gl^{-1})	40
Ignition loss (%)	< 1

The impurities determined by ICP-MS are (188): .

Al	< 20 ppm
Ti	< 20 ppm
Fe	< 20 ppm
Na	20 ppm

A3. CS1030E Silica Support (189)

CS1030E silica support is a high purity, moderate pore, synthetic amorphous silica extrudate. This support is designed particularly to function as a highly efficient catalyst carrier in applications where controlled pore size and narrow pore size distribution are desirable. For this support, catalyst impregnation using an aqueous slurry or incipient wetness technique can be achieved without significant loss of surface area or pore volume.

The typical properties of CS1030E are:

Physical Form	1/16" Extrudate
Surface Area (m^2g^{-1})	300
N_2 Pore Volume (cm^3g^{-1})	1.0
Average Pore Diameter (nm)	13
Crush Strength ($\text{Lb}_f/10$ mm particle)	> 20
Wt % loss on drying at 378 K	< 3.0

Typical chemical analysis:

Wt % Silica, as SiO_2	> 99.7
PPM Alumina, as Al_2O_3	< 300
PPM Sodium, as Na_2O	< 1000
PPM Calcium + Magnesium, as CaO	< 200

A4. CS2040 Silica Support (190)

CS2040 silica support is a high purity, large pore volume, synthetic amorphous granular silica gel. This support is essentially designed to function as a highly efficient catalyst carrier in applications where controlled pore size and narrow pore size distributions are desired.

The silica is stable in terms of surface area and pore volume when heated to temperatures up to 1173 K in air or other controlled atmosphere activations, e.g. a decrease of less than 10 % occurs in these properties after calcination in air for 16 hours at 1143 K. Pore diameter contraction occurs, however, after the support has been in contact with aqueous media and then dried (ref. 161, Table B1 (Appendix B) and Section 4.1.1).

The typical properties of CS2040 are:

Physical Form 30, 45 or 90 micron granular powders

Surface Area (m^2g^{-1}) 410

N_2 Pore Volume (cm^3g^{-1}) 2.1

Average Pore Diameter (nm) 20

Wt % loss on drying at 378 K < 6.0

Particle size distribution:

Wt % on 325 Mesh > 92

Wt % on 100 Mesh < 0.2

Typical chemical analysis:

Wt % Silica, as SiO_2 > 99.8

PPM Alumina, as Al_2O_3 < 300

PPM Sodium, as Na_2O < 300

PPM Calcium + Magnesium, as CaO < 200

Appendix B - Summary of Support Characterisation (191)

B1. Introduction

The department of Chemical Engineering, Cambridge University (Dr. L. Gladden *et al.*) has used NMR, neutron scattering and computer simulation techniques to study the structure of the various silica supports used in the preparation of the catalysts. The major problem in understanding the behaviour of silica-supported catalysts is the inability to characterise the structure of amorphous silica. The aim of this work was to overcome this problem.

It is commonly accepted that the structure of a non-crystalline solid can be described in terms of ring statistics; this description should be thought of as analogous to the unit cell description of crystalline materials. In the following discussion the 5 nm pore gel is nominally the same material as the standard ICI catalyst support (the two give identical ^{29}Si MAS NMR and CP MAS NMR spectra). The major findings of the work are summarised below.

B2. Neutron Diffraction Studies

Neutron diffraction experiments were undertaken on instrument D4B at ILL, Grenoble and LAD at ISIS. It was found that the more active catalysts (see Appendix C) were prepared from silicas with a higher concentration of small, strained, three-fold siloxane rings in their network. These siloxane rings consist of three silicon atoms bonded together via three bridging oxygen atoms. The percentage of three-fold siloxane rings incorporated into each silica network was determined by constructing computer models of

networks with varying ring statistics and then comparing their respective scattering functions with those obtained experimentally from diffraction studies. The results are presented in Table B1.

Table B1
Results of Neutron Diffraction Studies

Sample	Pore Diameter (nm)	BET Surface Area (m^2g^{-1})	Skeletal Density ^a (g cm^{-3})	% 3-fold Siloxane Rings
Bulk Silica	-	-	2.17-2.20	< 1
5 nm Gel	5.0	474	2.32	5
20 nm Gel	20.0	118	2.27	2
Densified Gel	-	0.29	2.21	< 1
CS2040 ^b	20.8	415	2.19	5
CS2040 ^c	11.5	426	2.16	2
Cab-O-Sil	-	194	2.20	1
‡	0.5	5	0.05	

a. Determined by helium pycnometry.

b. CS2040 before contact with water.

c. CS2040 after contact with water.

If it is assumed that all three-fold siloxane rings exist at the surfaces of silica structures (174) then the ICI 5 nm pore silica had 40 - 50 % of its surface made up of three-fold siloxane rings, CS2040 (before contact with water) 30 - 35 %, CS2040 (after contact with water) < 20 % and Cab-O-Sil 0 - 5 %. Three-fold siloxane rings are high energy structures relative to large ring species and catalytic activity appeared to correlate with the surface energy of the respective silica supports (see Appendix C).

It should also be noted that three-fold siloxane rings are known to readily interconvert to vicinal silanol groups upon exposure to water. NMR experiments have shown that the maximum number of three-fold siloxane rings were formed when the silicas were dehydroxylated at about 923 K.

B3. Magic Angle Spinning NMR (MAS NMR)

^{29}Si MAS NMR studies of the pure silicas have been performed on a Bruker MSL200 NMR spectrometer, operating at a spectrometer frequency of 39.76 MHz. Data were acquired using a $\pi/4$ pulse of duration 3 μs and a recycle delay of 60 s. TMS was used as a spectral reference. Deconvolution of the NMR lineshapes into component Gaussians was performed subject to the constraint that the lineshape should be fitted with the minimum number of component peaks; the peak falling at ca. -110 ppm was first positioned and its fit to the experimental lineshape optimised. If necessary, further peaks at ca. -100 ppm and ca. -91 ppm (corresponding to Q^3 and Q^2 sites, respectively) were introduced and the fit optimised by iterating on chemical shift, width and intensity of the component Gaussians. The results of this lineshape analysis strongly supported the interpretation of the neutron data previously discussed. Cab-O-Sil, the 20 nm pore gel, the densified gel and CS2040 (after contact with water) were all well fitted by two component Gaussians with the major component falling at ca. -110 ppm. However, the 5 nm pore gel and the CS2040 (before contact with water) did require a significant intensity at a chemical shift of ca. -105 ppm. Thus it was observed that samples which contained a significant number of three-fold siloxane rings

as determined by neutron diffraction, also required a Gaussian component at ca. -105 ppm. This component was not enhanced upon proton cross-polarisation and therefore was not a silanol species. Instead it can be assigned to Q^4 species in three-fold siloxane rings which will necessarily be associated with small Si-O-Si bond angles. Chemical shift and Si-O-Si bond angle have been seen to correlate as follows:

$$\delta \text{ (ppm)} = -0.59(\phi) - 23.21,$$

where ϕ is the Si-O-Si bond angle in degrees. The Q^4 peak centred at ca. -110 ppm was associated with Si-O-Si bond angles, $\phi > 145^\circ$ (which is typical of a four-, five- or six-fold siloxane ring), whereas a peak centred at ca. -105 ppm was associated with $\phi = 138^\circ$. Such a bond angle would be expected for a three-fold siloxane ring structure. Table B2, below, summarises the results of the line fitting analysis.

B4. Small Angle Neutron Scattering

Small angle neutron scattering (S.A.N.S.) experiments have been performed on instrument D17 at ILL, Grenoble. By using both natural and isotopically substituted nickel/silica it was possible to investigate the potential of S.A.N.S. to study simultaneously changes in both silica pore size and metal particle size as a function of thermal treatment of a nickel/silica catalyst. These studies were only performed on reduced samples of nickel supported on silica produced by ICI. The silica support had been hydrothermally processed to yield a pore diameter which could be observed using the S.A.N.S. technique.

Table B2

Results of MAS NMR Experiments on the Pure Silicas

Sample	Chemical Shift (ppm)	Peak Fitting Parameters	
		Peak Position (ppm)	Relative Area (%)
5 nm Gel	-109.0	-95.3	19
		-104.1	59
		-109.0	22
20 nm Gel	-111.9	-101.9	25
		-111.9	75
Densified Gel	-111.8	-95.8	20
		-111.8	80
CS2040 ^a	-111.9	-100.1	28
		-107.2	14
		-111.9	58
CS2040 ^b	-109.9	-100.9	28
		-109.9	72
Cab-O-Sil	-109.8	-98.6	29
		-109.8	71
\pm	0.5	0.5	5

a. CS2040 before contact with water.

b. CS2040 after contact with water.

Following reduction the catalysts were heated in flowing hydrogen at the temperatures indicated in Table B3. Analysis suggests a bimodal distribution in particle size;

the smaller particles being resistant to sintering up to ca. 1023 K. A S.A.N.S. study on a reduced nickel/silica sample heated to 1223 K in flowing hydrogen showed complete collapse of the pore structure and the loss of discrete nickel particles in the catalyst. These results were consistent with nickel silicate formation at a very high temperature. A summary of the results is presented in Table B3.

Table B3

Results of S.A.N.S. Studies on Nickel on ICI Silica

Pore Size Characteristics				
Treatment Temp. (K)	Surface Fractal Dimension, D_s	Mean Pore Diameter (nm)	Smallest Pore Diameter (nm)	BET (nm)
723	3.89	9.6	0.73	10.6
873	3.85	9.9	0.69	11.1
1023	3.71	11.8	0.68	11.4
Nickel Particle Characteristics				
Treatment Temp. (K)	Surface Fractal Dimension, D_s	Mean Particle Diameter (nm)	Smallest Particle Diameter (nm)	
723	6.00	9.9	0.82	
873	4.00	8.7	0.83	
1023	2.35	6.9	1.17	

BET pore size measurements were additionally performed on samples taken from the same batch as were used in the S.A.N.S. experiments and the results also listed in Table B3 for comparative purposes.

The general conclusions from the S.A.N.S. studies are as follows:

- i. The silica support was stable to thermal treatment at 723, 873 and 1023 K; i.e. there was no significant change in any of the parameters characterising the pore structure.
- ii. There were changes in the size of the nickel particles with treatment temperature. These results can be explained in terms of a bimodal distribution of nickel particle sizes with representative dimensions of particles being 1 - 2 nm and 20 - 40 nm. The larger particles were free to migrate on the surface and agglomerate at all treatment temperatures studied. The smaller particles appeared to be resistant to sintering up to ca. 1023 K, where the smallest particle diameter observed began to increase.

Appendix C - Catalyst Characterisation and Reaction
Chemistry

C1. Introduction

The department of Chemistry, Surrey University (Prof. J. R. Jones et al.) has used various methods of catalyst characterisation including T.P.R., using both the conventional method employing a T.C.D. and a novel method employing tritiated-hydrogen as the reducing gas and a radioactivity detector to monitor the hydrogen depletion in the eluant flow with temperature. The use of tritiated-hydrogen as the reducing gas was also utilised in an investigation to determine how much hydrogen was retained by the catalysts after reduction.

The Surrey group have also studied the kinetics and mechanism of the reductive amination of ethanol to give, predominantly, ethylamine.

The major findings of the work are presented below.

C2. T.P.R. Studies

T.P.R. experiments were performed by the Surrey group using a T.P.R. apparatus capable of operating in either a gas flow or gas recirculating mode; the recirculating mode was used for experiments involving the use of tritiated-hydrogen, with the water formed during reduction removed by a cold trap. The depletion of hydrogen in the 5 % v/v hydrogen in nitrogen reducing gas during a T.P.R. experiment was monitored either by a T.C.D. or, in case of tritiated-hydrogen experiments, by a radio-detector.

To ensure that comparable T.P.R. data to those presented in Section 4.1.2 were produced by this apparatus,

the T.P.R. experiments performed using the unreduced calcined catalysts were repeated under identical conditions to those used at Glasgow (i.e. $\beta = 5 \text{ K min.}^{-1}$ up to a final temperature of 1023 K). The T.P.R. profiles produced from these experiments were found to be similar to those obtained at Glasgow, with all the profiles of the calcined catalysts displaying L.T. peaks and those of the nickel on the ICI and CS2040 (non-aq.) silica catalysts exhibiting significant H.T. peaks.

T.P.R. experiments were then performed using the calcined catalysts with a relatively small amount of tritium (75 - 200 mCi) added to the 5 % hydrogen in nitrogen reducing gas mixture. This gas mixture was recirculated over each sample of catalyst whilst it was heated under the same conditions previously described. An 80 μl sample of gas was taken every five minutes during the heating process and analysed by the radio-detector. After the T.P.R. experiments were complete, the activities of the catalysts were assessed.

The T.P.R. profiles obtained (185) showed that, for all catalysts, no significant uptake of [^3H]-hydrogen occurred until the reduction of the supported nickel oxide began, generally at a temperature of ca. 573 K. The [^3H]-hydrogen was then consumed continuously up to 1023 K, which was the final temperature in the T.P.R. experiments. Samples of the pure ICI and Cab-O-Sil silicas were also used in control experiments. Both these supports consumed a small amount of [^3H]-hydrogen at a steady rate during heating; this loss became more significant beyond a temperature of 723 K. These uptakes of [^3H]-hydrogen were probably due to hydrogen

isotope exchange between surface water and silanol groups, with exchange facilitated by the presence of water vapour desorbed from the silicas during heating and not due to actual reduction of the supports. The [^3H]-hydrogen uptakes by the supports were relatively small compared to those of the calcined catalysts.

After the final temperature was reached, the catalysts were allowed to cool in the 5 % tritiated-hydrogen in nitrogen and then flushed with helium at room temperature. The activities of the catalysts, and hence the amounts of retained hydrogen, were then assessed (see Table C1).

Table C1

Amounts of Tritium Retained on the Catalysts After T.P.R.

Catalyst	Catalyst Activity [mCi (g catalyst) ⁻¹]
10 % Ni on ICI	11
10 % Ni on CS1030E	8
10 % Ni on Cab-O-Sil	2
1 % Ni on ICI	21
1 % Ni on ICI ^a	16
1 % Ni on CS2040 (non-aq.)	18
1 % Ni on CS1030E	14
1 % Ni on Cab-O-Sil	8
1 % Ni on CS2040 (aq.)	2
Pure ICI Silica ^b	8
Pure Cab-O-Sil Silica ^b	10

a. Duplicate experiment.

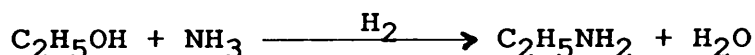
b. Control experiment.

It was found that, in general, the 1 % nickel on silica catalysts retained more tritium than 10 % nickel on silica catalysts. Additionally it was observed, for catalysts of the same metal loading, that the amounts of retained tritium were higher for catalysts prepared from silicas with higher metastable energies in the form of larger proportions of three-fold siloxane rings in their structures (see Appendix B). Therefore, the data presented in Table C1 lead to the conclusion that catalysts prepared from silica supports containing a larger percentage of three-fold siloxane rings in their structures led to more hydrogen (or tritium for reduction by labelled gas) being retained after reduction.

The observation that the 1 % nickel on silica catalysts retained more hydrogen after reduction than the corresponding 10 % nickel on silica catalysts may be explained by the majority of retained hydrogen being stored in the support (176). Spillover hydrogen is thought to associate with three-fold siloxane rings on the surfaces of silica supports (176) and this led to larger amounts of hydrogen being retained by the catalysts prepared from the higher energy supports. If an interaction also occurred in the catalysts between nickel and the three-fold siloxane rings on the surfaces of the supports as proposed in Section 5.1.2, then fewer three-fold siloxane ring sites will have been available for hydrogen storage on the support for catalysts of higher metal loading. Hence metal deposited on a support may adversely affect these storage sites for spillover hydrogen and so the more metal on the support, the less available sites for hydrogen storage exist on the surface of the support.

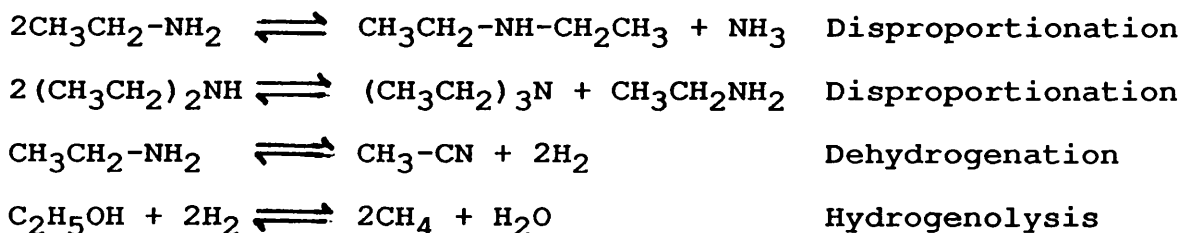
C3. Reductive Amination of Ethanol

The Surrey group also investigated the kinetics and, by means of isotopic labelling, the mechanism of the reductive amination of ethanol to give amine products. The reaction can be represented, in its simplest form, by the following equation;



In practice, however, significant quantities of diethylamine and triethylamine are formed by the disproportionation of the ethylamine. Acetonitrile (from the dehydrogenation of ethylamine) and methane (from the hydrogenolysis of ethanol) can also be produced.

These reactions are illustrated below;



The relative amounts of all the products are dependent on both the metal and the support from which the catalyst is prepared (192 - 194) and also the reaction conditions such as the temperature, pressure and the initial relative ratio of the reactants (192, 194, 195).

In the experiments performed at Surrey, a sample of each calcined catalyst was reduced using the apparatus described above following the standard reduction conditions outlined in Section 3.3.1(a). The reduced catalyst was then cooled to the temperature at which the reaction was to be studied; the reaction was studied for temperatures in the

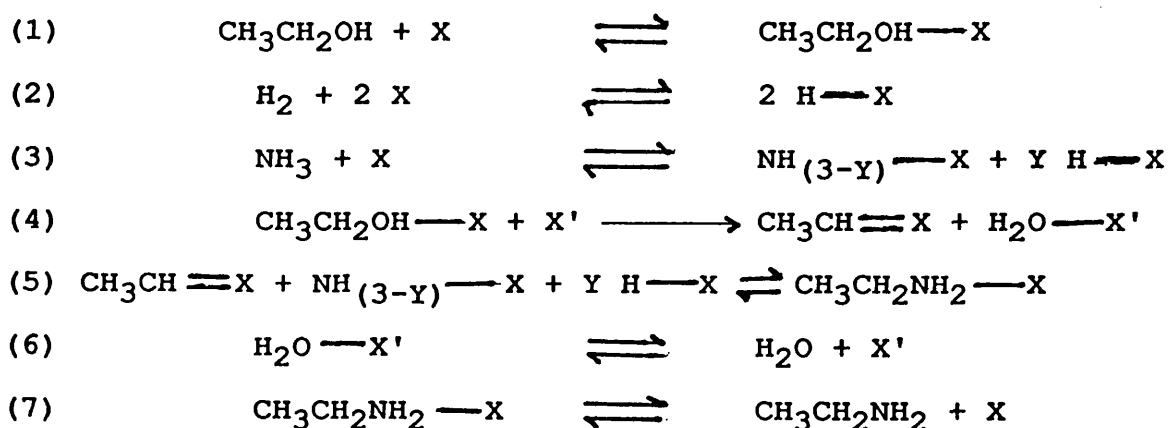
range 383 - 453 K. The reactor was then filled with hydrogen and isolated; the pressure of hydrogen for all the experiments was constant at 6 p.s.i.g. The apparatus was then heated (temperature = 383 K) and filled with hydrogen to the same pressure as the reactor together with ammonia and ethanol in a relative molar ratio to one another of either 1:1, 4:1 or 7:1, respectively. Each of these mixtures was recirculated for a time to mix the gases thoroughly before being directed through the reactor.

Under the reaction conditions chosen for amination it was observed that only the amine products were formed in significant amounts and that acetonitrile was present only in trace amounts (although at higher temperatures this increased) and methane was not detected. It was also found that the 1:1 ratio of ammonia:ethanol gave very poor yields of all the amine products. The yields of the amine products were found to be greatly improved on increasing this ratio to 4:1. On going to a ratio of 7:1 using the 10 % nickel on ICI and Cab-O-Sil silica catalysts, a difference in behaviour was noted. The rate of ethylamine formation increased for the 10 % nickel on ICI silica catalyst, while the corresponding rate decreased for the 10 % nickel on Cab-O-Sil silica catalyst. Therefore a higher ratio of ammonia to ethanol appeared to retard the amination reaction rate using the 10 % nickel on Cab-O-Sil silica catalyst.

Under identical reaction conditions, the catalysts prepared from supports of higher metastable energy (i.e. the nickel on ICI and CS2040 (non-aq.) silica catalysts) were found to catalyse the amination reaction at a much faster rate than catalysts prepared from lower energy supports

(i.e. the nickel on Cab-O-Sil and CS2040 (aq.) silica catalysts). The reaction rate was also found to be considerably slower for subsequent amination reactions performed using the catalysts; this indicated that deactivation occurred.

Experiments were performed to elucidate the mechanism of the amination reaction including labelling experiments using ^2H , ^3H and ^{13}C labels. From the results of these experiments, the mechanism for the reaction illustrated in Figure C1 was proposed. It was further suggested that stage (4) of this mechanism, dehydration of adsorbed ethanol, was the rate determining step.



where X and X' represent catalyst active sites and $3 \gg \text{Y} \gg 0$.

Figure C1 Proposed Mechanism of Reductive Amination of Ethanol

The faster rate of amination observed for catalysts prepared from higher energy supports was attributed to the three-fold siloxane rings on the surface of the high energy support aiding water removal in stage (4) by initially

reacting chemically with this water as illustrated in Figure C2.

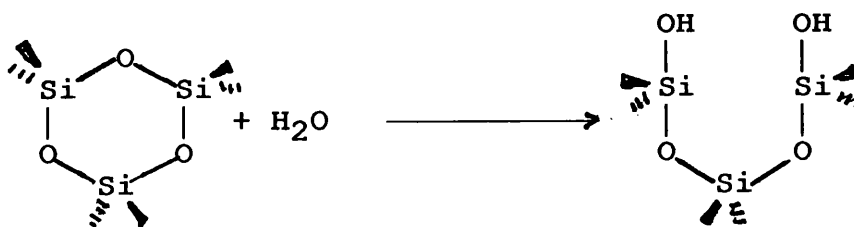


Figure C2 Reaction of Water with a Three-fold Siloxane Ring

Later, the vicinal silanol groups formed by the reaction illustrated in Figure C2 will have aided water removal from the metal crystallites by hydrogen bonding. Hence for catalysts prepared from the high energy silicas, the water formed in step (4) of the reaction mechanism illustrated in Figure C1 would have been swiftly removed from the nickel crystallites and subsequently the reaction rates were higher using these catalysts. Also potentially active intermediates could have been formed by the dissociative adsorption of ammonia and ethanol on the three-fold siloxane rings (illustrated below in Figures C3 and C4, respectively);

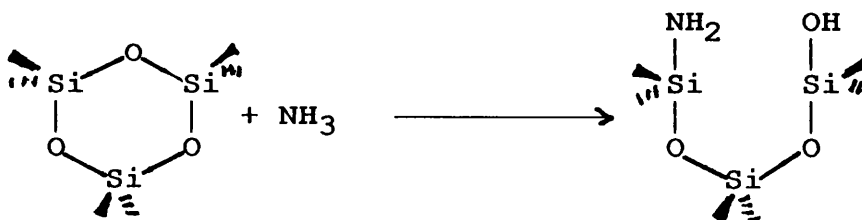


Figure C3 Reaction of Ammonia with a Three-fold Siloxane

Ring

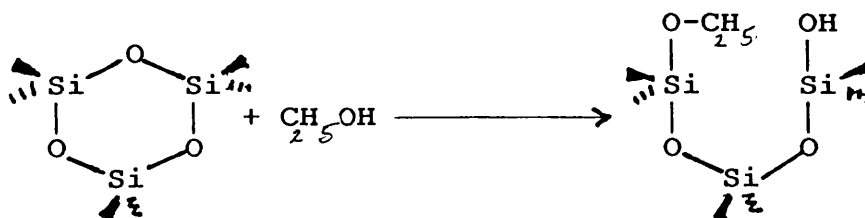


Figure C4 Reaction of Ethanol with a Three-fold Siloxane Ring

Morrow and Cody (177) have shown that strained siloxane linkages (such as those found in three-fold siloxane rings) act as Lewis acids and will strongly interact with Lewis bases such as water, ammonia and alcohols, in the manners illustrated in Figures C2, C3 and C4, respectively. All these interactions would be expected to enhance the reactivities of the catalysts, and hence catalysts with larger proportions of three-fold siloxane rings in their supports were found to be more active, i.e. the nickel on ICI and CS2040 (non-aq.) silica catalysts.

The relaxation and loss of these three-fold siloxane rings during the course of an amination reaction could also account for the observed deactivation of the catalysts.

The observation that the amination reaction rate using the 10 % nickel on Cab-O-Sil silica catalyst was relatively slow when a high ammonia:ethanol ratio was used may be explained by the fact that the concentration of three-fold siloxane rings on this silica was limited. Thus it was possible that high concentrations of ammonia swamped the three-fold siloxane ring sites on the Cab-O-Sil silica-supported catalyst and reduced their ability to remove water formed during the reaction.

REFERENCES TO THE LITERATURE

1. G. C. Bond, "Heterogeneous Catalysis; Principles and Applications", Clarendon Press, Oxford, 1974, pp. 62 - 113.
2. W. Carruthers, "Some Modern Methods of Organic Synthesis", 2nd Edition, Cambridge University Press, 1978.
3. R. T. Morrison and R. N. Boyd, "Organic Chemistry", 4th Edition, Allyn and Bacon Inc., Boston, 1983.
4. S. J. Thomson and G. Webb, "Heterogeneous Catalysis", University Chemical Texts, Oliver and Boyd, London, 1968, p14.
5. R. Burch and A. R. Flambard in *Scientific Basis for the Preparation of Heterogeneous Catalysts; 3rd International Symposium*, Louvain-La-Neuve, Belgian, 1982.
6. J. W. E. Coenen, *Appl. Catal.*, **54**, 65 (1989).
7. Y. Nitta, T. Utsumi, T. Imanaka and S. Teranishi, *Chem. Lett.*, 1339 (1984).
8. J. T. Richardson and R. J. Dubus, *J. Catal.*, **54**, 207 (1978).
9. M. Montes, Ch. Penneman de Bosscheyde, B. K. Hodnett, F. Delannay, P. Grange and B. Delmon, *Appl. Catal.*, **12**, 309 (1984).
10. J. A. Van Dillen, J. W. Geus, L. A. M. Hermans and J. Van der Meijden in *Proc. 6th Intl. Congr. Catalysis*, (G. C. Bond, P. B. Wells and F. C. Tompkins, Eds.), The Chemical Society, London (1976), p677.
11. C. H. Bartholomew and W. L. Sorensen, *J. Catal.*, **81**, 131 (1983).
12. A. Aguinaga, J. C. de la Cal, J. M. Asúa and M. Montes, *Appl. Catal.*, **51**, 1 (1989).
13. D. G. Mustard and C. H. Bartholomew, *J. Catal.*, **67**, 186 (1981).
14. M. Boudart, *Adv. in Catal.*, **20**, 153 (1969).
15. C. E. O'Neill and D. J. C. Yates, *J. Phys. Chem.*, **65**, 901 (1961).
16. P. H. Desai and J. T. Richardson, *J. Catal.*, **98**, 392 (1986).
17. A. I. Ahmed, S. M. Hassan, M. A. Morsi and S. Abdel-Hakam, *Bull. Soc. Chim. France*, **6**, 731 (1989).

18. A. Roman and B. Delmon, *J. Catal.*, **30**, 333 (1973).
19. M. Komiyama, *Catal. Rev. -Sci. Eng.*, **27**, 341 (1985).
20. As reference 4, p146.
21. J. L. Lemaitre, P. G. Menon and F. Delannay in "Characterization of Heterogeneous Catalysts", (F. Delannay, Ed.), Chemical Industries/15, Marcel Dekker, New York, 1984, pp 299 - 365.
22. W. Romanowski, "Highly Dispersed Metals", Ellis Horwood Series in Inorganic Chemistry, Halsted Press, Chichester, 1987 (English Trans.), pp. 11 - 29.
23. J. S. Smith, P. A. Thrower and M. A. Vannice, *J. Catal.*, **68**, 270 (1981).
24. A. Shastri, J. Schwank and S. Galvagno, *J. Catal.*, **100**, 446 (1986).
25. M. A. Vannice and R. L. Garten, *J. Catal.*, **56**, 236 (1979).
26. F. Arena, B. A. Horrell, D. L. Cocke, A. Parmaliana and N. Giordano, *J. Catal.*, **132**, 58 (1991).
27. D. J. C. Yates, W. F. Taylor and J. H. Sinfelt, *J. Amer. Chem. Soc.*, **86**, 2996 (1964).
28. C. H. Bartholomew and R. J. Farrauto, *J. Catal.*, **45**, 41 (1976).
29. F. E. Shephard, *J. Catal.*, **14**, 148 (1969).
30. A. Verma and D. M. Ruthven, *J. Catal.*, **19**, 401 (1970).
31. J. Freel, *J. Catal.*, **25**, 139 (1972).
32. P. I. Lee and J. A. Schwarz, *J. Catal.*, **73**, 272 (1982).
33. M. Primet, J. A. Dalmon and G. A. Martin, *J. Catal.*, **46**, 25 (1977).
34. J. A. Rabo, A. P. Risch and M. L. Poutsma, *J. Catal.*, **53**, 295 (1978).
35. R. W. Joyner and M. W. Roberts, *J. Chem. Soc., Faraday Trans. I*, **70**, 1819 (1974).
36. G. A. Martin, M. Primet and J. A. Dalmon, *J. Catal.*, **53**, 321 (1978).
37. G. Wedler, H. Papp and G. Schroll, *Surf. Sci.*, **44**, 463 (1974).
38. P. R. Wentreek, B. J. Wood and H. Wise, *J. Catal.*, **43**, 363 (1976).

39. J. A. Dalmon and G. A. Martin, *J. Catal.*, **84**, 45 (1983).
40. G. D. Renshaw, C. Roscoe and P. L. Walker Jr., *J. Catal.*, **22**, 394 (1971).
41. N. Sheppard and T. T. Nguyen in *Advances in Infrared and Raman Spectroscopy*, (R. J. Clarke and R. E. Hester, Eds.), Wiley, New York, 1978, vol. 4, p67.
42. As reference 22, pp170 - 172.
43. S. L. Anderson, T. Mizushima and Y. Udagawa, *J. Phys. Chem.*, **95**, 6603 (1991).
44. R. P. Eischens, W. A. Pliskin and S. A. Francis, *J. Chem. Phys.*, **22**, 1786 (1954).
45. R. P. Eischens, S. A. Francis and W. A. Pliskin, *J. Phys. Chem.*, **60**, 194 (1956).
46. J. T. Yates Jr. and C. W. Garland, *J. Phys. Chem.*, **65**, 617 (1961).
47. G. Blyholder, *J. Phys. Chem.*, **68**, 2772 (1964).
48. F. A. Cotton and C. S. Kraihanzel, *J. Amer. Chem. Soc.*, **84**, 4432 (1962).
49. C. S. Kraihanzel and F. A. Cotton, *Inorg. Chem.*, **2**, 533 (1963).
50. J. A. Dalmon, M. Primet, G. A. Martin and B. Imelik, *Surf. Sci.*, **50**, 95 (1975).
51. C. H. Rochester and R. J. Terrell, *J. Chem. Soc., Faraday Trans. I*, **73**, 609 (1977).
52. C. W. Garland, *J. Phys. Chem.*, **63**, 1423 (1959).
53. Y. Soma-Noto and W. M. H. Sachtler, *J. Catal.*, **34**, 162 (1974).
54. G. A. Martin and J. A. Dalmon, *J. Catal.*, **75**, 233 (1982).
55. G. Blyholder, *J. Phys. Chem.*, **79**, 756 (1975).
56. H. S. Luftman, Y-M. Sun and J. M. White, *Surf. Sci.*, **141**, 82 (1984).
57. H. Praliaud, J. A. Dalmon, C. Mirodatos and G. A. Martin, *J. Catal.*, **97**, 344 (1986).
58. R. P. Eischens and W. A. Pliskin, *Adv. in Catal.*, **10**, 1 (1958).
59. D. G. Blackmond and E. I. Ko, *J. Catal.*, **96**, 210 (1985).

60. C. H. Bartholomew, R. B. Pannell and J. L. Butler, *J. Catal.*, **65**, 335 (1980).
61. R. Van Hardeveld and F. Hartog, *Adv. in Catal.*, **22**, 75 (1972).
62. M. J. Heal, E. C. Leisegang and R. G. Torrington, *J. Catal.*, **42**, 10 (1976).
63. D. G. Blackmond and E. I. Ko, *J. Catal.*, **94**, 343 (1985).
64. A. M. Bradshaw and J. Pritchard, *Surf. Sci.*, **17**, 372 (1969).
65. H. L. Pickering and H. C. Eckstrom, *J. Phys. Chem.*, **63**, 512 (1959).
66. C. H. Bartholomew and R. B. Pannell, *J. Catal.*, **65**, 390 (1980).
67. M. A. Vannice, *J. Catal.*, **44**, 152 (1976).
68. G. A. Somorjai and M. A. Van Hove, *Prog. Surf. Sci.*, **30**, 201 (1989).
69. G. A. Somorjai, *J. Phys. Chem.*, **94**, 1013 (1990).
70. I. Toyoshima and G. A. Somorjai, *Catal. Rev. -Sci. Eng.*, **19**, 105 (1979).
71. W. C. Conner and C. O. Bennett, *J. Catal.*, **41**, 30 (1976).
72. G. C. A. Schuit and L. L. Van Reijen, *Adv. in Catal.*, **10**, 242 (1958).
73. A. Borgna, R. Fréty, M. Primet and M. Guenin, *Appl. Catal.*, **76**, 233 (1991).
74. As reference 1, p44.
75. R. J. Kokes and P. H. Emmett, *J. Amer. Chem. Soc.*, **82**, 1037 (1960).
76. C. S. Brooks and G. L. M. Christopher, *J. Catal.*, **10**, 211 (1968).
77. R. Mason and M. Textor in *Surface and Defect Properties of Solids*, (M. W. Roberts and J. M. Thomas, Eds.), Specialist Periodical Reports, Chemical Society, London, 1976, Vol. 5, p189.
78. A. R. West, "Solid State Chemistry and its Applications", Wiley, Chichester, 1984, pp 64 - 68.
79. As reference 22, p88.
80. As reference 21, pp 86 - 93.

81. R. Van Hardeveld and A. Van Montfoort, *Surf. Sci.*, **4**, 396 (1966).
82. T. E. Whyte Jr., *Catal. Rev.*, **8**, 117 (1973).
83. C. Raab, J. A. Lercher, J. G. Goodwin Jr. and J. Z. Shyu, *J. Catal.*, **122**, 406 (1990).
84. S-L. Guo, M. Arai and Y. Nishiyama, *Appl. Catal.*, **65**, 31 (1990).
85. M. Montes, J. Soupart, M. de Saedeleer, B. K. Hodnett and B. Delmon, *J. Chem. Soc., Faraday Trans. I*, **80**, 3209 (1984).
86. P. C. Flynn, S. E. Wanke and P. S. Turner, *J. Catal.*, **33**, 233 (1974).
87. As reference 22, p97.
88. M. Houalla, F. Delannay, I. Matsuura and B. Delmon, *J. Chem. Soc., Faraday Trans. I*, **76**, 2128 (1980).
89. M. Houalla, F. Delannay and B. Delmon, *J. Chem. Soc., Faraday Trans. I*, **76**, 1766 (1980).
90. N. W. Hurst, S. J. Gentry, A. Jones and B. D. McNicol, *Catal. Rev. -Sci. Eng.*, **24**, 233 (1982).
91. S. D. Robertson, B. D. McNicol, J. H. de Baas, S. C. Kloet and J. W. Jenkins, *J. Catal.*, **37**, 424 (1975).
92. D. Reinen and P. W. Selwood, *J. Catal.*, **2**, 109 (1963).
93. V. C. F. Holm, G. C. Bailey and A. Clark, *Ind. Eng. Chem.*, **49**, 250 (1957).
94. V. C. F. Holm and A. Clark, *J. Catal.*, **11**, 305 (1968).
95. G. A. Martin, C. Mirodatos and H. Praliaud, *Appl. Catal.*, **1**, 367 (1981).
96. J. C. Vedrine, G. Hollinger and T. M. Duc, *J. Phys. Chem.*, **82**, 1515 (1978).
97. B. Mile, M. A. Zammitt and A. G. Chapman, Interim Report to SERC, Grant No. GR/A/3531/0, 1978 - 1980.
98. J. B. Peri, *Discuss. Faraday Soc.*, **41**, 121 (1966).
99. M. Houalla and B. Delmon, *J. Phys. Chem.*, **84**, 2194 (1980).
100. E. E. Unmuth, L. H. Schwartz and J. B. Butt, *J. Catal.*, **61**, 242 (1980).
101. B. Mile, D. Stirling, M. A. Zammitt, A. Lovell and M. Webb, *J. Catal.*, **114**, 217 (1988).

102. M. W. Roberts and R. St. C. Smart, *J. Chem. Soc., Faraday Trans. I*, **80**, 2957 (1984).
103. J. W. E. Coenen and B. G. Linsen in "Physical and Chemical Aspects of Adsorbents and Catalysts", (B. G. Linsen, ed.), Academic Press, New York, 1970, pp 472 - 524.
104. J. R. Sohn and A. Ozaki, *J. Catal.*, **59**, 303 (1979).
105. S. J. Tauster, S. C. Fung and R. L. Garten, *J. Amer. Chem. Soc.*, **100**, 170 (1978).
106. S. J. Tauster and S. C. Fung, *J. Catal.*, **55**, 29 (1978).
107. S. A. Stevenston, G. B. Raupp, J. A. Dumesic, S. J. Tauster and R. T. K. Baker in "Metal-Support Interactions in Catalysis, Sintering and Redispersion", (S. A. Stevenston, J. A. Dumesic, R. T. K. Baker and E. Ruckenstein, Eds.), Van Nostrand Reinhold Company, New York, 1987, pp9 - 19.
108. X-Z. Jiang, T. F. Hayden and J. A. Dumesic, *J. Catal.*, **83**, 168 (1983).
109. X-Z. Jiang, S. A. Stevenston, J. A. Dumesic, T. F. Kelly and R. J. Casper, *J. Phys. Chem.*, **88**, 6191 (1984).
110. P. Turlier, J. A. Delmon and G. A. Martin, *Stud. Surf. Sci. Catal.*, **11**, 203 (1982).
111. M. A. Vannice, *J. Catal.*, **74**, 199 (1982).
112. R. Burch and A. R. Flambard, *J. Catal.*, **78**, 389 (1982).
113. J. D. Bracey and R. Burch, *J. Catal.*, **86**, 384 (1984).
114. M. A. Vannice and S-Y. Wang, *J. Phys. Chem.*, **85**, 2543 (1981).
115. E. I. Ko, J. M. Hupp, F. H. Rogan and N. J. Wagner, *J. Catal.*, **84**, 85 (1983).
116. E. I. Ko, J. M. Hupp and N. J. Wagner, *J. Chem. Soc., Chem. Comm.*, 94 (1983).
117. E. I. Ko, R. Bafrafi, N. T. Nuhfer and N. J. Wagner, *J. Catal.*, **95**, 260 (1985).
118. E. Kikuchi, H. Nomura, M. Matsumoto and Y. Morita, *Appl. Catal.*, **7**, 1 (1983).
119. T. Iizuka, Y. Tanaka and K. Tanabe, *J. Molec. Catal.*, **17**, 381 (1982).
120. K. Kunimori, H. Abe and T. Uchijima, *Chem. Lett.*, 1619 (1983).

121. S. J. Tauster, S. C. Fung, R. T. K. Baker and J. A. Horsley, *Science*, **211**, 1121 (1981).
122. P. G. Menon and G. F. Froment, *Appl. Catal.*, **1**, 31 (1981).
123. P. G. Menon and G. F. Froment, *Stud. Surf. Sci. Catal.*, **11**, 171 (1982).
124. F. S. Delk and A. Vavere, *J. Catal.*, **85**, 380 (1984).
125. T. Huizinga, J. Van Grondelle and R. Prins, *Appl. Catal.*, **10**, 199 (1984).
126. D. Briggs, J. Dewing, A. G. Burden, R. B. Moyes and P. B. Wells, *J. Catal.*, **65**, 31 (1980).
127. R. Burch and A. R. Flambard, *J. Chem. Soc., Chem. Comm.*, 965 (1981).
128. R. T. K. Baker, E. B. Prestridge and R. L. Garten, *J. Catal.*, **56**, 390 (1979).
129. A. G. Shastri, A. K. Dayte and J. Schwank, *J. Catal.*, **87**, 265 (1984).
130. J. A. Dumesic, S. A. Stevenston, R. D. Sherwood and R. T. K. Baker, *J. Catal.*, **99**, 79 (1986).
131. A. J. Simoens, R. T. K. Baker, D. J. Dwyer, C. R. F. Lund and R. J. Madon, *J. Catal.*, **86**, 359 (1984).
132. R. T. K. Baker, *J. Catal.*, **63**, 523 (1980).
133. T. Huizinga and R. Prins, *J. Phys. Chem.*, **85**, 2156 (1981).
134. B. J. Tatarchuk and J. A. Dumesic, *J. Catal.*, **70**, 308 (1981).
135. B. J. Tatarchuk, J. J. Chludzinski, R. D. Sherwood, J. A. Dumesic and R. T. K. Baker, *J. Catal.*, **70**, 433 (1981).
136. R. T. K. Baker, E. B. Prestridge and G. B. McVicker, *J. Catal.*, **89**, 422 (1984).
137. P. Mériaudeau, O. H. Ellestad, M. Dufaux and C. Naccache, *J. Catal.*, **75**, 243 (1982).
138. D. N. Belton, Y-M. Sun and J. M. White, *J. Phys. Chem.*, **88**, 1690 (1984).
139. S-M. Fang and J. M. White, *J. Catal.*, **83**, 1 (1983).
140. J. A. Horsley, *J. Amer. Chem. Soc.*, **101**, 2870 (1979).
141. G. M. Schwab, *Adv. in Catal.*, **27**, 1 (1978).

142. B. J. Tatarchuk and J. A. Dumesic, *J. Catal.*, **70**, 323 (1981).
143. C. S. Ko and R. J. Gorte, *J. Catal.*, **90**, 59 (1984).
144. J. Santos, J. Phillips and J. A. Dumesic, *J. Catal.*, **81**, 147 (1983).
145. G. B. Raupp and J. A. Dumesic, *J. Phys. Chem.*, **88**, 660 (1984).
146. L. M. Tau and C. O. Bennett, *J. Catal.*, **89**, 285 (1984).
147. R. T. K. Baker, J. J. Chludzinski and J. A. Dumesic, *J. Catal.*, **93**, 312 (1985).
148. H. C. Yao, M. Sieg and H. K. Plummer Jr., *J. Catal.*, **59**, 365 (1979).
149. F. M. Dautzenberg and H. B. M. Wolters, *J. Catal.*, **51**, 26 (1978).
150. G. J. den Otter and F. M. Dautzenberg, *J. Catal.*, **53**, 116 (1978).
151. K. Kunimori and T. Uchijima, *Stud. Surf. Sci. Catal.*, **17**, 197 (1983).
152. P. G. Menon and G. F. Froment, *J. Catal.*, **59**, 138 (1979).
153. K. Kunimori Y. Ikeda, M. Soma and T. Uchijima, *J. Catal.*, **79**, 185 (1983).
154. T. Ren-yuan, W. Rong-an and L. Li-wu, *Appl. Catal.*, **10**, 163 (1984).
155. G. A. Martin, R. Dutartre and J. A. Dalmon, *React. Kinet. Catal. Lett.*, **16**, 329 (1981).
156. H. Praliaud and G. A. Martin, *J. Catal.*, **72**, 394 (1981).
157. B. R. Powell and S. E. Whittington, *J. Catal.*, **81**, 382 (1983).
158. J. A. Dalmon and C. Mirodatos, *J. Molec. Catal.*, **25**, 161 (1984).
159. L. H. Dubois and R. G. Nuzzo, *J. Amer. Chem. Soc.*, **105**, 365 (1983).
160. R. K. Iler, "The Chemistry of Silica", Wiley - Interscience, New York, 1979.
161. M. Vignaux, P. Chiaranussati, L. F. Gladden, A. P. Sharratt, J. R. Jones, F. J. Robertson, G. Webb, R. J. Cross, S. D. Jackson, R. W. Griffiths, P. Chieux and A. C. Hannon, *J. Non-cryst. Solids*, **139**, 47 (1992).

162. A. Jones and B. D. McNicol, "Temperature Programmed Reduction for Solid Materials Characterisation", Chemical Industries/24, Marcel Dekker Inc., New York, 1986.
163. S. D. Jackson, F. J. Robertson and J. Willis, *J. Molec. Catal.*, **63**, 255 (1990).
164. J. Hu, J. A. Schwarz and Y-J. Huang, *J. Catal.*, **111**, 59 (1989).
165. H. L. Gruber, *J. Phys. Chem.*, **66**, 48 (1962).
166. L. Spenadel and M. Boudart, *J. Phys. Chem.*, **64**, 204 (1960).
167. D. Smith, D. White, T. Baird and J. Fryer, *J. Catal.*, **81**, 107 (1983).
168. J. R. Anderson, "Structure of Metallic Catalysts", Academic Press, New York, pp. 358-368.
169. M. P. Lapinski and J. G. Ekerdt, *J. Phys. Chem.*, **94**, 4599 (1990).
170. J. H. Anderson, *J. Catal.*, **26**, 277 (1972).
171. B. Mile, D. Stirling, M. A. Zammitt, A. Lovell and M. Webb, *J. Molec. Catal.*, **62**, 179 (1990).
172. P. Turlier, H. Pra liaud, P. Moral, G. A. Martin and J. A. Dalmon, *Appl. Catal.*, **18**, 389 (1985).
173. P. D. Maniar and A. Navrotsky, *J. Non-cryst. Solids*, **120**, 20 (1990).
174. D. R. Tallant, B. C. Bunker, C. J. Brinker and C. A. Balfe, *Mat. Res. Soc. Symp. Proc.*, **73**, 261 (1986).
175. M. E. Bartram, T. A. Michalske and J. W. Rogers Jr., *J. Phys. Chem.*, **95**, 4453 (1991).
176. S. D. Jackson, J. R. Jones, A. P. Sharratt, L. F. Gladden, M. Vignaux, F. J. Robertson, G. Webb, R. J. Cross and R. W. Griffiths, *Catalysis Today*, **10**, 323 (1991).
177. B. A. Morrow and I. A. Cody, *J. Phys. Chem.*, **80**, 1995 (1976).
178. L. Gladden, P. Chiaranussati and M. Vignaux, unpublished results.
179. L. L. Murrell and D. J. C. Yates, *Stud. Surf. Sci. Catal.*, **3**, 307 (1979).
180. G. F. Hart, B.Sc. (Hons) Dissertation, University of Glasgow, 1977.

181. G. Webb, *Catalysis Today*, **7**, 139 (1990).
182. J. A. Altham and G. Webb, *J. Catal.*, **18**, 133 (1970).
183. E. Crawford, M. W. Roberts and C. Kemball, *Trans. Faraday Soc.*, **58**, 1761 (1962).
184. G. A. Somorjai and F. Zaera, *J. Phys. Chem.*, **86**, 3070 (1982).
185. A. P. Sharratt, Ph.D. Dissertation, University of Surrey, 1991.
186. R. W. Griffiths, Private Communication.
187. Cabot Corporation Technical Data Sheet.
188. ICI Analytical Report, Job No. 010314910, 20th April 1987.
189. PQ Corporation, Data Sheet on CS1030E Silica.
190. PQ Corporation, Data Sheet on CS2040 Silica.
191. L. F. Gladden, P. Chiaranussati and M. Vignaux, Private Communication.
192. C. M. Barnes and H. F. Rase, *Ind. Eng. Chem. Prod. Res. Dev.*, **20**, 399 (1981).
193. A. Baiker and W. Richarz, *Ind. Eng. Chem. Prod. Res. Dev.*, **16**, 261 (1977).
194. R. J. Card and J. L. Schmitt, *J. Org. Chem.*, **46**, 754 (1981).
195. J. Pašek, P. Kondelik and P. Richter, *Ind. Eng. Chem. Prod. Res. Dev.*, **11**, 333 (1972).

